TAMPEREEN TEKNILLINEN YLIOPISTO
TAMPERE UNIVERSITY OF TECHNOLOGY

JUHA KURONEN

IMPROVING TRANSIENT SIMULATION OF PULVERIZED COAL-FIRED POWER PLANTS IN DYNAMIC SIMULATION SOFTWARE

Master of Science Thesis

Examiner: Professor Matti Vilkko
Examiner and topic were approved by the Council of the Faculty of Engineering Sciences on 9th December 2015

ABSTRACT

JUHA KURONEN: Improving transient simulation of pulverized coal-fired power plants in dynamic simulation software
Tampere University of Technology
Master of Science Thesis, 88 pages, 11 appendix pages
March 2016
Master's Degree Programme in Automation Technology
Major: Process Automation
Examiner: Professor Matti Vilkko

Keywords: pulverized coal-fired power plant, cyclic operation, coal mill, thermal stress, thermo-mechanical stress, dynamic simulation, transient, Apros

Pulverized coal-fired power plants are increasingly used in electric grid load compensation. The intermittent electricity production of wind and solar power plants causes sudden load changes in the electric grid which must be balanced by operating steam power plants cyclically. Rapid load changes cause new challenges to plant operators.

Dynamic simulation is a powerful tool for investigating the transient behavior of a power plant that is operated cyclically. Process changes and new control strategies are often needed when base load power plants are used in cyclic operation mode. New solutions can be tested with a computer-aided dynamic simulation software. A dynamic model of pulverized coal-fired power plant requires a realistic coal mill model. Also it is important to define thermo-mechanical stresses in stress-prone boiler components during the cyclic operation. These features improve the transient simulation of pulverized coal-fired power plants.

This thesis focuses on examining and improving the transient simulation of pulverized coal-fired power plants in dynamic simulation software Apros. The main objectives of this thesis are implementation and validation of a generic coal mill model as well as the verification and validation of Apros thermo-mechanical stress calculation. The coal mill model was implemented by using the user component feature of Apros, whereas the thermo-mechanical stress calculation was implemented with a stress solver component which has been earlier added to Apros component library.

Two pulverized coal-fired power plant simulation models were utilized in the validation experiments. Model of reference plant A was received from the plant operator whereas modelling of reference plant B was part of this work. The dynamic validation of the coal mill model was done by simulating the same load change transients that have been measured during cyclic operation of the reference plants. The stress calculation was verified against literary reference and validated against calculation based on standard EN-12952-3 (Water-tube boilers and auxiliary installations. Part 3: Design and calculation for pressure parts of the boiler). In addition stresses were defined during load change transients in critical once-through boiler components.

The validation of the coal mill model did not completely give desired results during the load changes. The model was unable to simulate the dynamics of the coal storage inside the mill realistically, when the plant load was changed. Apros stress calculation corresponded to the literary verification reference. It was noted in the validation that stress concentration factors should be used in Apros calculation when the stresses are defined in pipe connections. The stresses during the load change transients seemed realistic and they remained under the defined stress limits.

TIIVISTELMÄ

JUHA KURONEN: Hiilivoimalaitosten transienttisimuloinnin kehittäminen dynaamisessa simulointiohjelmistossa
Tampereen teknillinen yliopisto
Diplomityö, 88 sivua, 11 liitesivua
Maaliskuu 2016
Automaatiotekniikan koulutusohjelma
Pääaine: Prosessiautomaatio
Tarkastaja: Professori Matti Vilkko

Avainsanat: hiilivoimalaitos, syklinen käyttö, hiilimylly, lämpöjännitys, lämpömekaaninen jännitys, dynaaminen simulointi, transientti, Apros

Hiilivoimalaitoksia käytetään yhä enemmän sähköverkon tehonsäädössä. Tuuli- ja aurinkovoimaloiden epäsäännöllinen sähköntuotanto aiheuttaa sähköverkkoon äkillisiä tehonmuutoksia, joita on kompensoitava ohjaamalla höyryvoimalaitoksia syklisesti. Nopeat tehonmuutokset aiheuttavat uusia haasteita laitosoperaattoreille.

Dynaaminen simulointi on tehokas työkalu, kun tutkitaan voimalaitoksen tehonmuutosten aikaista käyttäytymistä. Peruskuormalaitoksella on yleensä tarpeellista tehdä prosessimuutoksia ja suunnitella uusia säätöstrategioita, kun laitosta aletaan ajaa syklisesti. Uusia ratkaisuja voidaan testata tietokonepohjaisella dynaamisen simuloinnin ohjelmistolla. Hiilivoimalaitoksen dynaamisessa mallissa tarvitaan realistinen hiilimyllymalli. On myös tärkeää määrittää lämpö-mekaaniset jännitykset jännityksille alttiissa kattilakomponenteissa syklisen käytön aikana. Nämä ominaisuudet kehittävät hiilivoimalaitosten transienttisimulointia.

Tämä työ keskittyy hiilivoimalaitosten transienttisimuloinnin tutkimiseen ja kehittämiseen dynaamisen simuloinnin ohjelmistossa Aprosissa. Työn päätavoitteita ovat geneerisen hiilimyllymallin toteuttaminen ja validointi sekä Aprosin lämpö-mekaanisten jännitysten laskennan verifiointi ja validointi. Hiilimyllymalli on toteutettu Aprosin user component -ominaisuudella, kun taas lämpö-mekaaninen jännityslaskenta on toteutettu stress solver -komponentilla, joka on aiemmin lisätty Aprosin komponenttikirjastoon.

Validointikokeissa hyödynnettiin kahden hiilivoimalaitoksen simulointimalleja. Referenssilaitoksen A malli saatiin käyttöön laitokselta, kun taas referenssilaitoksen B mallintaminen oli osa tätä työtä. Hiilimyllymallin dynaamisessa validoinnissa käytettiin samoja transientteja, jotka on mitattu referenssilaitoksilla, kun laitoksia on ajettu syklisesti. Jännityslaskenta verifioitiin kirjallista lähdettä vasten ja validoitiin EN-12952-3 standardiin (Vesiputkikattilat ja niihin liittyvät laitteistot. Osa 3: Paineenalaisten osien suunnittelu ja laskenta.) perustuvaa laskentaa vasten. Lisäksi määritettiin jännitykset läpivirtauskattilan kriittisissä komponenteissa tehonmuutosten aikana.

Hiilimyllymallin validointi ei täysin tuottanut haluttuja tuloksia tehonmuutosten aikana. Malli ei pystynyt simuloimaan realistisesti myllyn sisäisen hiilivaraston dynamiikkaa, kun laitoksen tehoa muutettiin. Aprosin jännityslaskenta vastasi kirjallista verifiointireferenssiä. Validoinnissa huomattiin, että Aprosin laskennassa on käytettävä muotokertoimia, kun jännityksiä määritetään putkiliitoksissa. Tehonmuutosten aikaiset jännitykset vaikuttivat realistisilta ja ne pysyivät määritettyjen jännitysrajojen alapuolella.

PREFACE

This thesis was done at the IT-systems unit of Fortum Thermal Production and Power Solutions as a part of development project related to upgrading coal-fired power plant modelling and simulation in dynamic simulation software Apros.

I would like to thank my supervisors at IT-systems for the opportunity to carry out this thesis work. Especially I want to thank the supervisor of the study, Sami Tuuri, for the topic and guidance throughout the work.

I want to express my gratitude to Martin Fricke from Trianel and Martin Wortel from STEAG for providing information and data from Lünen power plant (reference plant B) as well as the reference plant A contact person, who provided the plant simulation model and guided me during the work.

At the university I would like to thank the examiner, Matti Vilkko, who gave me instructions concerning the structure of the thesis. Finally great thanks to my family and friends for all the support during my studies.

Helsinki, March 23, 2016

Juha Kuronen

TABLE OF CONTENTS

SYMBOLS AND ABBREVIATIONS

Apros	A commercial dynamic simulation software
CHP	Combined heat and power
CO_2	Carbon dioxide
HP	High-pressure
IP	Intermediate-pressure
LP	Low-pressure
NO_X	Nitrogen oxides
O_2	Oxygen
P&ID	Piping and instrumentation diagram
SC	Supercritical
SO_X	Sulfur oxides
TH0	Apros thermal hydraulics accuracy level zero
TSO	Transmission system operator
UC	User component, feature in Apros software
USC	Ultra-supercritical
VTT	Technical Research Centre of Finland

a	Thermal diffusivity [m^2/s]
A	Cross-sectional area [m^2]
B	Coefficient for calculation of stress concentration factor
C	Coefficient for calculation of stress concentration factor
c	Specific heat capacity [J/kg]
D	Pipe diameter [m]
e	Wall thickness [mm]
E	Power consumed for grinding [%]
h	Enthalpy [kJ/kg]
k	Form loss coefficient
k_t	Stress concentration factor due thermal stress
k_p	Stress concentration factor due pressure stress
K_i	Identification parameter
l	Length [m]
L	Latent heat of vaporization [J/kg]
m	Mass [kg]
$\dot{m}$	Mass flow [kg/s]
Nu_D	Nusselt number
p	Pressure [bar],[MPa]
Δp	Pressure difference [mbar]
r	Radius [mm]
Re	Reynolds number
S_i	Source term for mass, momentum and energy
t	Time [s]
T	Temperature [°C]
u	Fluid velocity [m/s]
v	Temperature derivative [°C/s]
x	Position [m]
z	Ratio between pipe and vessel diameters

α	Heat transfer coefficient [W/m^2°C]
β	Thermal expansion coefficient [1/°C]
ξ	Friction coefficient
ζ	Coefficient for calculation of stress concentration factor
φ	Mass fraction of moisture in raw coal
λ	Thermal conductivity [W/m°C]
μ	Poisson's ratio
ν	Kinematic viscosity [m^2/s]
ρ	Density [kg/m^3]
σ	Stress [MPa]
τ	Time constant
ω	Rotation speed [r/s]

1. INTRODUCTION

The amount of renewable energy production has increased significantly in the past few years especially in Central and Northern Europe due to growing concern about the climate change and emission restrictions on the energy markets. The production of renewable energy, such as wind and solar power, depends on weather conditions which vary depending on the season and daytime. Therefore the power level of wind and solar plants is ever-changing. In addition the electric power output of these plants is challenging to control. The intermittent power generation leads to load fluctuations in the electric grid. The frequency of the grid is determined by electricity demand and supply, and the grid operator tries to maintain the balance between them. To balance the grid frequency some power plants are forced to compensate the load fluctuations by continuously controlling the power output of the plant.

In Nordic countries hydropower is traditionally used to compensate load fluctuations in the electric grid. However there is not enough capacity of hydropower in Central Europe to compensate varying load produced by wind and solar power plants. Also load varying operation of nuclear power plants is forbidden in most countries. Hence conventional steam power plants, typically pulverized coal-fired units, are increasingly participating in the compensation. This sets new challenges for the controllability and flexibility of these plants, especially if the plant has not been designed for load compensation.

Starkloff et al. noticed that these challenges can be divided into three categories. Firstly faster load transients between operational points as well as faster and more flexible start-up and shutdown processes are needed. Secondly the plant needs to be operated in broader range and the technical minimal load limit has to be re-evaluated. Thirdly the thermo-economical optimization of the plant within the whole operational range need to be done, since the operation in full load is reduced. [1 pp. 496–497]

In addition to new challenges the rate of load transients, start-ups and shutdowns are limited by thermo-mechanical stress in stress-prone plant components. Thermal stress is a consequence of temperature differences in the component material, whereas pressure (i.e. mechanical) stress is a consequence of medium pressure inside a vessel. Prolonged stress creates fatigue and creep-fatigue in the material and eventually cracks are starting to appear due to damage mechanisms. Uncontrollable stress reduces significantly the residual life time of stress-prone plant components.

1.1 Modelling and dynamic simulation

In order to respond to the load transient, flexibility, and thermo-economical optimization challenges, development and re-engineering work is typically required. This work may result e.g. in boiler heat surface constructional changes, burner upgrades, air division changes, instrumentation changes, or control strategy changes.

New solutions, such as process changes or control strategy changes, can be tested with computer-aided simulation tools.

Steady state simulation software are traditionally utilized for process optimization. Steady state models are composed of mass and energy balances for a stationary process which means the governing equations do not depend on time. For the above-mentioned new requirements for coal-fired power plants a steady-state approach is no longer valid and dynamic simulation becomes necessary.

Dynamic simulation is the use of a computer program to model the time varying behavior of a system. Dynamic model is capable of presenting the whole operating range of the process including transients between the operating points. Dynamic simulation is used in designing new processes as well as test and predict the operation of processes already in use. By using a simulator, experiments can be performed, which would never be possible on an actual plant due to e.g. economical or safety issues [2 p. 2].

Well-designed dynamic simulation model of pulverized coal-fired power plant creates conditions for the evolution of the control systems and prediction of the dynamic behavior as part of the whole energy system, where renewable energy production has a major part. The plant model should include a realistic coal mill (i.e. coal pulverizer) submodel. Mill model becomes especially necessary, when fast load changes are simulated, since the realistic fuel feed simulation depends mainly on the dynamic behavior of the mill. It is also necessary to define thermo-mechanical stresses in the simulation environment during the cyclic operation. Thereby the rate of start-ups, shutdowns and load changes can be optimized. These features improve considerably the transient simulation capability of pulverized coal-fired power plants in dynamic simulation software.

Before the simulation model is introduced, model needs to be verified and validated to prove the correctness of the model. Verification and validation are not isolated procedures that follow the modelling, but rather integral parts of the model development [3 p. 310]. Object of verification is to ensure that the model reflects accurately the intension of the modeler [4 p. 309]. Secondly verification confirms, whether the model is correctly implemented with the respect to the modelling concept. Model verification can be done for example by examining the model output under a variety of settings of input parameters. [3 p. 310–312]

Model validation is a method for demonstrating correspondence between the model and the real process. Validation is performed by testing the model against as many empirical data as possible. Successful tests give confidence that the model is valid, whereas failure in any fair test indicates that the model is in some way defective. [4 p. 309] In practice model is validated by simulating the model in different operating conditions and the simulation results are compared with data from the real process.

1.2 Objective of the thesis

Transient simulation of pulverized coal-fired power plants is increasingly important, since e.g. process changes and new control strategies of these plants can be easily tested by simulating the load-varying operation. The main objective of this thesis is to investigate and test new solutions related to an improved simulation model of a pulverized coal-fired power plant, which is capable of simulating transient load changes in a realistic way. These solutions are implemented in dynamic simulation software Apros.

To improve the pulverized coal-fired power plant simulation in Apros, a new coal mill model is implemented and tested. The model is implemented using the user component (UC) feature of Apros. The used model is based on the theory introduced in reference [5]. The coal mill model is validated against operational data from reference power plants.

Nowadays software related to calculation and analysis of thermo-mechanical stresses during the operation are commonly utilized in modern load following power plants. There is also a need for defining the stresses in the simulation environment. Since the stresses restrict the magnitude and rate of the load changes, start-ups and shutdowns, allowable and safe operation can be easily tested with simulation tools. Stress calculation enables a new way to optimize the plant operation in dynamic simulation software, and thereby it improves the transient simulation of pulverized coal-fired power plants.

A stress solver component was added to Apros component library few years ago. In this work the calculation of the stress solver is verified against literary reference and validated against stress calculations based on operational plant data. Furthermore stresses are defined during load change transients from two reference plant models.

For the simulation experiments two reference power plant models were utilized. Reference power plant model A was received from the plant operator and the mill and stress solver were attached to it. Modelling of the reference plant B was included in this work. The modelling procedure and the validation of the plant model are presented in the thesis.

1.3 Structure of the thesis

After the introduction the background of cyclic power plant operation is presented in Chapter two. Chapter three discuss the basic theory of pulverized coal-fired power plants and introduction of dynamic simulation software Apros is given in Chapter four.

The theory and methods used in coal mill and stress solver component implementation are considered in Chapters five and six, respectively. Chapter seven introduces the model and modelling methods of reference power plant B. Simulation experiments are introduced and the results are analyzed in Chapter eight. Conclusions of the study are given in Chapter nine.

2. CYCLIC OPERATION

Due to market liberalization and rapid expansion of intermittent renewable energy production large pulverized coal-fired power plants, which have primarily designed for base load operation, are now increasingly operated at varying load levels for electric grid load adjustment [6 p. 550]. Also new units are designed and constructed for this purpose. Operation of electricity-generating power plants at varying load levels is called cycling. Cycled power plants adjust their power output as the supply and demand for electricity fluctuates during the day. Cycling involves start-ups, shutdowns, load following and minimum load operation in response to changes in load of the electric grid [7 p. iv].

Fluctuating power generation of solar and wind power plants in Germany in 2014 is illustrated in Figure 1. Respectively, daily production of conventional power plants is presented in Figure 2. The power produced by wind and solar power plants is not steady, which can been seen from the figures, and thus the load following power plants are needed to even up the load in the electric grid,

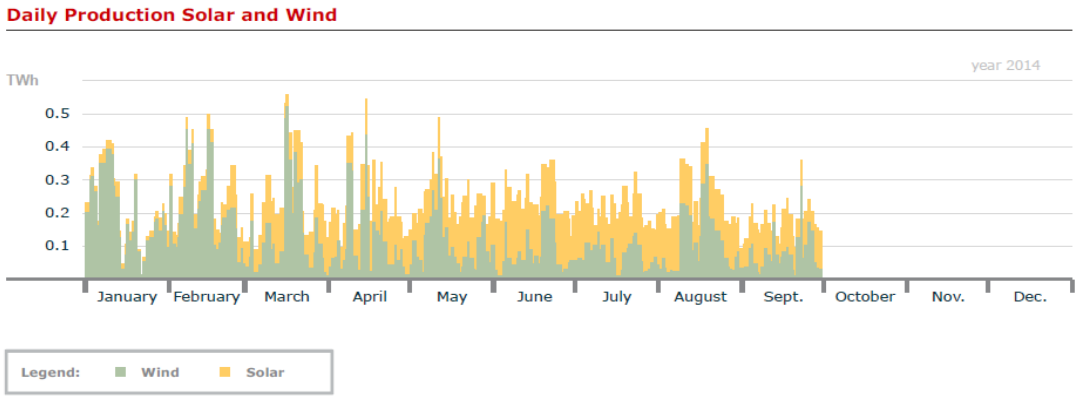

Figure 1. *Daily electricity production of solar and wind power plants in Germany in 2014. [8]*

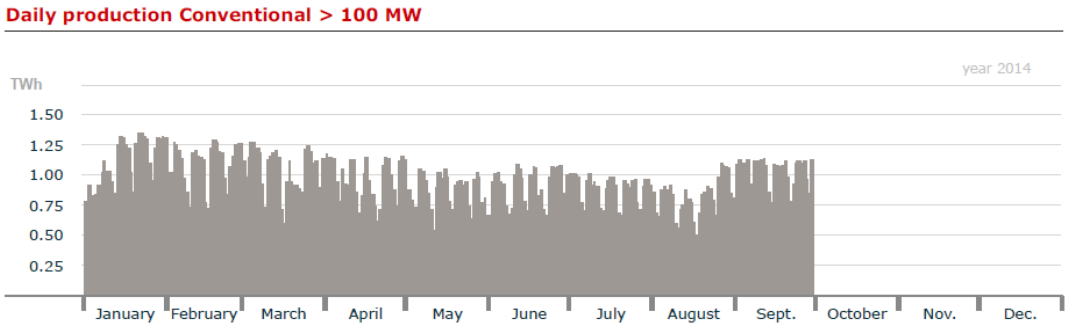

Figure 2. *Daily electricity production of conventional power plants in Germany in 2014. [8]*

Cyclic operation inflicts several concerns in the power plant. Base load plants were primarily designed to resist creep damages throughout a service life of more than 40 years. However fast temperature and pressure changes during cyclic operation cause significant thermo-mechanical stresses in the boiler and turbine structures. Stresses lead to fatigue-related damages which these units were not designed to withstand. [6 p. 550] Furthermore this type of off-design operation increases operational costs due to increased wear and tear of the plant components.

In order to use old base load power plants in cyclic operation mode, process changes and new control systems must be implemented. The plant operation should be flexible and the controllability of the plant must be fast and accurate. Also the pollution control becomes more complicated when flue gas temperatures and pressures vary with sudden changes in the load.

2.1 Utilization rate of power plants

The consumer demand of electricity varies significantly from day to night, on weekly patterns as well as seasonally. In Nordic countries the highest loads are produced on cold winter mornings. The renewable energy production depends on multiple factors, such as weather conditions, time of the day and season. The load cannot be controlled as effectively as in conventional steam power plants. The electricity production load should approximately equate the electricity demand all the time, and therefore different types of power plants are needed to cover the demand. The type of the power plant can be categorized by the utilization rate.

Expensive facilities, such as nuclear and large coal-fired power plants are often used as base load plants, which means they run continuously at maximum output. Base load plants are shutdown only for annual service and in fault situations. Usual characteristics of a base load unit are poor controllability, high investment costs and low operating

costs [9 p. 103]. Due the above-mentioned changes in the energy markets base load units are also increasingly operated cyclically in off-design mode.

Intermediate and peak-load units are traditionally operated cyclically to cover the variations in the consumer demand. Intermediate facilities can be operated for extended periods at a time, but generally they do not operate all the time as base load units. The power output of intermediate units is controlled daily to cover the hourly electric demand, and therefore good controllability is a basic condition. Investment and operating costs are at average level compared to other plant types. [9 p. 103–104]

Peak-load power plants are operated only for short periods of time during the year when the power demand is in its peak. Gas turbines and oil-fired condensing units are usually used for this purpose. These plants can be brought online quickly to meet the rapidly increasing demand for power, and can then be taken offline quickly as power demand diminishes. Investment costs of a peak-load unit are low, whereas operating cost are high [9 p. 104].

2.2 Grid load control

Frequency describes the balance between generation and demand in the electric grid. The nominal grid frequency in Europe is 50 Hz and in the Nordic interconnected grid it is allowed to vary between 49,9 and 50,1 Hz. If the grid frequency drops below 50 Hz, the consumer demand is bigger than production. Correspondingly, supply is larger than demand, if the frequency is over 50 Hz. Since the demand varies as a function of time, power reserves are needed to maintain the balance. [10 p. 30]

Control of the electric load in the grid is divided into primary-, secondary- and tertiary control. The minimum requirements for each control method are generally specified in local grid codes, which are determined by the transmission system operators (TSOs).

Primary control is the automatic, stabilizing action of load-following power plants active power controls and it acts in the time frame of seconds [11 p. 5]. In conventional power plants such fast load changes can be achieved by using the heat storage of the boiler. Stored heat can be utilized by opening the throttled turbine control valve or closing the main condensate control valve, and thereby more generator power can be produced momentarily.

For example in Germany a plant that is participating in the primary control, is obligated to change its power output 2 % of nominal power in 30 seconds [12 p. 24]. Primary control is a proportional control method which corrects the deviation between the generation and demand but the steady-state error remains [13 p. 32].

Secondary control takes effect after about 30 seconds and acts in the time frame of minutes. In Germany the secondary control action must be implemented in 5 minutes

and the power change is done by modifying the fuel feed of the plant [14]. Secondary control removes the steady state error between generation and demand after the primary frequency control action and restores primary control reserves [13 p. 32]. The load change transients examined in this thesis are used for secondary control.

German TSO has determined that tertiary control reserve must be activated within 15 minutes. The control action could last several hours in case of several incidents [14]. Figure 3 shows the approximate time frame of grid frequency control.

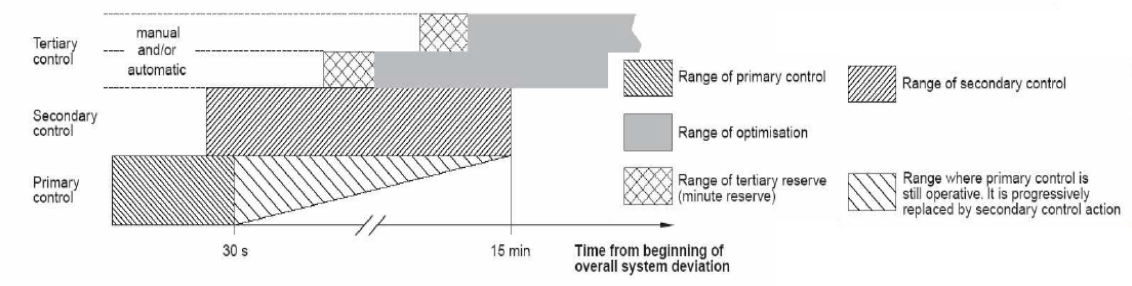

Figure 3. *Time frame of grid load control. [13 p. 33]*

In Nordic countries hydroelectric-power is traditionally used for grid load control. In Central Europe not enough hydropower is available, and therefore fossil condensing and combined heat and power (CHP) plants are utilized. Especially pulverized coal-fired power plants, that are designed for base load operation, are increasingly used in secondary level load control.

2.3 Damage mechanisms

All power plant operating regimes result in reduction of plant service life through a combination of multiple damage mechanisms which accumulate over time. Base load units are mostly operated in steady state conditions in which the load, and hence temperatures, pressures and fluid flows remain substantially constant over long periods of time. Furthermore the thermo-mechanical stresses remain also constant. Base load operation gives mainly rise to creep-related damages, which are defined as a material deformation due to constant stress under high temperature. The component materials are originally designed to withstand damages caused by creep. [6 p. 551]

When plants that are designed to operate in creep conditions are subjected to cyclic operation, the impact of fatigue-related mechanisms increases. When the plant is shut down, re-started or its load is changed rapidly, components filled with water or steam, are subjected to considerable temperature transients at high pressure, and furthermore to thermo-mechanical stresses. Stresses initiate fatigue and creep-fatigue which creep-resistant materials are less able to withstand, and this increases significantly the life consumption of boiler and turbine components. [6 p. 551.] Fatigue is defined as the tendency of a material to fracture when the material is subjected to cyclic loading.

Thermo-mechanical stresses in plant components are calculated based on component material properties as well as temperature and pressure measurements. The lifetime of the component can be estimated on the grounds of the stress definition. The lifetime calculation is determined in standard EN-12952-3 [15]. The lifetime calculation is not included in the scope of this thesis. Only the thermo-mechanical stress calculation is discussed.

3. PULVERIZED COAL-FIRED POWER PLANT

Theoretical background of pulverized coal-fired power plant is presented in this chapter. In Figure 4 a simplified illustration of an entire pulverized coal-fired power plant is presented.

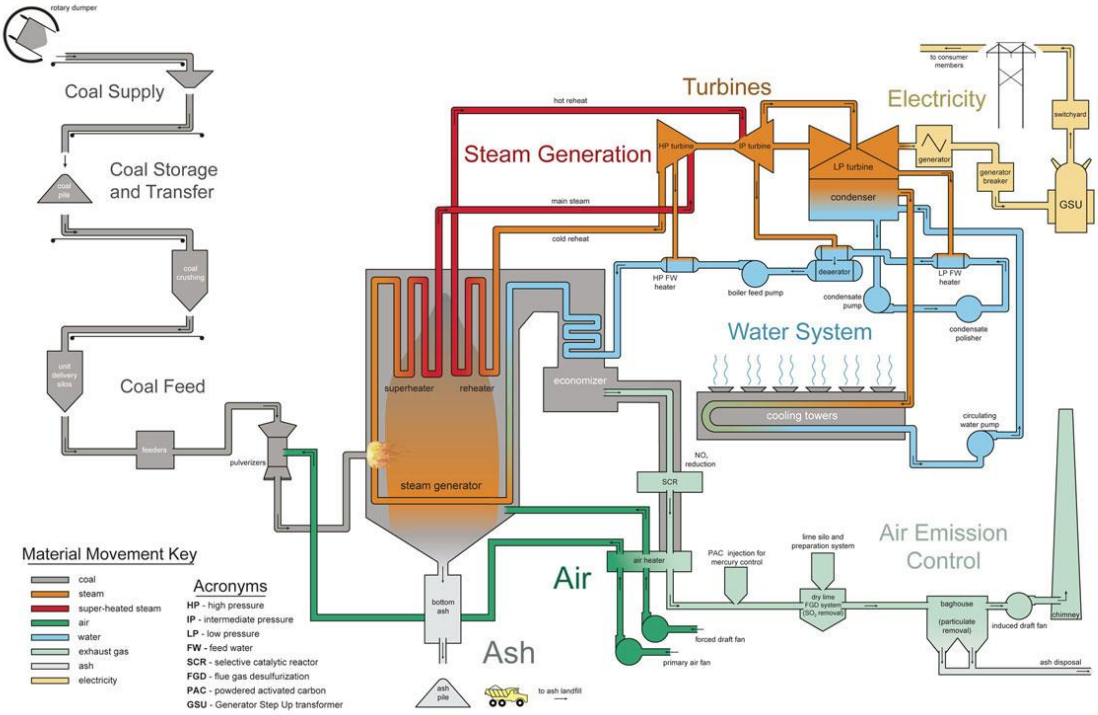

Figure 4. *Schematic diagram of a pulverized coal-fired power plant. [16]*

Coal has historically played a significant role in energy production and approximately 48% of the world power generation was supplied by coal-fired power plants in 2013 [17 p. 154]. In Germany almost half of the electricity was generated with brown or hard coal in 2014 as can been seen from Figure 5. In the next few decades coal will continue to be used to satisfy the world's energy demand despite of increased production of renewable energy. Benefits of coal are its stable supply and low price. Major disadvantages in the combustion of coal are high carbon dioxide (CO_2) emissions as well as high levels of air pollutants, such as particulate emissions, sulfur- (SO_X) and nitrogen oxides (NO_X). [18 p. 8349]

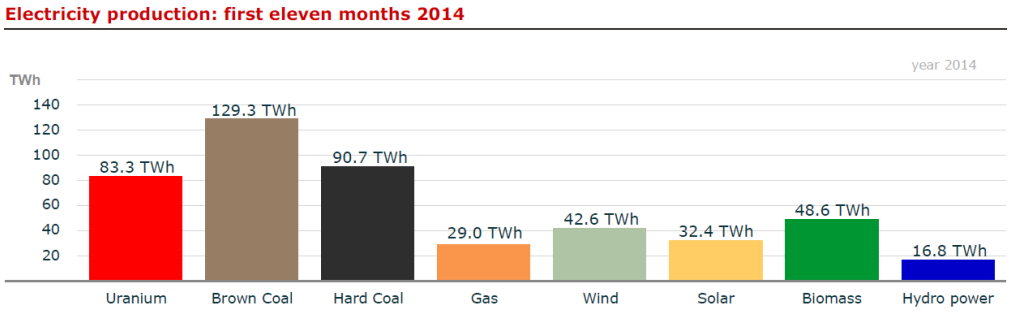

Figure 5. *Electricity production in Germany in 2014.[8]*

Pulverized coal-fired power plants account approximately 97% of the world's coal-fired capacity. The conventional types of coal-fired power plant technology have an efficiency of around 35%, which means that 35% of the energy in one unit of coal is transferred into electricity. Pulverized coal-fired units can have a size of up to 1000 MW and they are commercially available worldwide. [19]

New technologies are needed to increase the efficiency and decrease emissions. Ultra-supercritical (USC) boilers, which operate at high pressures and temperatures, can have efficiency as high as 45 %.

3.1 Operation of the plant

Raw coal is usually dispatched to the plant as crushed diameter of 10–50 mm pieces and it is stored outdoors in open or roofed coalfield near the plant constructions. From the coalfield raw coal is conveyed to the boiler unit coal bunkers with belt conveyors. [20 p. 455] Bunker operates as a buffer storage and a metering device for the coal mills. From the bunker coal is batched to the coal mills with a feeder device.

Raw coal and preheated primary air are fed to coal mills, where the coal is dried and pulverized. Mixture of pulverized coal and primary air is transported from the mills to burners in the furnace. Besides primary air also secondary- and tertiary air are fed to the furnace to ensure the complete burning of the coal. Main functions of the burner are controlled ignition of the coal powder and mixing of coal powder and combustion air [20 p. 457]. Ignited coal-air mixture produces heat which is transferred into water via the boiler heat exchanger surfaces (i.e. economizers, evaporator tubes, superheaters and reheaters).

In the boiler economizer is generally placed between the last reheater and air preheater. Its function is to heat the water to the saturation temperature corresponding to the boiler pressure, before water goes to the evaporator tubes. This raises the average temperature of heat supply in the boiler which raises the boiler efficiency.

Evaporator tubes, where the saturated liquid is converted to saturated steam, are placed on the walls of the boiler, and they serve also as wall structure of the boiler. Depending on the boiler type, water is either partially or completely vaporized in the evaporator zone. Evaporator tubes are placed in the lower part of the boiler where the radiant heat transfer is predominant form of heat transfer between burning coal and heat surfaces.

Superheating is used to raise the temperature of steam above the saturation temperature in constant pressure. Superheating raises the average temperature of heat supply in the boiler, and thereby increases boiler efficiency. Superheating has also an additional beneficial effect: it results in drier steam in low-pressure (LP) turbine. A turbine operating with less moist steam is more efficient and less prone to blade damages. [21 p. 37] Superheaters are divided into radiant and convection superheaters. Radiant superheaters are usually placed at the top of the furnace. Therefore radiation from the combustion flames to superheater tubes is the main heat transfer form. Convection superheaters are typically located in so called second pass in the flue gas duct of the boiler, and the heat is mainly transferred by convection between the flue gases and superheater tubes.

In modern high-pressure (HP) boilers, after the high-pressure turbine, partially expanded steam is reheated in constant pressure to increase the temperature and energy content of the steam. This also increases the mean temperature of heat supply in the boiler and the efficiency of the plant. By reheating the steam, expansion of the steam can be carried out to lower pressures, without raising the steam moisture content too much. Expansion to lower pressures improves the process efficiency. In high-pressure boilers there can be several turbine and reheating sections. Since the superheater and reheater tubes are subjected to high temperatures and pressures, their materials must be carefully selected [21 p. 96].

Air preheater is located in the final stage of the flue gas duct. It recovers heat from the flue gases before cleaning and exhausting them to atmosphere. Preheating the air improves plant efficiency by saving fuel that would otherwise be used for heating the air [21 p. 103]. Preheater brings down the flue gas temperature to 120–150 °C. Dew point of sulfuric acid sets a limit for the lowest temperature of the flue gas. Preheated air is a requirement for the operation of pulverized coal-fired boilers, in which heated air is used to dry moist coal. Arrangement of the heat surfaces in a once-trough boiler is illustrated in Figure 7.

Besides economizer feedwater is also preheated in low- and high-pressure feedwater preheaters. Extraction steam from the turbine is used to accomplish the preheating and the pressure level of the steam depends on the extraction point of the turbine. Closed-type heat exchangers, where the feedwater does not mix with the extraction steam, are usually utilized in preheating. Feedwater passes through the heat exchanger tubes while the extraction steam transfers its energy to the water and condensates on the shell side.

The condensate is fed from higher-pressure to the next lower-pressure preheater and from the lowest-pressure preheater condensate is led to the condenser. [21 p. 51–53]

The primary function of the condenser is to condensate the exhaust steam from the low-pressure turbine and thus recover the feedwater for reuse in the cycle. The pressure of the condenser is determined by the temperature of the cooling substance, which can either be water or air depending on the geographic location of the plant. This pressure equals to the saturation pressure of the condensing steam. Lowering of condenser pressure increases the work of the turbine, improves the plant efficiency and reduces the steam mass flow for a given plant output. [21 p. 219] A disadvantage of lowering the final pressure of steam expansion is that it increases the size of low-pressure turbine, because low pressure increases the specific volume of the steam. Furthermore size of the low-pressure turbine is proportional to investment costs of the plant.

From the boiler hot, pressurized steam is passed to the turbine, where the expansive steam rotates the turbine blades. Turbine and generator are connected to the same shaft and turbine transmits its rotation energy to the generator. Rotating generator produces electricity. The low-pressure steam leaving the turbine is passed to the condenser, and the condensed water is transported by the condensate pumps to the feedwater tank. From there water is pumped back to the boiler for conversion into steam again and the process continues.

3.2 Once-through boiler

Boilers used in power plants can be divided into two types: once-through boilers and drum-type boilers. Large pulverized coal-fired boilers in high-efficiency power plants are usually once-through boilers, as both boilers in the reference plants in this thesis [22 p. 20]. Once-through boiler technology is further introduced in this section.

A once-through boiler can be thought as a long, externally heated tube [22 p. 17]. Water goes through the economizer, evaporator section and superheating sections changing sequentially to saturated water, saturated steam and superheated steam in one continuous pass. Once-through boilers are further divided into Benson and Sulzer type boilers, which are named after their inventors. The principle of these types is shown in Figure 6. No drum is required to separate liquid water from steam and no water recirculation takes place in Benson boiler, and so the point where all the water has been evaporated may vary as a function of load and operation strategy. After the evaporator steam is passed straight to the superheating section. [21 p. 99] Sulzer boiler includes a water separator vessel, where water and impurities are separated from the steam. Separator ensures, that water is not passed to superheaters during part-load operation, start-up or shutdown. It also provides a fixed point where the superheating starts as drum in drum-type boilers.

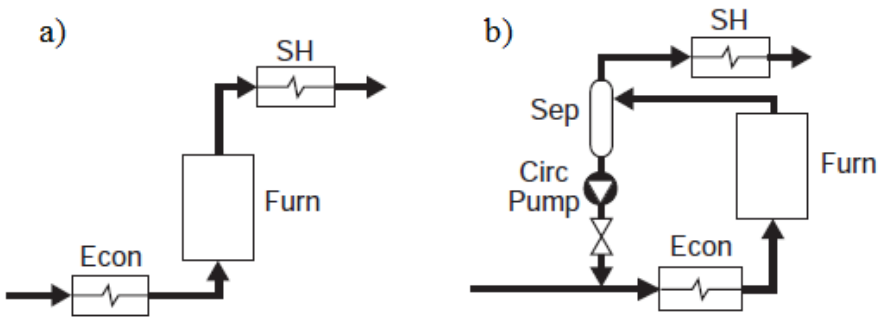

Figure 6. *Principle of a) Benson boiler and b) Sulzer boiler. [23 p. 158]*

In once-through boiler heated water coming from the economizer is partially vaporized in the evaporator tubes, where the concentration of steam rises to 80-85 %. Liquid-steam mixture flows into post-evaporator, where the remaining moisture is vaporized and steam is slightly superheated. Actual superheating occurs in the radiant and convection superheaters. [24 p. 47]

Once-through boilers can operate either at subcritical or supercritical steam pressures but typically they are used pressure above 200 bars. [25 p. 101] Once-through boiler is the only boiler type suited to supercritical-pressure operation (above 221 bar), because the latent heat of vaporization at supercritical pressures is zero, and therefore liquid and vapor are one and the same, so no separation in a drum is necessary. [21 p. 99]

Once-trough boiler does not contain a thick-walled drum, which makes its dynamic behavior faster than in drum-type boiler. Therefore faster load changes can be made, since drum is not a restrictive factor, although e.g. headers and water separators are prone to thermo-mechanical stress. In once-trough boiler requirements for the feedwater purity are high, since all the feedwater chemicals pass through the turbine. In addition in once-through boiler the water inventory is much smaller than in drum-type boiler, and hence the control of the boiler is rather complicated. Schematic diagram of a typical pulverized-coal fired once-trough boiler is presented in Figure 7.

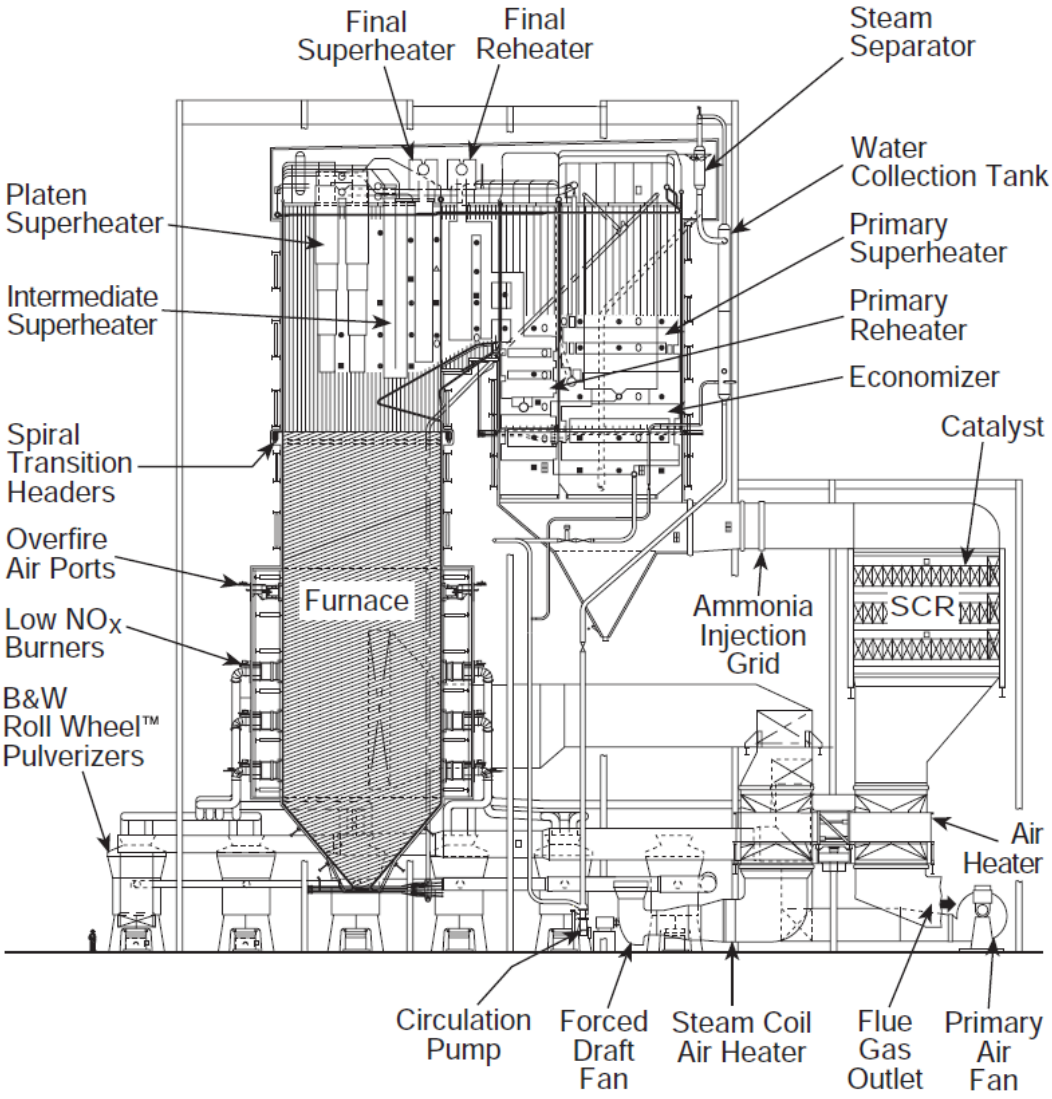

Figure 7. *Typical pulverized coal-fired once-through boiler. [23 p. 423]*

3.3 Ultra-supercritical boiler technology

The thermodynamic efficiency of the Rankine steam cycle increases if temperature and pressure of the superheated live steam entering the turbine are raised. When steam pressure and superheat temperature are increased above 221 bar and 540 °C the steam becomes supercritical (SC). In supercritical conditions heated water does not produce a two phase mixture of liquid and steam as in subcritical steam, but instead it changes directly from liquid to steam. The boiler is classified as ultra-supercritical (USC) when the main and reheat steam temperatures exceed 580 °C. In subcritical once-through boilers superheat pressure is around 180 bar and temperature is around 540 °C. The operating ranges of subcritical, supercritical and ultra-supercritical boilers are illustrated in Table 1. [26]

Table 1. *Approximate pressure, temperature and efficiency ranges for subcritical, supercritical and ultra-supercritical boiler technologies. [26]*

	Live steam pressure [bar]	**Live steam temperature [°C]**	**Efficiency [%]**
Subcritical	< 221	< 565	33–39
Supercritical (SC)	221–250	540–580	38-42
Ultra-supercritical (USC)	> 250	> 580	> 42

Efficiency of a USC boiler can be as high as 45 % when efficiency of subcritical boilers is around 35 %. A potential 50 % efficiency is foreseen for USC technology with the availability of proper boiler materials [27 p. 129].

USC technology is a cost effective option to reduce emissions of generated electricity. As the efficiency of the plant is increased, less fuel is burned per unit of electricity generated. Since coal-fired power plants are under pressure due to ever-tightening emission restrictions, USC technology provides one solution to this problem.

Increasing steam pressures and temperatures pose new challenges for the materials used in the boiler. Conventional boiler materials are not able to last long, and the damage of exposure would happen quickly in USC conditions. Nickel alloys are usually used in USC boilers and steam turbines. Research is focusing on the development of new steels for boiler tubes and on high alloy steels that are resistant to corrosion.

3.4 Control of the power plant

Dukelow [28 p. 2] listed the main objectives of the boiler control system in steam power plant as follows:

- To cause the boiler to produce a continuous supply of steam at desired condition
- To operate the boiler at lowest cost for fuel and other boiler inputs, consistent with high levels of safety and full boiler design life
- To safely start-up, shutdown, monitor online operation, detect unsafe conditions and take appropriate actions for safe operation.

By utilizing the control system of the power plant it is possible to make fast and accurate load changes with small energy losses. Boiler controls ensure that steam is produced in desired pressure and temperature safely and economically. Besides the boiler the other important component in the power plant is the steam turbine. Steam turbine

has a significant role when it comes to controlling the pressure of the steam. Boiler and components relating to boiler have a major influence on the other controls of the plant. [25 p. 157]

Nowadays steam power plants must increasingly participate in load control of the electric grid. This underlines the importance of the control system which is used to execute the load changes. [25 p. 157]

3.4.1 Block control

The coordination of the turbine and boiler operation is realized by the block control (unit control), which generates set points for the boiler and turbine to keep the desired load set point while maintaining the desired operating pressures and temperatures [29 p. 1]. Block control includes the functionality required to control the boiler and turbine as an integrated unit consistent with generation requirements but constrained by the unit capability. Block control typically consists of the following functionalities: unit load demand target and rate of changes; runback logic that ensures overall unit loading is constrained by the availability of major equipment; boiler master that provides demand for fuel, air and feedwater; turbine master that provides demand for turbine controls. The principle of block control is presented in Figure 8.

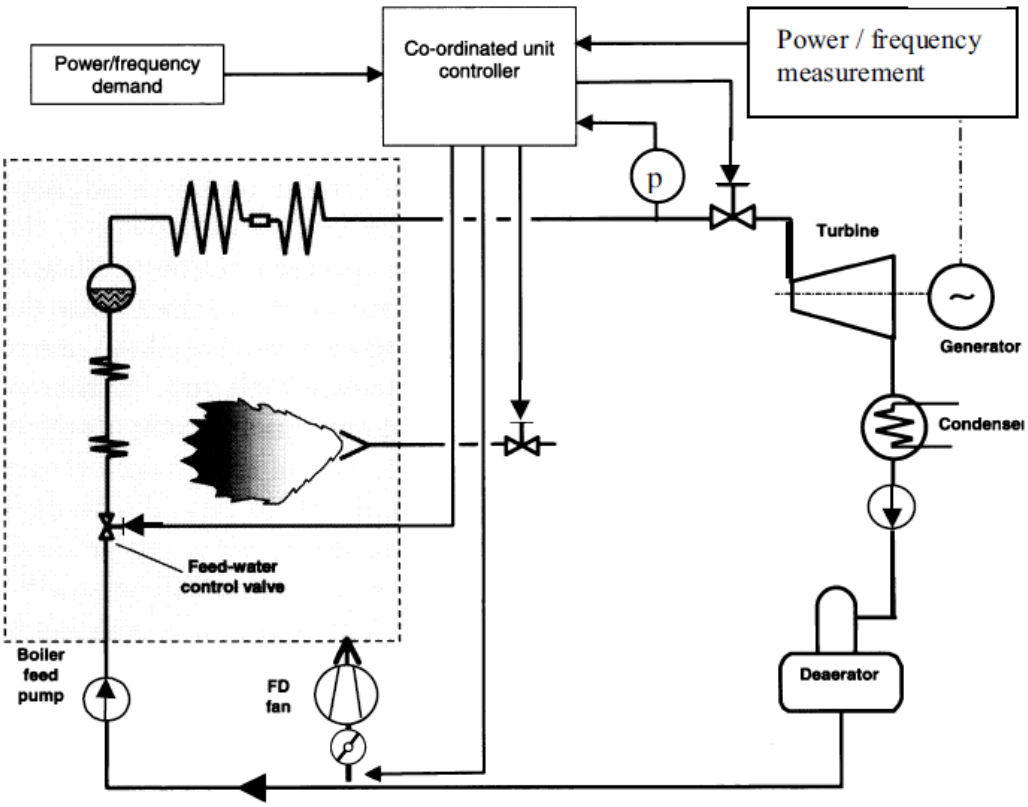

Figure 8. *Principle of block control.[13 p. 23]*

Electric power control is the main control of the power plant that produces electricity as its main product. Especially in power plants used in grid load compensation accurate power control is essential. The plant power output set point is adjusted through block control. Depending on the pressure control method, turbine power is controlled either by means of fuel feed or turbine control valve. The heat inventory of the boiler can be utilized to get momentarily more steam from the boiler by opening the turbine control valve. This action provides a fast but limited response to power output set point changes, and therefore it can be used in primary grid load control.

3.4.2 Steam pressure control

Power plant can be operated either in fixed pressure or sliding pressure control mode. In large once-through boilers, especially in SC or USC boilers, the normal operation mode is sliding pressure mode. However, due to numerous different operating situations including start-ups, shutdowns and various exceptional conditions, e.g. equipment malfunctions, there are also other operation modes, such as fixed pressure mode, available.

In natural sliding pressure mode, turbine control valve is constantly in fully open position, and the power output of the unit is controlled with fuel feed to the furnace. In modified or throttled sliding pressure mode, the turbine control valve is slightly throttled, so that fast limited load changes can be executed by adjusting the valve position [24 p. 16]. In sliding pressure mode, both in the natural and modified modes, steam pressure varies as function of load and a certain variant pressure correspond the power produced by the turbine. As the turbine power, boiler thermal power and feedwater flow increase also the steam pressure rises. Therefore the steam pressure is not directly controlled but it slides as a function of the power. The turbine power is controlled by adjusting the fuel flow into the boiler.

3.4.3 Fuel feed control

Coal flow into the furnace is determined by the block control as a function of power output set point. Usually a simple linear or quadratic function between the load and coal flow is designed.

The coal composition, heat value and moisture content depend on the type of the coal and plants utilize different types of coals. Therefore the coal flow set point is adjusted with heat value correction. Heat value correction is based on the enthalpy difference between water at the inlet of the boiler and steam at the outlet of the boiler. Designed enthalpy difference is compared with measured enthalpy difference and the coal heat value is corrected according to the enthalpy deviation. Thereby the changing coal content can be considered in the fuel feed control.

3.4.4 Air control

Air-fuel ratio is kept at desired level by controlling the amount of combustion air in the furnace. The combustion will be incomplete, if there is not enough air in the furnace. On the other hand excess air in the furnace produces flue gas losses, and nitrogen oxide emissions will increase. [25 p. 163]

The main control criteria in combustion air control are the fuel flow to the boiler and the concentration of oxygen in the flue gas. In practice air flow is controlled according to boiler load set point and in parallel with the fuel flow control. Also there can be a feed-forward from the fuel flow to the air flow control, so disturbances can be predicted before they can be seen in the boiler load. [25 p. 163]

Because the mass flow of the solid fuel cannot be measured accurately, oxygen (O_2) correction is used to correct the amount of combustion air in the furnace. Oxygen analysis of the flue gas is forwarded as a feedback to the air flow controller. O_2-correction is used as a fine adjustment in the combustion air control. [25 p. 163]

In pulverized coal-fired boiler air is fed to the furnace usually in three different phases. Primary air is controlled according to fuel feed and it is blown trough the coal mills transporting pulverized coal to the furnace. The primary air is composed of hot and cold air flows, which are mixed to provide the right temperature after the coal mill. Primary air is not enough for complete combustion in the furnace, and therefore secondary air is needed. Secondary air is fed as a function of load and oxygen concentration in the flue gas. Tertiary air is fed to ensure the combustion of combustible gases in the upper part of the furnace and to reduce NO_X-emissions. Phasing of the air feed is a powerful way to reduce NO_X-emissions.

3.4.5 Feedwater control

In once-through boiler the control of the water-steam balance is based on measurements of feedwater flow, steam mass flow and temperatures. [24 p. 15] The feedwater flow set point is a function of the power set point and it is typically adjusted with enthalpy correction. Enthalpy correction is based on the desired enthalpy of the steam after the evaporator. Steam enthalpy after the evaporator is calculated as a function of temperature and pressure, which are measured from the process. Calculated enthalpy is compared with the design enthalpy which is also a function of the power set point. The deviation of these two leads to a correction in the feedwater flow.

Feedwater flow and pressure can be controlled either with control valve or with feed water pump. Also combination between these two can be used. Nowadays control with feedwater pump is implemented with a frequency converter which provides a fast and

accurate control. Control with a control valve is a cheaper option, but disadvantage is the pressure loss that it produces. [24 p. 15]

3.4.6 Steam temperature control

To maximize the efficiency of the power plant, temperature of superheated steam is designed as high as possible. Function of steam temperature control is to keep steam temperature in its set point value to prevent exceeding of maximum material temperatures and too fast temperature transients. Also turbine has its own restrictions considering steam temperature and transient rate of the temperature. [24 p. 15]

Temperature of superheated steam is usually controlled by spraying feed water among steam in one or several phases. [24 p. 15] Also steam at a lower temperature can be used. Steam temperature set points after each superheater are determined as a function of the power set point and the temperature signal before the superheater is usually used as a derivative feedforward.

3.4.7 Furnace pressure control

Furnace pressure is usually set to be lower than ambient pressure outside the boiler to avoid leakages from the furnace. Good combustion conditions can be provided by stabilizing furnace pressure. [24 p. 25] Furnace pressure is controlled by a induced draft fan, which is located in the end of the flue gas duct.

Fluctuations in furnace pressure change the pressure difference across the combustion air dampers which complicate the combustion air control. Also large furnace pressure fluctuations can damage the boiler. [24 p. 25]

3.5 Reference plants

Simulation models and operational measurement data of two pulverized coal-fired power plants were utilized for the validation of the proposed coal mill model and Apros stress calculation. Simulation model of reference power plant A was received from the plant whereas modelling of the reference plant B was part of this thesis. Both units are operated cyclically for compensating load fluctuations in the electric grid.

3.5.1 Reference plant A

The owner and location of reference plant A are confidential. Pulverized coal-fired power plant A was commissioned in the 1970s. The gross power output of the plant is approximately 820 MW and the net power output is 750 MW. The once-through boiler of the plant operates at subcritical range with live steam temperature of approximately 530 °C and live steam pressure of 190 bar.

Originally the plant was designed for base load operation, but due to major changes in the energy production in recent years, plant is now used for grid load compensation. The plant simulation model was originally developed for testing a new control system.

3.5.2 Reference plant B

Reference plant B is pulverized coal-fired power plant Lünen which is located in western Germany and it is owned by German energy company Trianel Kohlekraftwerk Lünen GmbH & CO.KG. The facility was introduced in 2013 and it represents state of the art technology. The once-through boiler is ultra-supercritical with live steam temperature of 600 °C and live steam pressure of 287 bar. The gross power capacity of the plant is 813 MW and the net power is 750 MW. [30 p. 2] Also the plant is able to produce 90 MW district heat for the Lünen region.

The plant efficiency is 46 %, which is the world's highest class in coal-fired power plants [30 p. 2]. The plant can be categorized as intermediate unit, since it is designed for both base load and cyclic operation. Due to increased renewable energy production in Germany the plant is mostly used for load compensation. The plant is presented in Figure 9. Dynamic modelling of the plant was included in this thesis.

Figure 9. *Pulverized coal-fired power plant Lünen. [30 p. 4]*

4. APROS - DYNAMIC SIMULATION SOFTWARE

Apros is a multifunctional software for full-scale modelling and dynamic simulation of industrial processes and different types of power plants. Apros is the result of a quarter century's development work by VTT (Technical research centre of Finland) in co-operation with Fortum. It is used by a multiple power plant operators, engineering companies, research institutes, safety authorities and universities all over the world. Development started in 1986 for internal use and first commercial version, Apros 1.0, was released in 1991. Latest version, Apros 6.05, was published in September 2015 and it is used in this thesis.

Apros combines accurate first-principles, physical process modelling with automation modelling. With Apros it is easy to design, test and see how the process and the control system work together, and the whole integrated system can be studied and optimized simultaneously in detail. The main uses of simulation models and dynamic simulation are:

- Design engineering
- Developing and testing new control strategies
- Testing process changes
- Safety analysis
- Training operators.

The major Apros products are Apros Combustion and Apros Nuclear. Apros Combustion is for conventional thermal power plants simulation including coal-fired power plants, combined-cycle power plants etc. In the past few years several commercial coal-fired units have been modelled and analyzed with Apros Combustion [31][32][33]. Apros Nuclear has been widely used for designing and safety analysis of nuclear power plants [34][35][36]. In this thesis Apros Combustion was utilized.

4.1 General description of the software

In Apros process modelling is based on thermal hydraulics, which is described using time-dependent conservation equations for mass, momentum and energy as well as correlations for friction and heat transfer [37]. Conservation equations for one-dimensional homogenous two-phase flow are

(mass) $$\frac{\partial A\rho}{\partial t} + \frac{\partial A\rho u}{\partial x} = S_1 \quad (1)$$

(momentum) $$\frac{\partial A\rho u}{\partial t} + \frac{\partial A\rho u^2}{\partial x} + \frac{\partial Ap}{\partial x} = S_2 \quad (2)$$

(energy) $$\frac{\partial A\rho h}{\partial t} + \frac{\partial A\rho uh}{\partial x} = S_3, \quad (3)$$

where A is the cross-sectional area of the component, ρ is the density of the fluid, u is velocity of the fluid, h is enthalpy of the fluid, t is time, x is position and S_1–S_3 are source terms for mass, momentum and energy.

In the modelling user interface the model is regarded as a network of thermal hydraulic nodes (i.e. control volumes) and branches (i.e. connections between nodes). So-called calculation level network is created and managed automatically by the process component level, where the user operates. The calculation level structure depends on the user given nodalization parameters (i.e. parameters of nodes and branches). The equation solver provides tools for solving large systems of linear equations arising from the discretization and linearization of partial differential equations with respect to space and time.

The user has access to a set of predefined process component models, that are conceptually analogous with concrete devices, and hide all solution algorithms. The component libraries of Apros cover a comprehensive set of process components, such as pipes, valves, pumps, heat exchangers, reactors, tanks, measurements, PID controllers, electric generators etc.

Every process component contains a calculation level, which is constructed with calculation level objects (i.e. nodes and branches). Components are composed together to form a subprocess, which can be used as a part of an integrated process model. The user drags and drops appropriate process components from model library palettes, draws connections and enters process related input data. Parameterization is straightforward in the graphical user interface. [38]

The complete model information can be saved into a model snapshot file containing the model configuration and its state data at the time instant. Similarly, at any time, the user can load a snapshot once saved in the past. Model can be exported to a file, which can be merged to another model. This way user can build up model libraries for re-use of models in other projects. [38]

4.2 User component

User component (UC) is a feature that allows user to create re-usable own structures consisting of basic Apros components and other user components. User component can be exported, just like a model, and reused or shared with other users.

The internal functioning, input- and output terminals of the UC are determined in a configuration diagram. After the configuration user can add instances of this configured master-UC to models. UC can also be modified anytime by creating new versions of the existing master-UC.

One feature of the UC is the possibility to lift properties from the internal structure to be presented as properties of the UC. With configuration properties user can modify the internal parameters. State properties cannot be modified, but they provide information about the important state variables inside the UC. [39 pp. 166-170] In this thesis the coal mill model was implemented with a UC.

5. COAL MILL MODEL

Coal mill model is an essential part of a cyclically operated pulverized coal-fired power plant model, and a valid mill model improves the accuracy of the plant's transient simulation. Load changes, start-ups and shutdowns can be simulated realistically if the dynamics of the coal mill model corresponds to the dynamic behavior of a real mill.

Maffezzoni have noted that coal mills are the primary cause for slow load following capability and plant shutdowns [40]. The problem of the transient performance of coal mills has been recognized for some time. [41 p. 64]. This is because usually there are not enough measurements from the mill, and also the raw coal flow measurements are typically based on the feeder belt speed which makes them inaccurate. The lack of measurements complicates the plant power control as well as the mill modelling and validation of the model. Therefore an unambiguous method for transient coal mill modeling has not yet been presented.

5.1 Model description

Coal mill is a mechanical device for grinding raw coal. Pulverized coal is then used for combustion in steam generating furnaces of fossil fuel power plants. There are several types of coal mills. The most common types are roll mill, hammer mill, drum mill, blower mill and ball ring mill [24 p. 27]. In this thesis model of a generic roll mill is considered.

The operation of a coal mill is as follows. Raw coal is transported on a conveyor or with a feeder and dropped into the mill where it lands on a grinding table and is pulverized by rollers. Primary air is used as carrier gas for pulverized coal and to dry moist raw coal. The temperature of air is controlled by mixing hot and cold air with each other. Also flue gas or a mixture of flue gas and air can be used as a carrier gas. Air is blown from the bottom of the mill and it picks up fine coal particles transporting them into the classifier section. Only the finest coal particles escape the mill, whereas heavier particles fall back to the grinding table. With rotary classifier it is possible to control the speed of rotation and therefore, if it is needed, increase quickly the amount of pulverized coal escaping the mill. If the classier speed is decreased, larger coal particles can pass through the classifier. [5 p. 2]

Mass fraction of moisture in raw coal before the mill is usually 6–14 % and pulverized coal moisture after the mill is around 0,5–2,0 %. Vaporized moisture from the coal stays in the primary air which is fed to the furnace. [20 p. 456]

The coal mill model used in this thesis was first introduced in reference [5]. The model is rather simple compared to models introduced e.g. in references [42] and [43]. In reference [42] the interior of the mill is divided into four zones and coal particles are distributed into 10 different size groups, whereas model introduced in reference [43] includes submodels for different operation regimes. These types of complex models are challenging to implement and tune the model parameters to replicate the real mills dynamic behavior. The coal mill model used in this thesis is a so called graybox-model based on physical knowledge and parameter identification methods. The following assumptions are made in the model:

- Coal in the mill is either raw or pulverized, i.e. two particle size fractions are considered.
- The temperature of the mill is assumed to be the same as the temperature of the coal-air-mixture in the outlet of the mill.
- Heat emitted from the mill to its environment is negligible.
- The mill interior is divided into three different zones. [5 p. 2]

Notation used in the model is described in Table 2.

Table 2. *Notation used in the coal mill model.*

Variable	Name	Unit
m_c	Raw coal mass on the grinding table	kg
m_{pf}	Mass of pulverized coal on the grinding table	kg
m_{cair}	Mass of pulverized coal carried by air	kg
$\dot{m}_{cin}$	Raw coal mass flow to the mill	kg/s
$\dot{m}_{cin,dry}$	Dry coal mass flow to the mill	kg/s
$\dot{m}_w$	Mass flow of moisture	kg/s
$\dot{m}_{pf}$	Mass flow of pulverized coal in the air	kg/s
$\dot{m}_{cout}$	Mass flow of pulverized coal out of the mill	kg/s
$\dot{m}_{ret}$	Mass flow of coal returning to the grinding table	kg/s
$\dot{m}_{air}$	Primary air mass flow	kg/s
Δp_{pa}	Primary air differential pressure	mbar
Δp_{mill}	Pressure drop across the mill	mbar
T_{in}	Primary air inlet temperature	°C
T_{out}	Outlet temperature of air-coal mixture	°C
E	Power consumed for grinding	%
E_e	Power consumed for running an empty mill	%
ω	Classifier rotation speed	r/s
K_i	Identification parameter	-
τ_9	Time constant	-
c_i	Specific heat capacity	J/kg
L_v	Latent heat of vaporization of water	J/kg
φ_m	Mass fraction of moisture in raw coal	-

Figure 10 presents schematic diagram and operational principle of a generic roll mill.

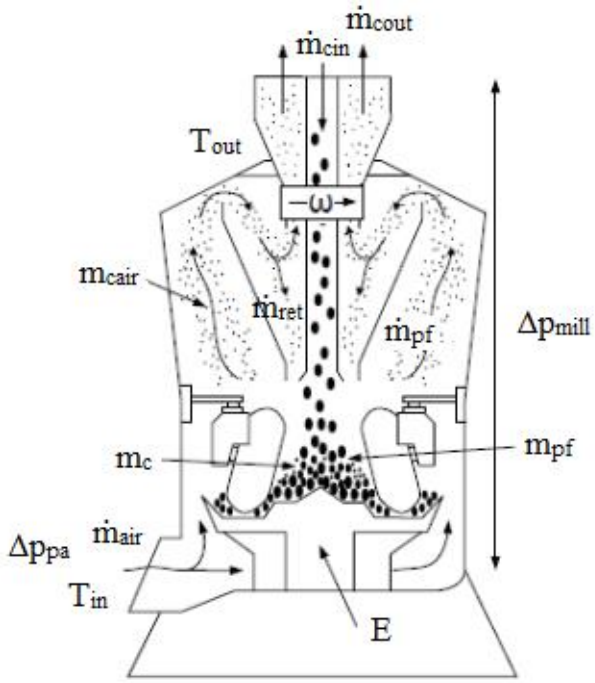

Figure 10. *Schematic picture of a roll mill. [5 p. 2]*

The following nine equations constitute the coal mill model. The rate of change of raw coal mass on the grinding table is proportional to the mass flow of dry raw coal, the flow of returning particles from the classifier section and the grinding rate of raw coal:

$$\frac{d}{dt}m_c(t) = \dot{m}_{cin,dry}(t) + \dot{m}_{ret}(t) - K_1 m_c(t). \quad (4)$$

The mass of pulverized coal on the grinding table depends on the grinding rate and the mass flow of pulverized coal in the air:

$$\frac{d}{dt}m_{pf}(t) = K_1 m_c(t) - \dot{m}_{pf}(t). \quad (5)$$

The mass of grinded coal particles in the pneumatic transport inside the mill depends on the mass flow of pulverized coal picked up from the grinding table, the coal mass flow out of the mill and the mass flow of coal returning to the grinding table:

$$\frac{d}{dt}m_{cair}(t) = \dot{m}_{pf}(t) - \dot{m}_{cout}(t) - \dot{m}_{ret}(t). \quad (6)$$

The mass of pulverized coal particles picked up from the grinding table by the primary air inside the mill is proportional to the primary air flow and the mass of pulverized coal on the grinding table:

$$\dot{m}_{pf}(t) = K_5 \dot{m}_{air}(t) m_{pf}(t). \quad (7)$$

The mass flow of pulverized coal out of the mill depends on the mass of coal lifted from the grinding table and classifier rotation speed:

$$\dot{m}_{cout}(t) = K_4 m_{cair}(t) \left(1 - \frac{\omega(t)}{K_6}\right). \quad (8)$$

The classifier speed is limited between $0 \leq \omega(t) < K_6$.

Mass flow of coal returning to the grinding table from the classifier section is

$$\dot{m}_{ret}(t) = K_9 m_{cair}(t), \quad (9)$$

where K_9 is an inverse of travel time constant τ_9, $K_9 = \frac{1}{\tau_9}$.

Equation for pressure drop across the mill is

$$\Delta p_{mill}(t) = K_7 \, \Delta p_{pa}(t) + K_8 m_{cair}(t), \quad (10)$$

where primary air differential pressure Δp_{pa} is measured inside the mill.

The power consumed for grinding is

$$E(t) = K_2 m_{pf}(t) + K_3 m_c(t) + E_e, \quad (11)$$

and it takes into account the grinding of raw and ground coal.

The output temperature of the mill can be solved from the energy balance of the mill

$$\frac{d}{dt} T_{out}(t) = \frac{1}{K_{11}} [c_a \dot{m}_a(t) T_{in}(t) + c_w \dot{m}_w(t) T_a + c_c \dot{m}_{cin,dry}(t) T_a - c_a \dot{m}_a(t) T_{out}(t) - c_c \dot{m}_{cout}(t) T_{out}(t) - c_w \dot{m}_w(t) T_{out} - \dot{m}_w(t) L_v + K_{10} E(t)], \quad (12)$$

where c_a, c_w and c_c are specific heat capacities of air, water and coal, respectively. Identification parameter K_{11} can be considered as mass of the mill structure which produces thermal inertia when temperature is changing inside the mill. [5 p. 3] In reference [5] energy balance does not include the heat of moisture that is exiting the mill i.e. $c_w \dot{m}_w(t) T_{out}$. It is considered in Equation (12).

Dry coal mass flow into the mill is

$$\dot{m}_{cin,dry} = (1 - \varphi_m) \dot{m}_{cin}, \quad (13)$$

and mass flow of water coming into the mill with raw coal is

$$\dot{m}_w = \varphi_m \dot{m}_{c,in}. \quad (14)$$

Identification parameters K_1–K_{11} have been estimated with an optimization procedure. The goal of the procedure is to minimize the error between measured and estimated process values. Depending on the coal mill there might be a need to change the parameters so that the model simulates the real coal mills behavior as well as possible. Identification parameters have been estimated for four different coal mills in reference [5]. There are slight deviations between the parameter sets. Reference [5] contains more specific information about tuning the parameters and the optimization procedure.

The coal mill model in reference [5] is made for nominal operation of the mill. Also the reference model assumes that all the moisture, that raw coal contains, is vaporized in all conditions . This assumption is not truly valid, since certain amount of moisture stays in the coal after the pulverization. Apros flow model takes this into consideration.

5.2 Implementation

The proposed coal mill model was implemented in Apros by using the user component feature, which allows the user to create re-usable own structures consisting of basic Apros components and other user components.

The purpose of the coal mill UC is to provide a generic model for coal pulverization, which can be tuned to match multiple types of mills used in pulverized coal-fired power plants. Capability of simulating transient operation is a required feature for the model. The realistic simulation of a pulverized coal-fired power plant requires a realistic coal model, which can be used in different types operation modes. Theoretical background of the mill model was introduced in the previous section and the implementation is illustrated in this section. The UC symbol and property view are shown in Figure 11. From the property view user can tune the mill model by changing the values of configuration parameters and follow the values of state variables.

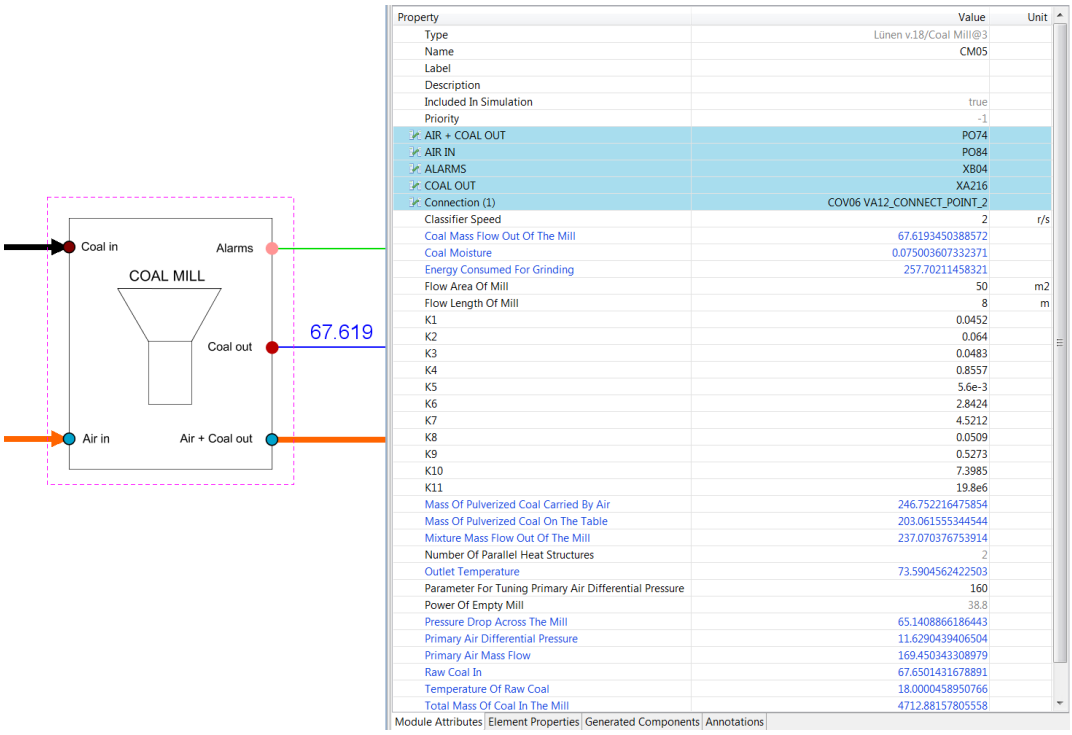

Figure 11. *Coal mill user component symbol and property view.*

There are two input and three output terminals in the coal mill UC. The first input is the raw coal flow into the mill. The raw coal line is modelled with flow model zero (TH0 – Thermal hydraulics accuracy level 0). TH0 is a convenient way to model solid material flows in Apros. TH0 includes an option to use plug flow mode, which is used for defining the delays in the flow line. The plug flow velocity is assumed to be constant across any cross-section of the pipe perpendicular to the axis of the pipe. Mass flow, temperature and composition of the raw coal are measured from the raw coal line and they are used to calculate internal states and outputs of the mill. The composition of the coal is user definable.

The second input is the primary air flow into the mill. Primary air is used to dry moist raw coal and carry pulverized coal to the furnace. The primary air mass flow into the mill is approximately two times bigger than the raw coal mass flow. A suitable air-coal ratio ensures the mixing of coal and air and complete combustion in the furnace. Air flow line is modelled with homogenous (level two) flow model.

Internal states and outputs of the mill are defined according to Equations (4)–(14) and coal flows inside the mill are illustrated in Figure 12. The predominant parameters for tuning the model are K_1, K_4, K_5, K_6, K_9 and ω. K_1 describes the grinding rate of raw coal, K_5 defines the amount of coal picked up from the grinding table by the primary air and K_9 is used for determining the mass of coal dropping from the classifier zone back to the grinding table. K_4, K_6 and classifier speed ω are used for determining the pulverized coal flow out of the mill.

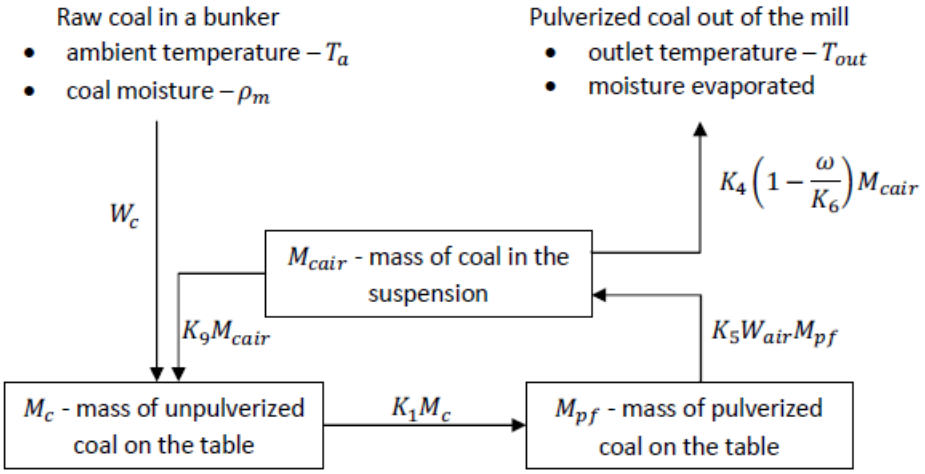

Figure 12. *Flow diagram of the coal mill. [5 p. 2]*

The output temperature of the air-coal mixture is defined according to Equation (12). Coal mill is a thick-walled metallic device, which contains a significant heat storage. Thus thermal inertia of the structure should be observed, when the temperature distribution inside the mill is defined. Parameter K_{11} is considered as mass of the mill, which affects the thermal dynamics of the mill. Inside the UC a heat structure module is utilized to simulate the heat transfer in the mill structure. User can adjust the mass of iron in the structure by modifying a configuration parameter. The outer surface of the mill is assumed to be ideally insulated so no heat is transferred from outer surface to surroundings.

The pressure difference across the mill is determined in accordance with Equation (10). The pressure drop is divided into two factors: primary air differential pressure and pressure drop caused by the stored coal inside the mill. User can adjust the magnitude of primary air differential pressure by modifying a form loss coefficient in the primary air line trough configuration parameters. The effect of coal is taken into account by adjusting another form loss coefficient inside the mill as a function of stored coal. Pressure differences are defined in Apros by equation

$$\Delta p = (k + \xi \cdot \frac{l}{D}) \cdot \frac{\rho v^2}{2}, \tag{15}$$

where k is form loss coefficient (i.e. flow resistance coefficient), ξ is friction coefficient, l is length of the pipe, D is diameter of the pipe, ρ is density of the fluid and v is velocity of the fluid.

The air-coal mixture flow out of the mill is the third output in Figure 11 and it is modelled with homogeneous flow model. Air, coal and coal moisture are handled separately inside the component and they are mixed at the output of the mill taking into account the right mass- and energy balances. The mass flow of pulverized coal out of the mill is

calculated according to Equation (8) and it is mixed with primary air and coal moisture. In the model the amount of vaporized moisture is defined as a function of temperature and pressure.

The pulverized coal flow can be also read from the second output in Figure 11. This is an analog signal, which can be used in coal flow control as an estimate. Usually pulverized coal flow is not measurable in a real plant.

The first input in Figure 11 is for alarms. Temperature, air-coal ratio, pulverized coal mass on the grinding table and primary air mass flow are followed inside the mill to secure safe and reliable operation. Binary signal from this output indicates, whether the critical variables are inside allowed limits or not. If one of them exceeds the operating range, alarm is triggered to warn the user.

6. STRESS CALCULATION

Thermo-mechanical stresses (i.e. thermal and pressure stresses) restrict the rate of start-ups, shutdowns and load changes in the power plant. These rates can be optimized based on stress calculation. Also the lifetime consumption of the boiler components can be defined using the stress calculation. Hence it is important to include the stress calculation in the simulation environment. Inclusion of this feature in the simulation software also gives variety and improves the transient simulation of pulverized coal-fired power plants. The theoretical background of thermo-mechanical stress calculation used in Apros is introduced in this chapter.

6.1 Thermal stress

Thermal stress forms a major constrain for the plant's power control during cyclic operation. Thermal stress is formed as a consequence of temperature differences especially in boiler component walls. Limitations must be taken into account particularly in start-ups, shutdowns and load changes since they are the most critical phases during plant operation due to temperature gradients that they cause in thick-walled boiler elements. Economically thinking start-ups, shutdowns and load changes are intended to be done as quickly as possible. In these situations thermal stresses in boiler materials have to be known to avoid fatigue, creep and cracking of the boiler element materials. Thermal stresses are often a major factor in determining boiler elements material life cycle.

Temperature deviations can be measured from the wall material, and on that basis, stress concentrated on the material can be calculated [44 p. 2]. EN-12952-3 standard enables to determine the residual life of the boiler elements as well as the allowable heating and cooling rates for boiler pressure components [15].

Especially thick-walled boiler elements, such as headers and drums, are prone to thermal stress, when temperature of the medium changes rapidly. In once-through boilers uneven distribution of medium in parallel evaporator and superheater tubes causes temperature differences in the tubes which inflict thermal stress.

The temperature difference between the medium and the wall is a function of heat transfer coefficient which controls the effectiveness of heat transfer. Increase of the medium flow rate improves heat transfer between medium and wall surface. Hence medium temperature changes are reflected faster to element wall surface. For this reason biggest thermal stresses occur in places with biggest fluid velocity differences, e.g. connections between headers and pipes. The shape of the element can increase the material stress,

e.g. stress can be significantly larger in sharp corners of a header compared to straight wall due to differences in heat transfer. [45 p. 7]

Also insulation of the outer surface of the wall might have a significant impact on the stress values. If the insulation is assumed to be ideal, the outer surface of the element wall eventually settles to the same value as the inner surface temperature, when the medium temperature is changed. If the outer surface does not have ideal insulation, temperatures of inner and outer surface deviate from each other also in steady state situation, which inflicts thermal stress. In reality insulation in boiler components is never ideal. [45 p. 7]

6.1.1 Quasi-stationary temperature field

Thermal stress calculation in Apros is based on a quasi-stationary temperature field, which is now defined. Let us consider a cylindrical thick-walled boiler component which contains pressurized medium, e.g. water. When the temperature of water inside the component changes at constant rate, it can be assumed that the temperature derivate in the inner surface of the component is constant. It is also assumed that the outer surface is well insulated. When the temperature of medium changes, temperature derivate in the outer surface of the component is smaller than in the inner surface. After a while the outer surface temperature derivate settles on the same value as the inner surface temperature derivate. The situation, when the surface temperature derivatives are equal and the temperature difference between surfaces is constant, is called quasi-stationary state. If the water temperature inside the element decreases, quasi-stationary temperature field is also generated, but the temperature difference is opposite in sign. [44 pp. 6–10]

Figure 13 illustrates a formation of a quasi-stationary temperature field in a thick-walled boiler component. When the wall inner surface is heated, its temperature starts to rise at a certain rate. After a short delay, the outer wall surface temperature also starts to rise. After 20 minutes the outer surface temperature derivate reaches the same value as the inner surface temperature derivate and the temperature difference between the surfaces is constant. Thus a quasi-stationary temperature field is formed. The outer surface of the wall is assumed to be ideally insulated, and therefore the outer surface temperature eventually reaches the same temperature as in the inner surface.

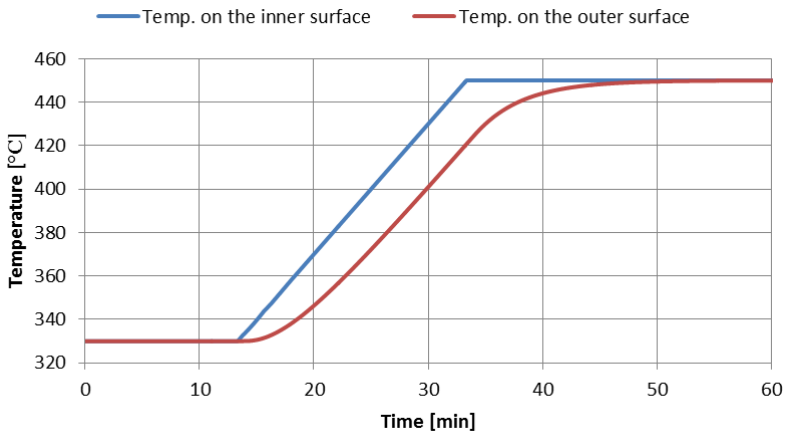

Figure 13. *Temperature change in a thick wall.*

The basic assumption, on which the boiler regulations allowing to calculate the permissible temperature change rates of boiler components are based, is the quasi-stationary state of the temperature field in simple-shaped component, such as cylindrical wall. [46 p. 4084] The biggest thermal stresses occur during quasi-stationary phase because the temperature difference between wall surfaces is at the maximum value. When the transient is over, outer surface temperature reaches the inner surface temperature, if ideal insulation on the outer surface is assumed. [44 pp. 6–10]

Equation for temperature distribution in quasi-stationary temperature field inside the boiler component wall is derived in reference [44 pp. 12–14]. Distribution is

$$T(r) = T_s + \frac{v}{4 \cdot a}(r^2 - r_s^2) - \frac{v \cdot r_u^2}{2 \cdot a} ln\left(\frac{r}{r_s}\right), \tag{16}$$

where r is radius of the cylindrical component, $T(r)$ is temperature as a function of radius inside the wall, T_s is the temperature of the inner surface of the component, v is the temperature derivative during quasi-stationary phase, a is thermal diffusivity of the material, r_s is the radius of the inner surface and r_u is the radius of the outer surface. [44 p. 14]

6.1.2 Stress formation

If the temperature of medium inside the cylindrical component increases during quasi-stationary phase, temperature in the components wall decreases when moving from the inner surface towards the outer surface according to Equation (16). Metal, as is well known, expands when temperature increases. When temperature in the walls inner surface is higher than in the outer surface, metal expands more forcefully in the inner surface. This generates a compression stress on the inner surface. Correspondingly tensile stress is generated on the outer surface. If the medium temperature inside the component

decreases, tensile stress is generated on the inner surface and compression stress on the outer surface. [44 p. 21]

Definition of thermal stress on the surface of the wall can be done by calculating the temperature difference between the surface temperature and the mean temperature of the wall. The mean temperature is

$$T_m = \frac{2}{r_u^2 - r_s^2} \cdot \int_{r_s}^{r_u} r \cdot T(r) \cdot dr. \quad (17)$$

The overall stress is three dimensional and it is divided into three components: tangential, radial and axial stress. Figure 14 illustrates directions of these components in a cylindrical element.

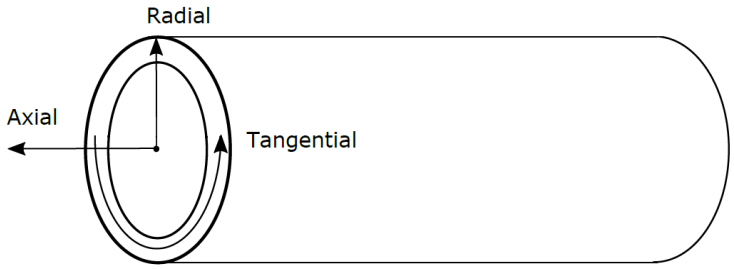

Figure 14. *Stress components.*

Figure 15 visualizes the difference between compression and tensile stress in radial direction. Compression stress tends to shrink the structure, whereas tensile stress tends to expand the structure. The same principal stands for tangential and axial stress.

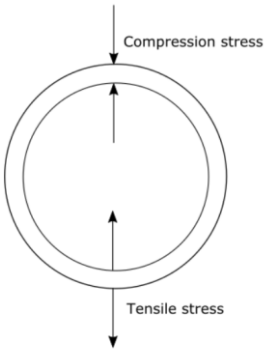

Figure 15. *Compression and tensile stress in radial direction.*

Thermal stresses in the shell of the cylindrical component can be calculated with the following equations:

$$\sigma_{tt} = \frac{\beta \cdot E}{1-\mu} \cdot \left[\frac{r^2 + r_s^2}{r^2 \cdot (r_u^2 - r_s^2)} \cdot \int_{r_s}^{r_u} r \cdot T \cdot dr + \frac{1}{r^2} \cdot \int_{r_s}^{r} r \cdot T \cdot dr - T \right] \quad (18)$$

$$\sigma_{tr} = \frac{\beta \cdot E}{1-\mu} \cdot \left[\frac{r^2 - r_s^2}{r^2 \cdot (r_u^2 - r_s^2)} \cdot \int_{r_s}^{r_u} r \cdot T \cdot dr - \frac{1}{r^2} \cdot \int_{r_s}^{r} r \cdot T \cdot dr \right] \quad (19)$$

$$\sigma_{tz} = \frac{\beta \cdot E}{1-\mu} \cdot \left[\frac{2}{r_u^2 - r_s^2} \cdot \int_{r_s}^{r_u} r \cdot T \cdot dr - T \right], \quad (20)$$

where σ_{tt} is tangential, σ_{tr} radial and σ_{tz} axial thermal stress, E is modulus of elasticity, β coefficient of thermal expansion and μ Poisson's ratio. [44 p. 25]

Biggest thermal stress values are located on the inner surface of the component. [44 p. 25–26] In the inner surface $r = r_s$ and the preceding equations simplify to

$$\sigma_{tts} = \frac{\beta \cdot E}{1-\mu} \cdot (T_m - T_s) \quad (21)$$

$$\sigma_{trs} = 0 \quad (22)$$

$$\sigma_{tzs} = \frac{\beta \cdot E}{1-\mu} \cdot (T_m - T_s), \quad (23)$$

where σ_{tts} is tangential, σ_{trs} radial and σ_{tzs} axial thermal stress in the inner surface of the component wall.

As a resultant of tangential, radial and axial stress a three dimensional state of stress is formed. To solve the overall material stress comprised of these three components, a combined stress (i.e. comparison stress) is formed. Combined stress can be compared with allowed stress values of the material in question. Combined stress is defined with

$$\sigma_{tv} = \sigma_{max} - \sigma_{min}, \quad (24)$$

where σ_{max} is the maximum value of σ_{tt}, σ_{tr}, σ_{tz} and σ_{min} is the minimum value of these three terms. [44 p. 28]

6.2 Pressure stress

In addition to thermal stress, shell of the cylindrical component is strained by stresses caused by pressure inside the component. Tangential σ_{pt}, radial σ_{pr} and axial pressure stress σ_{pz} can be calculated with following equations:

$$\sigma_{pt} = p \cdot \frac{(r_u^2 + r^2)/r^2}{(r_u^2 - r_s^2)/r_s^2} \quad (25)$$

$$\sigma_{pr} = -p \cdot \frac{(r_u^2 - r^2)/r^2}{(r_u^2 - r_s^2)/r_s^2} \quad (26)$$

$$\sigma_{pz} = p \cdot \frac{r_s^2}{r_u^2 - r_s^2}, \quad (27)$$

where p is pressure inside the boiler vessel. Also the maximum pressure stress values, as thermal stress values, are located on the inner surface of the component wall. [44 p. 31] In the inner surface $r = r_s$ and the preceding equations simplify to

$$\sigma_{pts} = p \cdot \frac{r_u^2 + r^2}{r_u^2 - r_s^2} \tag{28}$$

$$\sigma_{prs} = -p \tag{29}$$

$$\sigma_{pzs} = p \cdot \frac{r_s^2}{r_u^2 - r_s^2}, \tag{30}$$

where σ_{pts} is tangential, σ_{prs} radial and σ_{pzs} axial pressure on the inner surface of the component wall.

Combined pressure stress is defined with

$$\sigma_{pv} = \sigma_{max} - \sigma_{min}, \tag{31}$$

where σ_{max} is the maximum value of σ_{pt}, σ_{pr}, σ_{pz} and σ_{min} is the minimum value of these three terms.

6.3 Combined effect of stresses

When the temperature derivate *v* in the inner surface of the component is positive, compression stress is generated on the inner surface and tensile stress in the outer surface due to temperature distribution in the wall. Hence in the inner surface thermal stress and pressure stress are opposite in sign. This concerns expressly tangential and axial stresses. In the outer surface the stresses have the same sign instead. In some operating conditions the overall stress will be bigger in the outer surface. [44 p. 35]

When the temperature derivate in the inner surface of the element wall is negative, thermal and pressure stresses are equal in sign in the inner surface and opposite in sign in the outer surface. Thus the overall stress is concentrated in the inner surface more forcefully than in the outer surface. Decrease of medium temperature creates a more powerful stress in the inner surface than increase of medium temperature. [44 p. 35]

The boiler components material stress is composed of interaction between thermal and pressure stresses. The overall net stresses can be calculated from Equations (18)–(20) and (25)–(27). The net stresses are

$$\sigma_t = \sigma_{tt} + \sigma_{pt} \tag{32}$$

$$\sigma_r = \sigma_{tr} + \sigma_{pr} \tag{33}$$

$$\sigma_z = \sigma_{tz} + \sigma_{pz}, \tag{34}$$

where σ_t is tangential, σ_r is radial and σ_z is axial net stress. In the inner surface of the component wall overall stresses can be calculated according to Equations (21)–(23) and (28)–(30) as follows

$$\sigma_{ts} = \frac{k_t.\beta E}{1-\mu} \cdot (T_m - T_s) + p \cdot \frac{k_p(r_u^2+r^2)}{r_u^2-r_s^2} \tag{35}$$

$$\sigma_{rs} = -k_p p \tag{36}$$

$$\sigma_{zs} = \frac{k_t \beta E}{1-\mu} \cdot (T_m - T_s) + p \cdot \frac{k_p . r_s^2}{r_u^2-r_s^2}, \tag{37}$$

where σ_{ts} is tangential, σ_{rs} is radial and σ_{zs} is axial overall stress.

Thermal and pressure stress terms can be multiplied with stress concentration coefficients k_t and $k_{p,}$ respectively. Stress concentration factors are used when stresses are calculated at the crotch corner at the inner surface of an intersection between a cylindrical vessel and a tube attached to the vessel opening. Biggest stress values are located on these crotch corners due changing fluid velocity. The addition on the stress amplitude can be taken into consideration by using stress concentration factors. [44 pp. 50-51] [15 pp. 112-117] Stress concentration factor due to thermal stress for cylindrical and spherical shells is

$$k_t = \left\{ \left[2 - \frac{\alpha+2700}{\alpha+1700} z + \frac{\alpha}{\alpha+1700} (\exp(-7z) - 1) \right]^2 + 0{,}81 z^2 \right\}^{1/2}, \tag{38}$$

where $z = \frac{d_{mb}}{d_{ms}}$ and α is heat transfer coefficient between the fluid and the wall. Diameter of the tube d_{mb} and diameter of the vessel d_{ms} are determined according to Figure 16. Heat transfer coefficient α is defined 1000 W/m^{2}K for steam and 3000 W/m^{2}K for water.

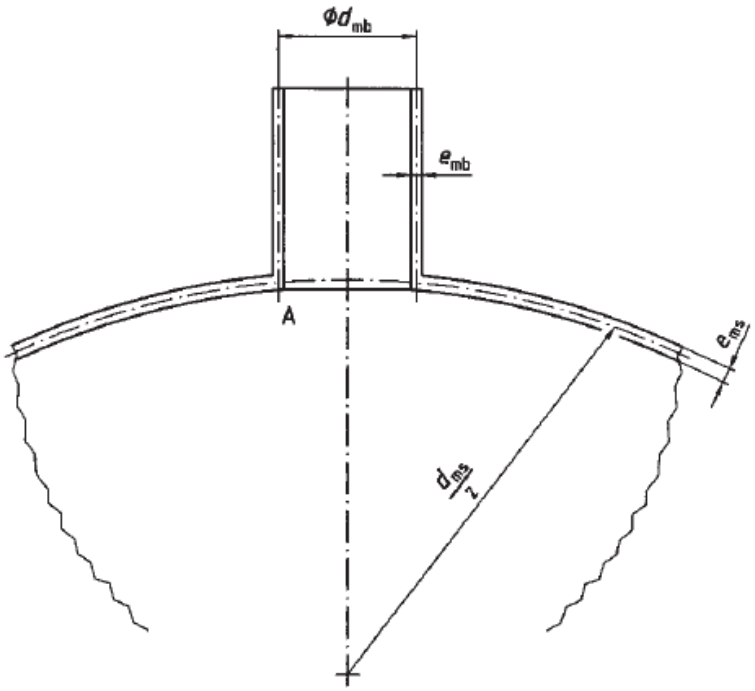

Figure 16. *Dimensions of the vessel and the attached tube. [15 p. 117]*

Stress concentration factor k_p due to pressure stress for cylindrical shells is

$$k_p = 2{,}2 + e^B \cdot \zeta^C, \tag{39}$$

where variables *B*, *C* and ζ are calculated with the following equations

$$B = -1{,}14\left(\frac{e_{mb}}{e_{ms}}\right)^2 - 0{,}89\left(\frac{e_{mb}}{e_{ms}}\right) + 1{,}43 \tag{40}$$

$$C = 0.326\left(\frac{e_{mb}}{e_{ms}}\right)^2 - 0{,}59\left(\frac{e_{mb}}{e_{ms}}\right) + 1{,}08 \tag{41}$$

$$\zeta = \frac{d_{mb}}{d_{ms}}\sqrt{\frac{d_{ms}}{2e_{ms}}}, \tag{42}$$

where e_{mb} is the wall thickness of the tube and e_{ms} is the wall thickness of the vessel.

The combined effect of net stresses is defined with

$$\sigma_v = \sigma_{max} - \sigma_{min}, \tag{43}$$

where σ_{max} is the maximum value of σ_t, σ_r, σ_z and σ_{min} is the minimum value of these three terms. [44 p. 36]

6.4 Thermo-mechanical stresses in once-through boiler

In once-through boilers superheater headers, which are located in the boiler room outside the furnace, are the most prone boiler elements for thermo-mechanical stresses. Especially the interface between the header and inlet/outlet pipes is a location, where significant temperature differences in the wall material can be observed. The fluid velocity increases considerably when the fluid flows from the header to the tube. Fluid velocity difference between the header and the tube results in a difference in the convective heat transfer coefficient between the superheated steam and the header wall. Furthermore the differences in the heat transfer coefficient leads to temperature differences between the header and the tubes. The temperature difference can be over 20 °C in normal steady state operation [47 p. 6]. Convective heat transfer coefficient between the steam and the wall is

$$\alpha = \frac{Nu_D \cdot \lambda}{D} \tag{44}$$

where Nu_D is Nusselt number, λ is thermal conductivity of the fluid and D is diameter of the tube. Nusselt number for internal turbulent flow can be solved from Dittus-Boelter equation

$$Nu_D = 0.023 \cdot Re_D^{0.8} \cdot Pr^{0.4} \tag{45}$$

where Re_D is Reynolds number and Pr is Prandtl number. Equation (45) is valid for fully developed turbulent flow, i.e. Reynolds number is over 10 000. Reynolds number can be calculated from equation

$$Re_D = \frac{u_m \cdot D}{\nu} \tag{46}$$

where u_m is the fluid velocity and ν is the kinematic viscosity of the fluid. Reynolds number is a function of fluid velocity and thereby heat transfer coefficient is dependent on fluid velocity. Equations (44)–(46) are used for modelling the superheater heat transfer surfaces.

Besides the greatest thermo-mechanical stresses occur in the connection area between the header and the tube, also the material is most fragile in the welded joint. A plant-scale superheater outlet header and welded tube stubs are illustrated in Figure 17.

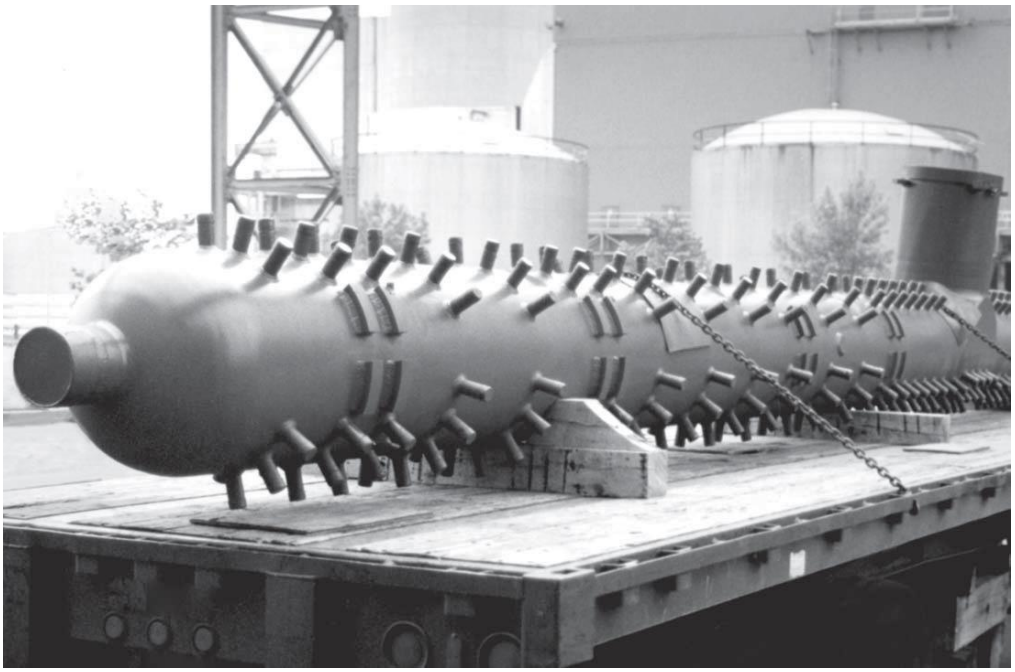

Figure 17. *Superheater header. [23 p. 211]*

The ligament area between header openings, where the biggest stress values occur and the material is most fragile, is shown in Figure 18.

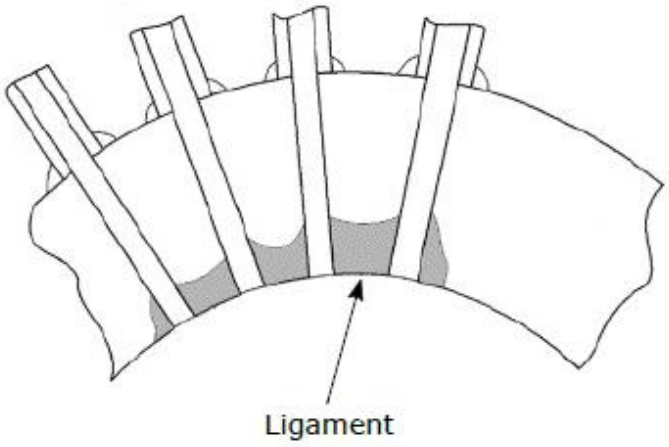

Figure 18. *Ligament area of superheater header and pipes. [48 p. 350]*

Water separator is another once-through boiler component prone to thermal and pressure stress. Water separator is located between the evaporator and the primary superheater in once-through boiler. Its function is to separate liquid water and steam, so only steam can enter the superheating section. During the start-up of the plant liquid water exits the evaporator and the separator prevents water flowing into the superheaters.

As superheater header also water separator is thick-walled and it is connected to smaller inlet- and outlet tubes. However the fluid velocity differences are not as big as in super-

heater header since the welded inlet and outlet tubes in the separator wall openings are usually wider than tubes connected to the superheater header. Typical vertical water separator is shown in Figure 19. The same heat transfer principles presented in Equations (44)–(46) are also valid for water separator.

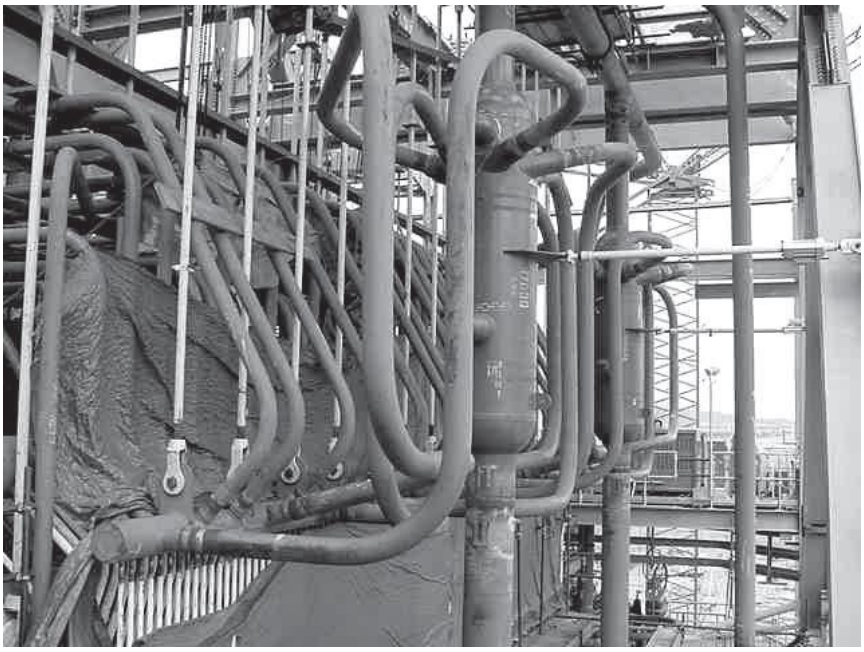

Figure 19. *Vertical water separator. [23 p. 157]*

7. REFERENCE PLANT MODEL

In this chapter the simulation model of reference plant B is concerned. The main features of the model sections and the modelling phases are introduced. Before starting the modeling process, it is necessary know the purpose of the model and the accuracy needed from the model. In this work the main purpose was to simulate cyclic operation of the power plant, validate the new coal mill component beside the power plant model and examine the dynamic behavior of the coal mill during the transients. In addition thermo-mechanical stresses in critical boiler components are defined during the transients. Coal mill model and stress calculation improve the transient simulation of pulverized coal-fired power plants in the simulation environment.

For these purposes the main processes of the power plant must be included in the model. These are air and fuel feed section, boiler including water-steam circuit, furnace and flue gas duct as well as turbine section. These sections include several smaller subprocesses. Also all the main control loops of the power plant are included in the model and a major part of the Apros-model consists of plant's control system. Water and steam temperatures, pressures and mass flows in the boiler should equate with the real process, so that the load change transients can be simulated accurately. Therefore the boiler section needs to modelled carefully.

In this thesis the reference plant B was modelled. The plant model is based on real design specifications, piping and instrumentation diagrams (P&ID's) and control diagrams. The model was supplemented with coal mill and stress solver components

Since a development of a plant simulator was not the aim in this work, the model was adapted to the specific needs for the simulation experiments. In other words the modelled sections and control loops include simplifications compared to the real plant. Simplifications are also discussed in this chapter.

A schematic process diagram of the plant model is presented in Figure 20. The scope of the model can been seen in the figure, i.e. which process sections are included in the model.

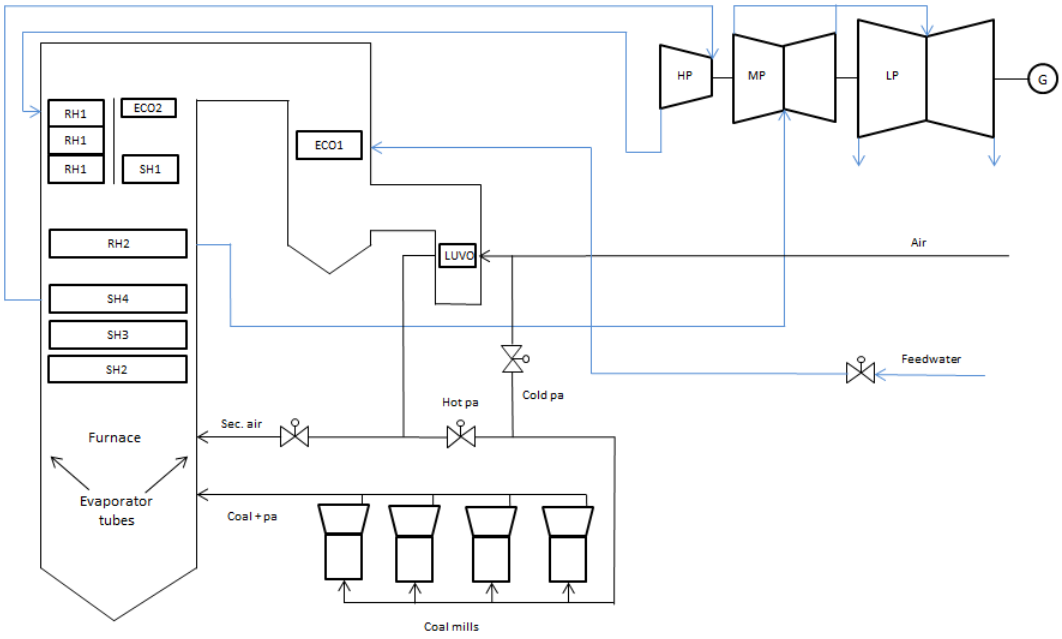

Figure 20. *Schematic diagram of the plant model.*

7.1 Air and fuel feed section

Air and fuel feed sections are linked together since air flow is controlled according to fuel flow and the primary air is fed to the furnace through the coal mills.

In the model air is passed to the furnace in two phases, whereas in the real plant the number of feed lines is much larger. Primary air, which is fed through the coal mill, makes up about 30 % of all combustion air. Primary air is mixture of cold and preheated hot air. Hot air is preheated with flue gases in the air preheater, and cold and hot air are mixed at the inlet of the coal mill to control the coal mill temperature. Inside the mill primary air dries the moist coal, picks up the pulverized coal and transports it to the furnace. The coal mill UC is tuned to simulate the behavior of the four mills of the real plant. After the coal mill the air-coal mixture flow is distributed to burners in the furnace.

Secondary air makes up the major part of the combustion air, around 70 %. Secondary air is preheated and mixed with fuel-rich primary air in the furnace to give a proper air-fuel ratio. The amount of air depends on the air-coal ratio and the desired oxygen content in the flue gas. Primary- as well as secondary air are blown to the burners in two parallel flow lines. Process diagram of the air- and fuel feed section is presented in Figure 21.

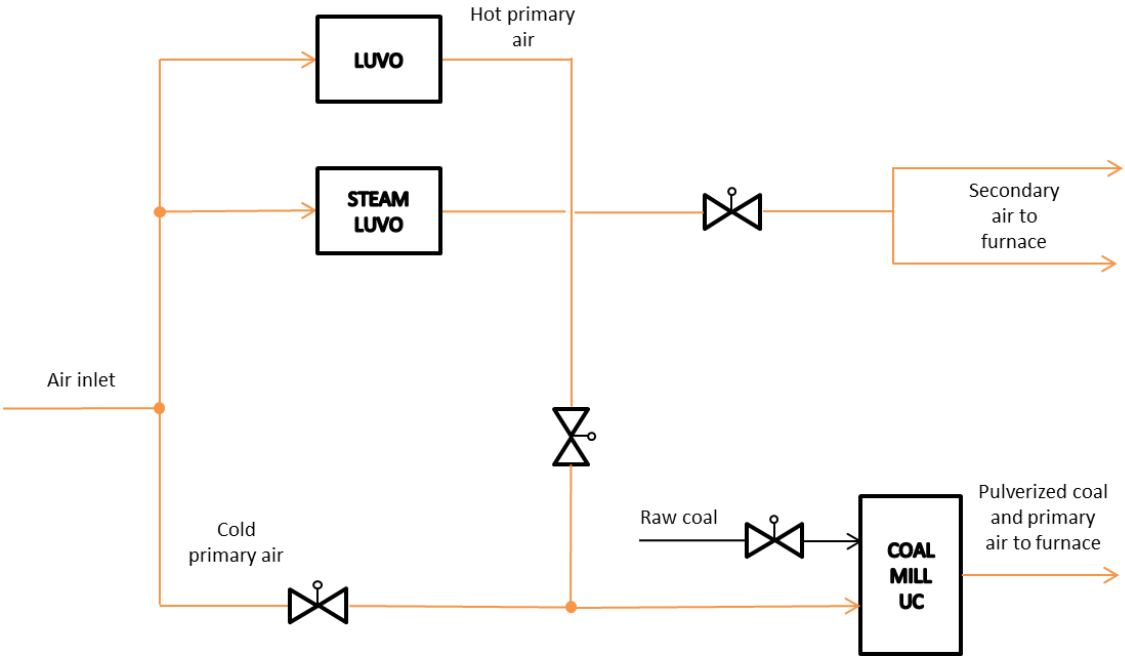

Figure 21. *Air and fuel feed section model diagram.*

7.2 Boiler

The heat transfer between the flue gas and water-steam circuit is modelled by including all the real heat exchange surfaces into the model. These are economizers, evaporator, superheaters and reheaters. Also the water sprayers, which control the temperature of the superheated steam, are modelled. The boiler model was tuned to various steady state load levels and it was compared with plant data. Once the model was able to simulate the steady state load levels, it could be tested with load change transients.

In order to keep up the correspondence between the real plant and the model the heat-exchange surfaces of the boiler must be modelled accurately. Heat transfer areas, pipe volumes and masses are fixed according to plant documentation. The heat transfer coefficients, radiation emissitivies and view factors of the heat exchange surface are adjusted empirically.

Flue gas section consists of the combustion chamber, burners and the flue gas duct. Burners in the combustion chamber are modelled by connecting the primary air-coal lines and secondary air lines at different levels of the furnace. In Apros point-modules include attributes for the mixing and ignition of the fuel-air mixture. When these attributes are selected correctly and the mixture ratio and the temperature are at appropriate level, fuel ignites and produces heat in the furnace.

The dimensions of the furnace and flue gas duct are equal to ones in the real plant. Both the furnace and the flue gas duct are modelled with pipe-modules and the heat transfer between the flue gas and the water-steam circuit is modeled with heat exchanger com-

ponents. A schematic diagram of the boiler model is presented in Figure 22. The color of the flow line indicates the substance inside it: the blue color indicates water or steam and the orange color indicates flue gas.

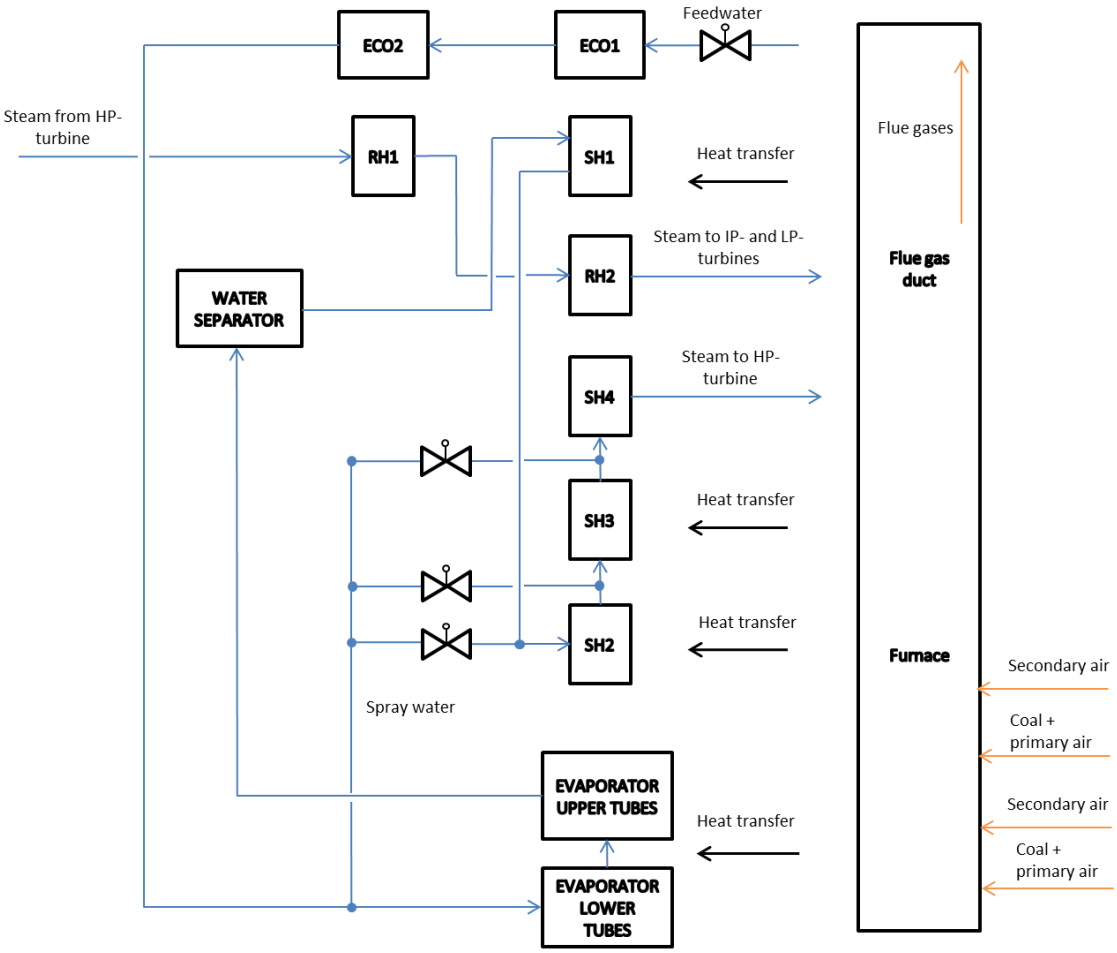

Figure 22. *Boiler model diagram.*

7.3 Turbine section

Turbine section includes high-pressure (HP), intermediate-pressure (IP) and low-pressure (LP) turbines, steam extractions, turbine control valve and turbine shaft. Superheated steam flows from the final superheater to the HP-turbine through the turbine control valve, which is kept fully open. After the HP-turbine steam is reheated in the steam generator and brought to IP- and LP-turbines

The mechanical power produced by the turbines is transformed to electric power via shaft component. The model scope does not include the condenser, where the steam is passed after the LP-turbine, but the pressure after LP-turbine is fixed according to the conditions in the condenser.

The turbine plant model is presented in Figure 23. Turbine sections are composed of turbine components, which are connected to a turbine shaft. After each turbine section, part of the steam is extracted to be taken to the water preheaters and district heat exchangers.

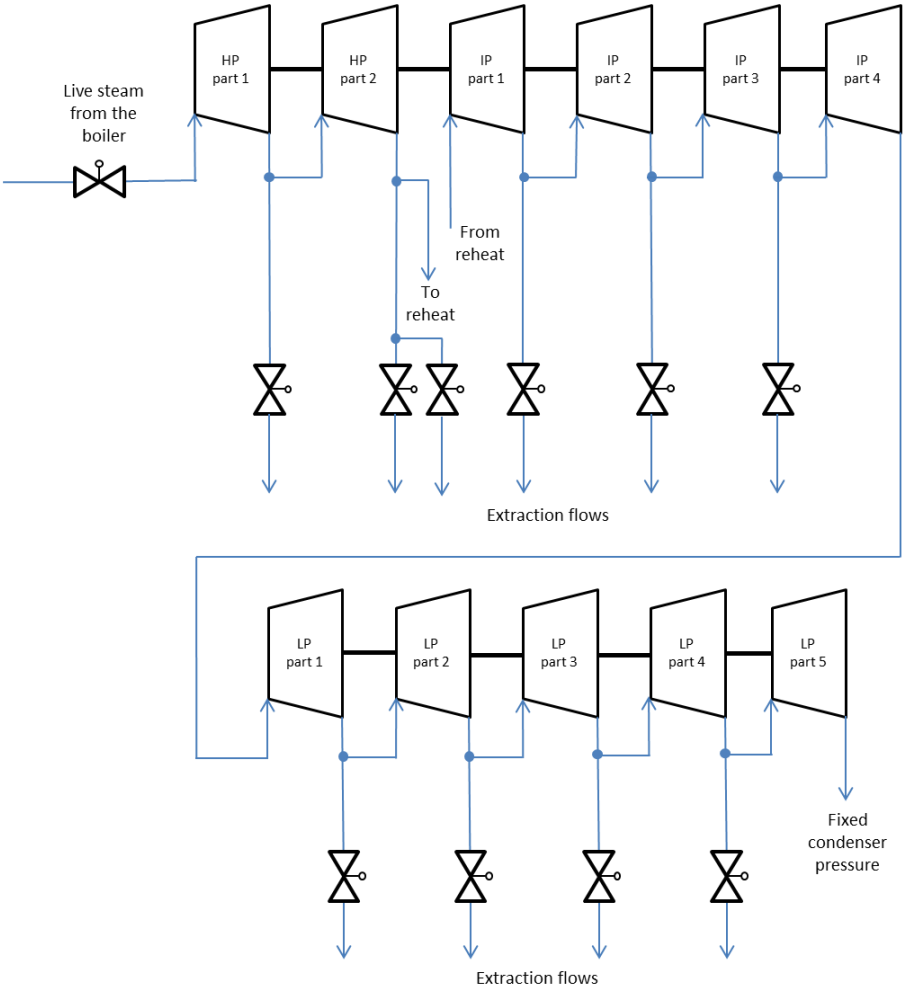

Figure 23. *Turbine plant model diagram.*

7.4 Control loops

The main control loops of the plant are modelled and tuned in Apros. These loops are:

- Block control
- Coal flow control including heat value correction
- Primary air and temperature control of the coal mill
- Secondary air control including O_2-correction
- Live steam temperature control
- Reheated steam temperature control
- Feed water control including enthalpy correction
- Extraction flow controls

The user gives the set point for the gross power output of the generator via block control. All the other controlled variables get their set points as a function of the power set point. The user given set point signal is corrected with a power correction controller according to the deviation between the power set point and measured generator power. The block control diagram is presented in Figure 24.

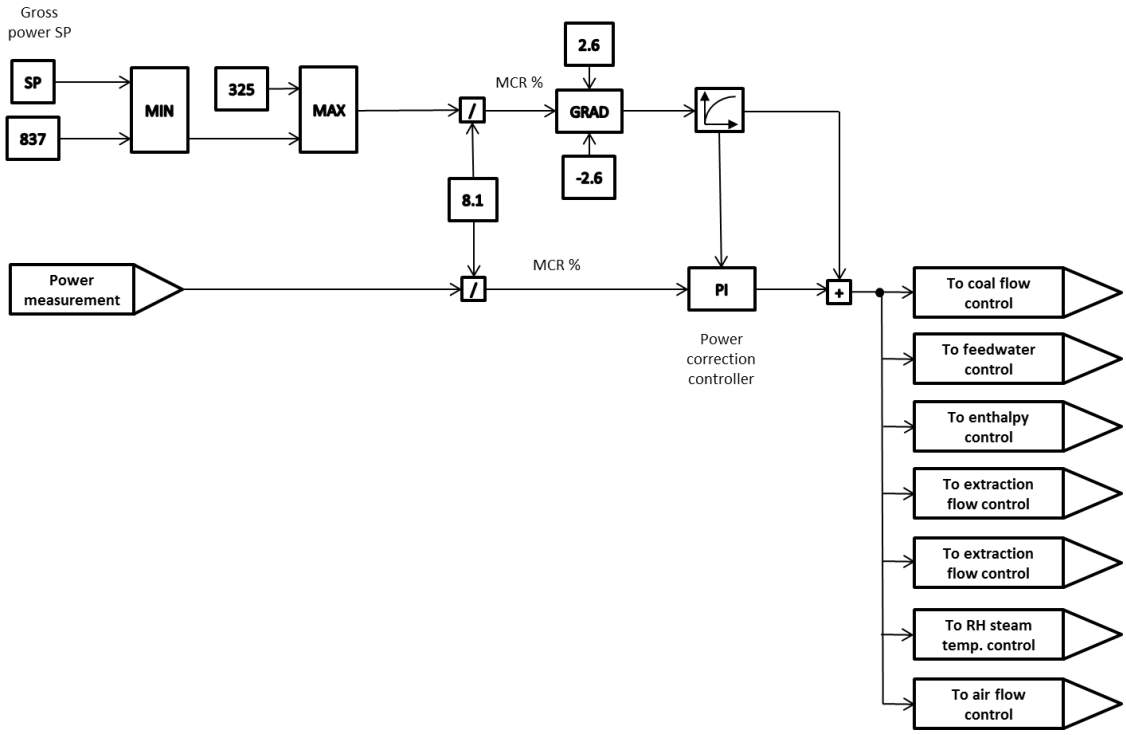

Figure 24. *Block control diagram.*

Set point for the coal flow is determined as a function of the power set point. Set point is then corrected with a heat value correction, which takes into consideration the changing content of the raw coal. Coal flow control diagram is showed in Figure 25.

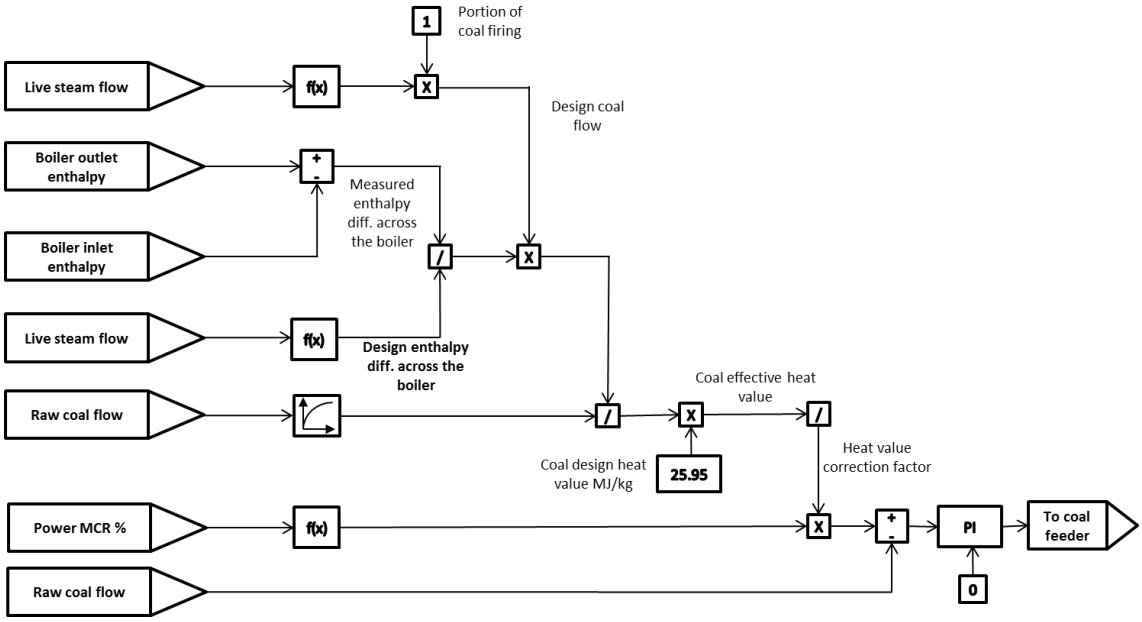

Figure 25. *Coal flow control diagram.*

The amount of primary air is controlled according to the coal flow. The mass flow of primary air is approximately two times bigger than the coal mass flow. The temperature of the air-coal mixture after the coal mill is controlled with the ratio of preheated and cold primary air.

The amount of secondary air is adjusted according to the total air demand, which is a function of power set point and coal flow set point. Secondary air set point is corrected with O_2-control, which adjusts the volume of oxygen in the flue gas to the desired level. A typical set point for oxygen volume in the flue gas after the economizer is around 3 %. Secondary air-, primary air- and coal mill temperature control loops are pieced together in air control diagram, which is presented in Figure 26.

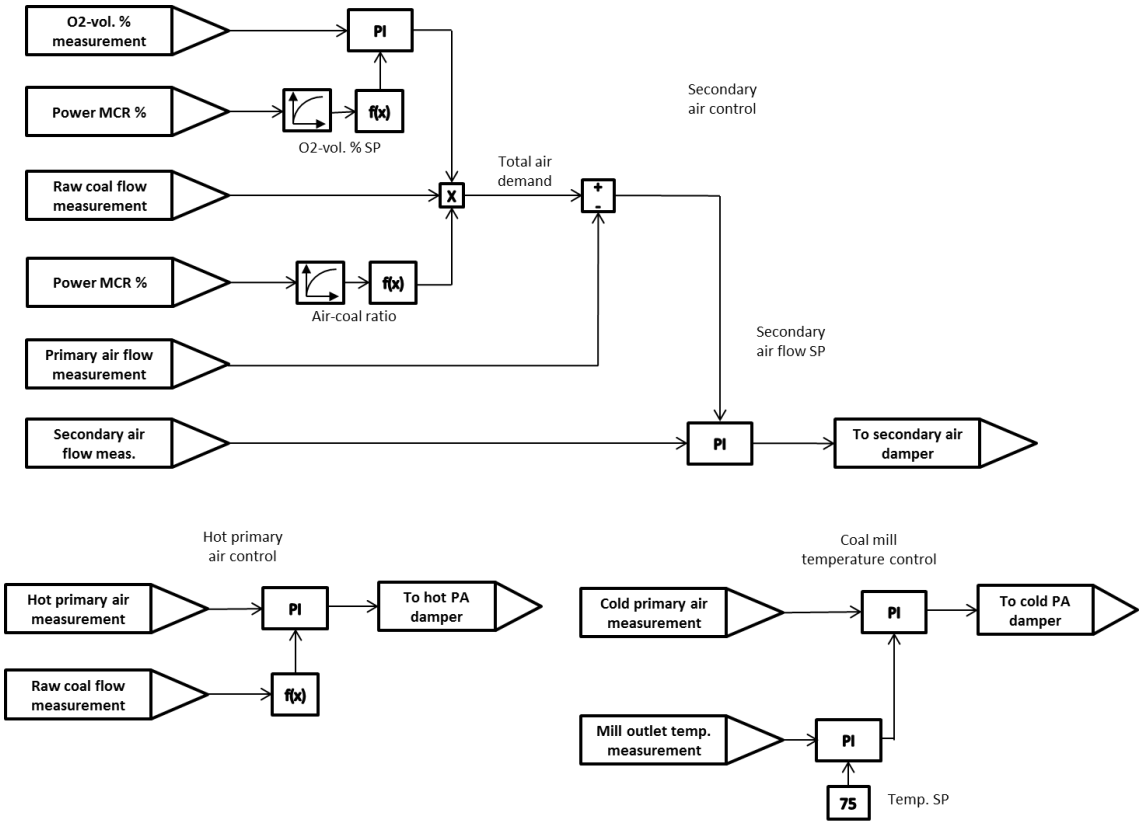

Figure 26. *Air control diagram.*

The live steam temperature is controlled by spraying saturated water among the live steam. The water is sprayed in three phases. There are four superheaters in the boiler. Steam temperature is controlled after the secondary-, tertiary- and final superheater. Live steam temperature set point after the final superheater is a function of the power set point. For the other attemperators the temperature set point is determined by the temperature difference across the attemperator. Reheated temperature is controlled correspondingly. Live steam temperature control diagram is showed in Figure 27.

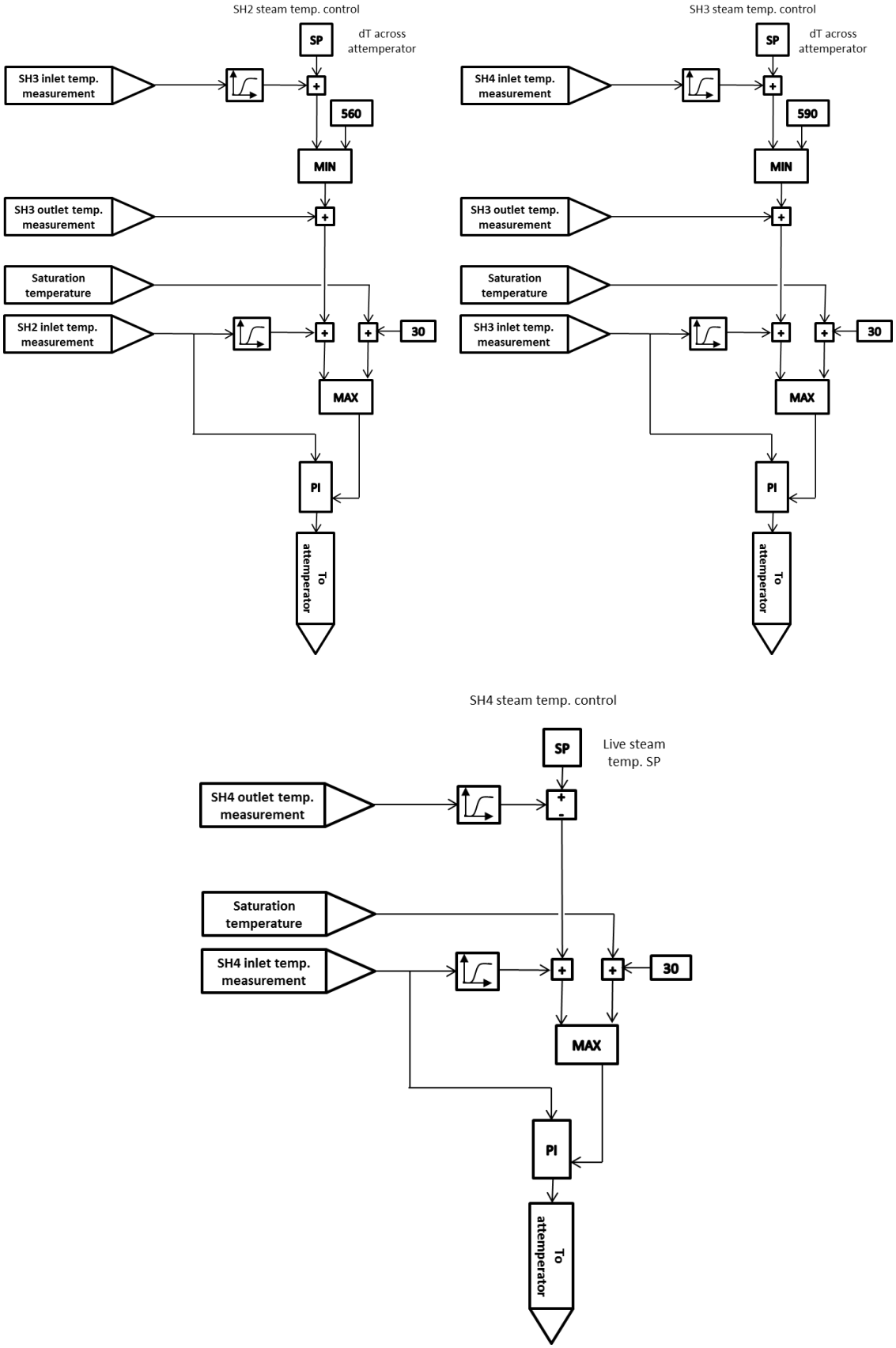

Figure 27. *Live steam temperature control diagram.*

The feedwater flow is controlled with a control valve. Set point for the feedwater mass flow is a function of power set point and the set point is modified with the enthalpy correction, which corrects the set point according to steam enthalpy after the evaporator. Correction factor is calculated according to the deviation between the design enthalpy and measured enthalpy. Since the steam enthalpy is a function of temperature and pressure, enthalpy correction controls the steam temperature and pressure after the evaporator. The feedwater control diagram is presented in Figure 28.

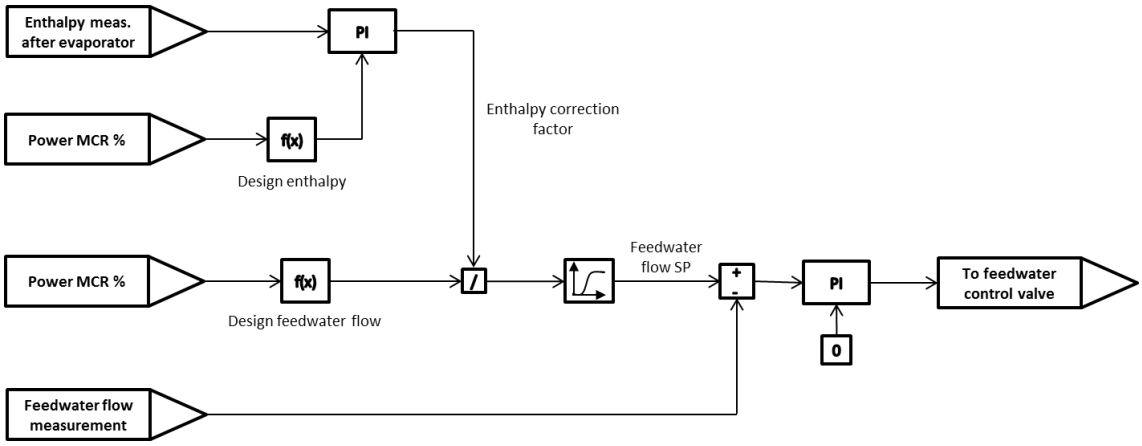

Figure 28. *Feedwater control diagram.*

Although the feedwater section is not included in the model, the extraction flows from the turbines must be modelled to achieve the right mass balance in the water-steam cycle. Extraction flows are controlled according to the power level. The set points for different power levels were collected from the plant's data repository. The extraction flow controls consist of multiple individual valve controls.

7.5 Simplifications

There are several simplifications in the model of reference plant B compared to the real plant. Simplifications are done to delimit the scope of the model, the time used for the modelling and to leave out some insignificant model parts. On the other hand some simplifications produce inaccuracies to the model.

The feedwater section and district heat section of the plant were not included in the model. However the extraction flows from the turbines to water preheaters and district heat exchangers were modeled to achieve the right feedwater mass balance. Also many other insignificant processes and control loops were left out of the model scope.

A notable difference between the model and the real plant are the time constants and delays of different processes, since they were unknown. Another significant inaccuracy in the model is the set points of the key process variables, which are determined as a

function of power output of the plant. Functions were determined on the grounds of collected measurement data from plant data repository. Exact functions, which are used in the control system of the plant, were not known. In addition tuning parameters of the controllers were not known. Parameters were adjusted by comparing the responses of the model and plant measurement data.

Various parallel structures were replaced with simplified layouts in the model. For example the superheating sections in the real plant are divided into two or four parallel steam flow lines. In the model these are modelled with just one flow line and the dimensions of the flow line were calculated according to the parallel lines of the plant. Furthermore the piping of the model is simplified version of the real layout, since accurate modeling of piping was not in the scope of the model.

8. SIMULATION EXPERIMENTS AND RESULTS

In this chapter the simulation experiments are introduced and the results are analyzed. Experiments were carried out to verify and validate the Apros stress calculation, validate the proposed coal mill model and reference plant B model as well as calculate thermo-mechanical stresses during reference plants cyclic operation. Furthermore these tested features improve the transient simulation of pulverized coal-fired power plants in the simulation environment. The simulation experiments are introduced in Table 3.

Table 3. *Simulation experiments.*

Chapter	Experiment
8.1	Apros thermal- and pressure stress calculation is compared against calculation from literary reference. The temperature field inside the component wall is quasi-stationary and the pressure inside the component is constant.
8.2	Simulation experiments that were carried out utilizing reference plant A model are discussed in this chapter.
8.2.1	Apros thermal- and pressure stress calculation is validated against calculation that is based on standard EN-12952-3. A plant cold start is simulated using reference plant A measurement data.
8.2.2	Coal mill UC is validated using reference plant A model. The original plant model has its own mill model. The original mill model is replaced with coal mill UC. Original plant model and plant model with coal mill UC are compared by simulating the same transient with both models.
8.2.3	Thermal- and pressure stresses are calculated during the same transient that was used in coal mill validation.
8.3	Simulation experiments that were carried out utilizing reference plant B model are discussed in this chapter.
8.3.1	The plant model and coal mill UC are validated by comparing model responses and plant measurement data.
8.3.2	Thermal- and pressure stresses are defined during the same transient that was used in plant and coal mill validation.

8.1 Verification of Apros stress calculation

Stress solver module is used to calculate thermal and pressure stresses in Apros. In this section stresses calculated by the module are verified against stresses calculated in literary reference [44]. Thermal stress verification is done by simulating a quasi-stationary state in thick-walled superheater header. Calculation of thermal stress both in reference [44] and in Apros is based on a quasi-stationary temperature field. During the simulation header wall is heated from 340 °C to 460 °C, whereas in reference [44] the temperature field is analytically solved.

The wall material is high-temperature structural steel 13CrMo44, which is commonly used in boiler drums and headers. The inner radius of the header is 120 mm and the outer radius is 180 mm, so the header wall is 60 mm thick. The temperature change rate (i.e. derivative) is maintained constant, 0,1 °C/s, which is 6 °C/min. The material properties of 13CrMo44 are presented in Table 4. Material properties are assumed to be constant and they are taken at temperature 450 °C.

Table 4. *13CrMO44 material properties at temperature 450 °C.*

Property	**Value**	**Unit**
Thermal diffusivity, a	$7{,}0 \cdot 10^{-6}$	m^2/s
Thermal conductivity, λ	25	W/mK
Density, ρ	7770	kg/m^3
Specific heat capacity, c_p	460	J/kgK
Thermal expansion coefficient, β	$15{,}2 \cdot 10^{-6}$	1/°C
Modulus of elasticity, E	167	kN/mm^2
Poisson's ratio, μ	0,3	-

Simulated inner and outer surface temperatures as a function of time are presented in Figure 13. Quasi-stationary temperature field is reached after 20 minutes and it lasts around 13 minutes.

Quasi-stationary temperature field in superheater header wall is illustrated in Figure 29. Temperature is presented as a function of header radius. The reference temperature field is presented in a state, where the wall inner temperature is 450 °C and outer surface temperature is approximately 420,4 °C.

Simulated and reference temperature fields correspond to each other as can be seen from the figure. Small temperature deviations are caused by the discretization of equations in Apros. In Apros the temperature is not solved in every point of the header wall but the wall is divided into calculation nodes. In this simulation the wall is divided into

50 nodes. If the nodalization is more scattered, the simulation result will be less accurate. Dense nodalization of course increases the software simulation time, since there are more difference equations to calculate. In normal situation 50 nodes in a 60 mm thick wall is not necessary. There are less calculation points in the reference than in the simulation.

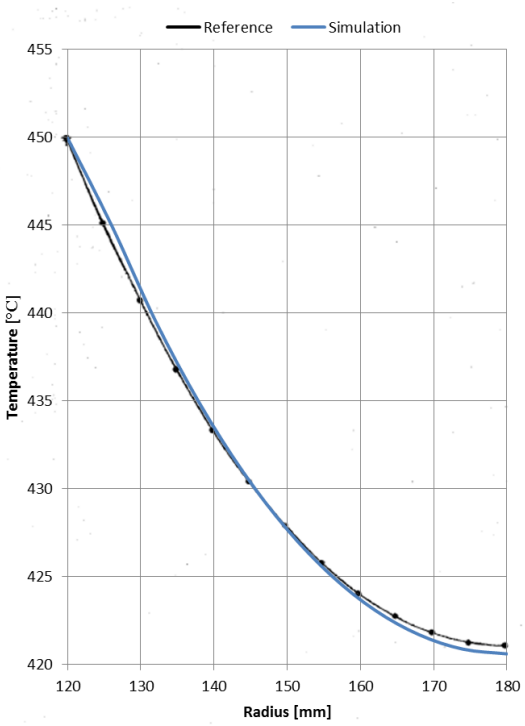

Figure 29. *Quasi-stationary temperature field in superheater header wall.*

Tangential, radial and axial thermal stresses are presented in Figure 30 a). The biggest absolute tangential and axial thermal stress values are located in the wall inner surface. The negative stress value is considered as compression stress and positive stress value as tensile stress. Axial thermal stress is a sum of tangential and radial thermal stresses, which can be seen from the Figure and solved from Equations (18)–(20). The simulation gives approximately the same result as was presented in reference [44].

Combined thermal stress, which is defined in Equation (24), is presented in Figure 30 b). The biggest combined thermal stress is located in the inner surface of the wall, whereas the smallest stress is in the middle of the wall.

a) b)

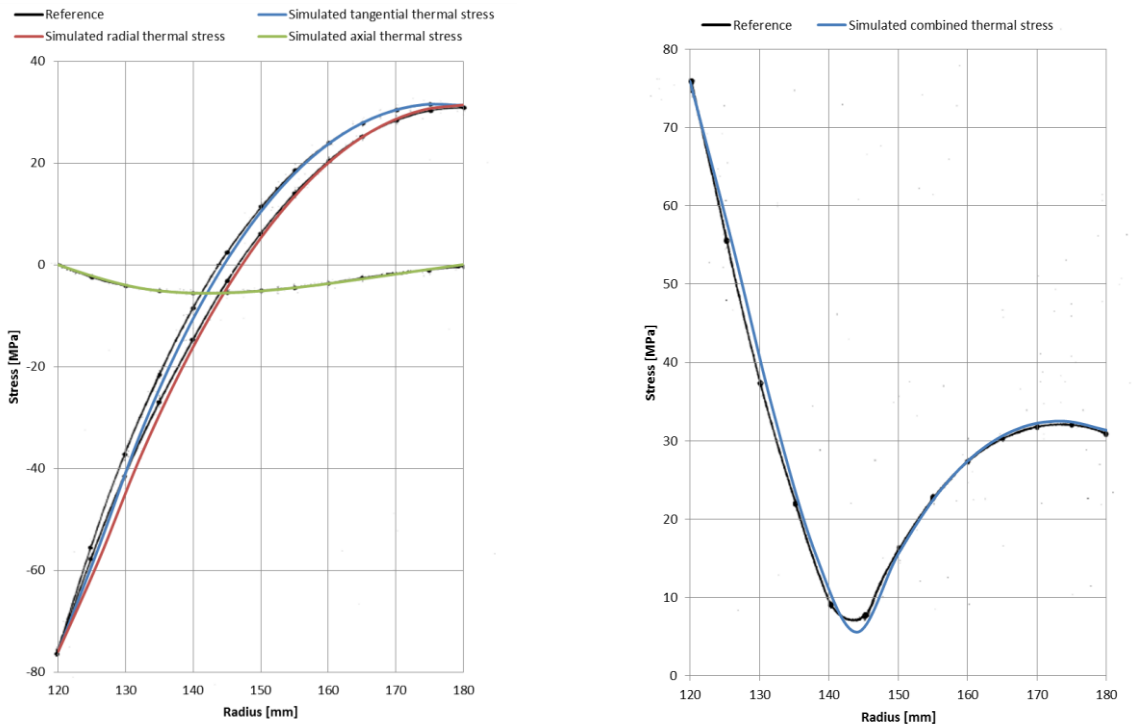

Figure 30. *a) Thermal stress components and b) combined thermal stress during quasi-stationary state.*

Pressure stress validation is carried out with a simulation, where the header inner pressure is 100 bars. Constant pressure creates constant pressure stress against the wall. Tangential, radial and axial pressure stress components defined in Equations (25)–(27) are presented in Figure 31 a). The highest pressure stresses are located in the inner surface of the wall. Axial pressure stress is constant throughout the wall. Combined pressure stress, which is defined in Equation (31), is illustrated in Figure 31 b). Combined pressure stress decreases almost linearly from the inner surface to the outer surface.

a) b)

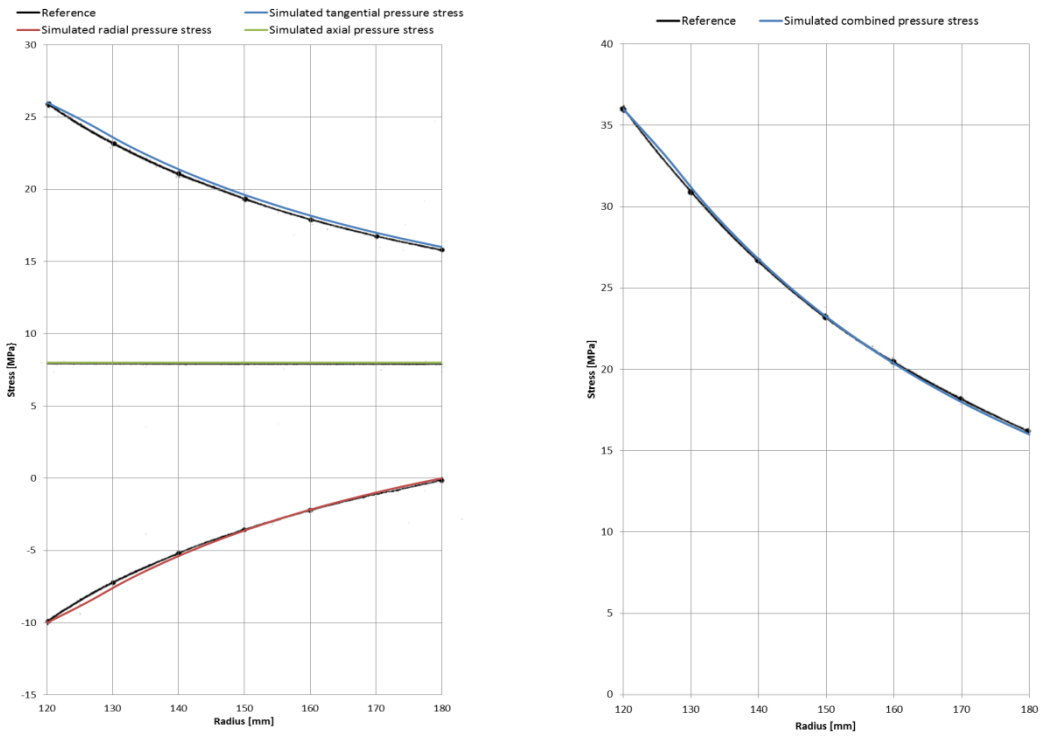

Figure 31. *a) Pressure stress components and b) combined pressure stress when the header inner pressure is 100 bars.*

In Figure 32 net stress components and combined net stress corresponding to previous simulations are presented. Temperature field of the wall is quasi-stationary and the header inner pressure is constant 100 bars. Tangential, radial and axial net stresses are defined with Equations (32)–(34). Maximum absolute net stresses appear in the wall inner and outer surfaces. All net stress components are at maximum in the inner surface when the temperature derivate in the wall is positive. Correspondingly, the biggest combined net stress values are located in the wall surfaces.

a) b)

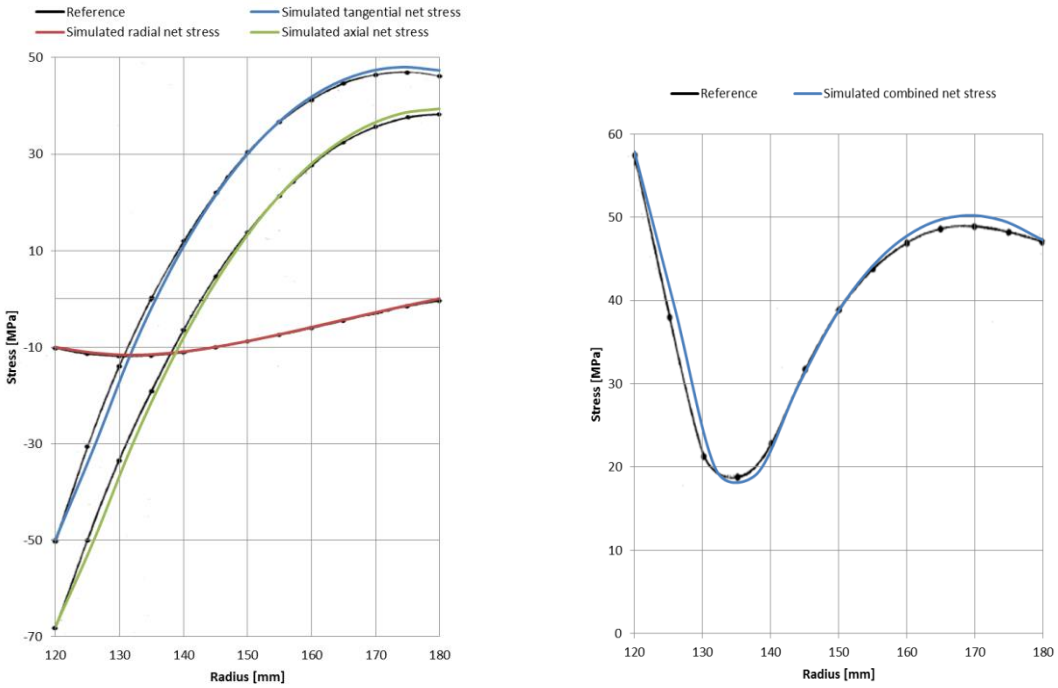

Figure 32. *a) Net stress components and b) combined net stress during quasi-stationary state. Header inner pressure is 100 bars.*

Based on the verification results Apros stress calculation corresponds with calculation in reference [44].

8.2 Reference plant A

In this section simulation experiments and results considering reference plant A model are introduced.

8.2.1 Validation of Apros stress calculation

In this chapter thermo-mechanical stresses calculated by the Apros stress solver module are validated against stress values calculated in reference [49]. In the reference stresses are determined according to standard EN 12952-3 [15]. The stress equations in the standard differ slightly from the ones proposed in Chapter 6.

Stresses are calculated using measured cold start-up data from reference plant A. Stresses are defined in the inner surface of a water separator wall in an interface between the separator tank and a tube attached to a tank opening. Dimensions of the separator tank and the tube attached to the tank are listed in Table 5.

Table 5. *Reference plant A water separator and tube dimensions.*

Component	Outside diameter [mm]	Wall thickness [mm]
Water separator tank	717,0	66,0
Tube	219,1	41,0

The material of the separator is metal alloy 15NiCuMoNb5. Material properties are listed in Table 6. Thermal conductivity, specific heat capacity, thermal expansion coefficient and modulus of elasticity are defined as a function of temperature.

Table 6. *15NiCuMoNb5 material properties.*

Property	Value	Unit
Thermal conductivity, λ	$38{,}273 + 0{,}0215 \cdot T - 5 \cdot 10^{-5} \cdot T^2$	W/m°C
Density, ρ	7850	kg/m^3
Specific heat capacity, c_p	$440{,}27 + 0{,}3804 \cdot T + 0{,}0003 \cdot T^2$	J/kg°C
Thermal expansion coefficient, β	$1 \cdot 10^{-5} + 2 \cdot 10^{-8} \cdot T - 1 \cdot 10^{-11} \cdot T^2$	1/°C
Modulus of elasticity, E	$212{,}42 - 0{,}0547 \cdot T - 4 \cdot 10^{-5} \cdot T^2$	kN/mm^2
Poisson's ratio, μ	0,3	-

Fluid pressure, mass flow and temperature measurements in the water separator and the power output during the cold start are presented in Figure 33 and the reference stresses are presented in Figures 34 a) and 35 a). In Figures 34 a) and 35 a) tangential thermal, pressure (i.e. mechanical) and net stress (i.e. total stress) in the water separator inner wall during the cold start are showed.

Temperature and pressure in the separator start to raise after 300 minutes. Rapid temperature increase causes a compression thermal stress whereas the pressure increase causes a tensile pressure stress in the wall inner surface. As was noted in Chapter 6.3 thermal and pressure stresses are opposite in sign, when temperature inside the vessel increases.

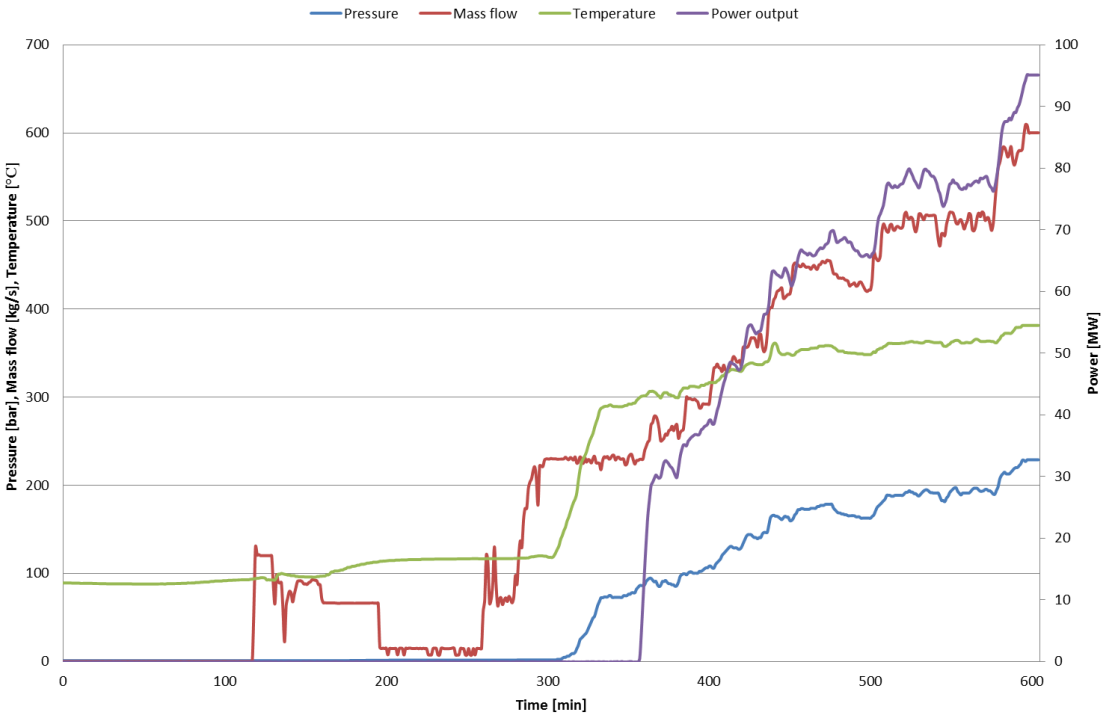

Figure 33. *Measured variables in water separator during the cold start.*

The validation is done by simulating the same cold start as in reference [49] by using the real pressure and temperature measurements, which are presented in Figure 33. Tangential thermal, pressure and net stresses are calculated according to Equations (21), (28) and (32) respectively. The calculation is done with Apros stress solver -module.

The most notable uncertainty related to the validation considers the heat transfer coefficient between the fluid and the separator inner wall. The fluid phase inside the separator and the flow velocity of the fluid change during the start-up, which cause changes in the heat transfer coefficient. Therefore the cold start simulation is performed in two different ways. The first case is simulated with a variable heat transfer coefficient, i.e. Apros calculates the heat transfer coefficient in every time step according to Equation (44). This case is presented in Figure 34.

a)

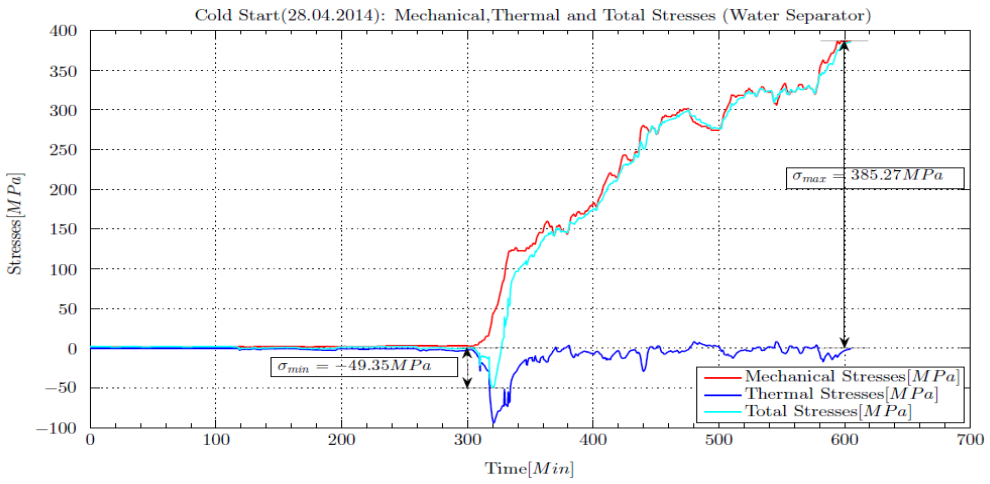

b)

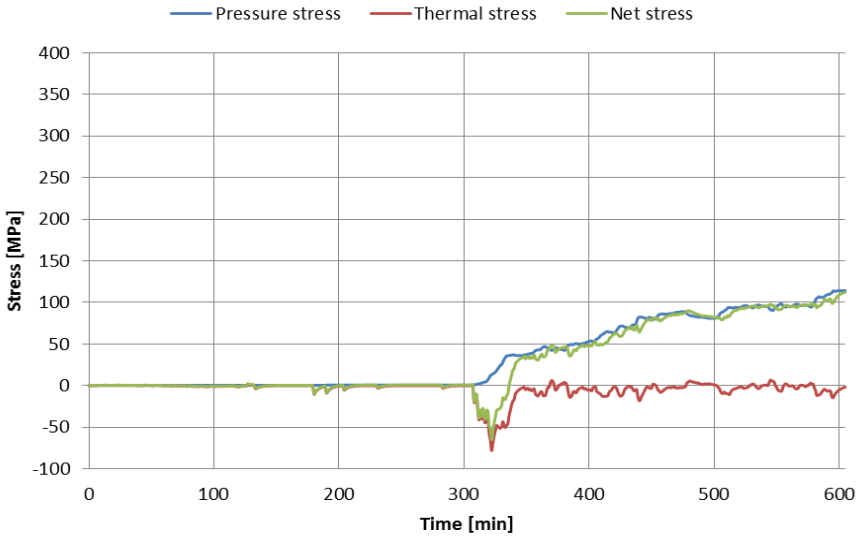

c)

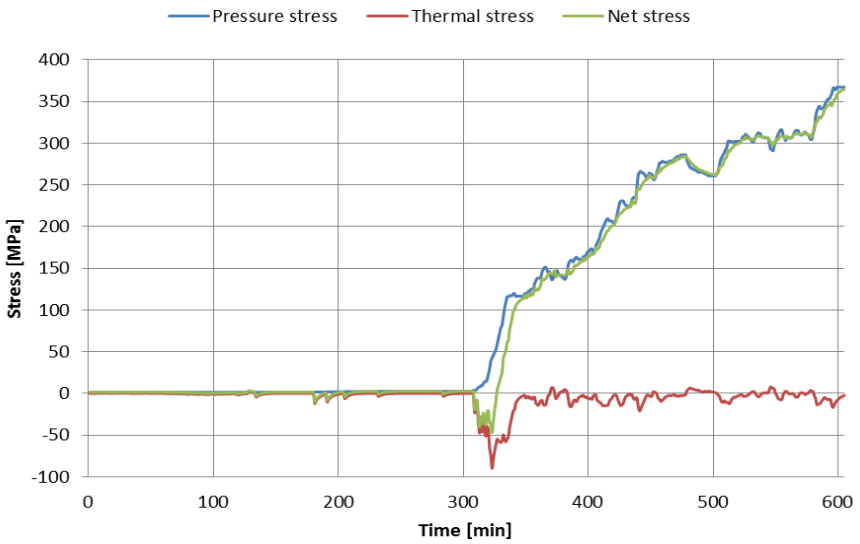

Figure 34. *a) Tangential reference stresses [49 p. 80], and simulated tangential stresses with variable heat transfer coefficient, a) without stress concentration factors and b) with stress concentration factors k_p = 3,291 and k_t = 1.151.*

When stress values between Figures 34 a) and 34 b) are compared, it can be seen that the stress curves have the same shape but the scale of the stress values is different. E.g. the pressure stresses in the reference calculation are over three times bigger than in Apros simulation. This can be explained by the fact that Apros stress solver does not use stress concentration factors, which are used in Equation (35) and in the reference calculation. When the simulated stress values are multiplied with relevant stress concentration factors $k_p = 3.291$ and $k_t = 1.151$, the compared stress values are much closer to each other as can be seen from Figure 34 c). The concentration values are calculated according to Equations (38)–(42) as follows:

$$z = \frac{d_{mb}}{d_{ms}} = \frac{219{,}1-41{,}0}{717{,}0-66{,}0} = 0{,}273579 \tag{47}$$

$$k_t = \left\{\left[2 - \frac{\alpha+2700}{\alpha+1700}z + \frac{\alpha}{\alpha+1700}(\exp(-7z) - 1)\right]^2 + 0{,}81z^2\right\}^{1/2} \tag{48}$$

$$= \left\{\left[2 - \frac{1000+2700}{1000+1700}0{,}2736 + \frac{1000}{1000+1700}(\exp(-7 \cdot 0{,}2736) - 1)\right]^2 + 0{,}81 \cdot 0{,}2736^2\right\}^{1/2} = 1{,}150611$$

$$B = -1{,}14\left(\frac{e_{mb}}{e_{ms}}\right)^2 - 0{,}89\left(\frac{e_{mb}}{e_{ms}}\right) + 1{,}43 = -1{,}14\left(\frac{41{,}0}{66{,}0}\right)^2 - 0{,}89\left(\frac{41{,}0}{66{,}0}\right) + 1{,}43 = 0{,}43719 \tag{49}$$

$$C = 0.326\left(\frac{e_{mb}}{e_{ms}}\right)^2 - 0{,}59\left(\frac{e_{mb}}{e_{ms}}\right) + 1{,}08 = 0.326\left(\frac{41{,}0}{66{,}0}\right)^2 - 0{,}59\left(\frac{41{,}0}{66{,}0}\right) + 1{,}08 = 0{,}83929 \tag{50}$$

$$\zeta = \frac{d_{mb}}{d_{ms}}\sqrt{\frac{d_{ms}}{2e_{ms}}} = \frac{219{,}1-41{,}0}{717{,}0-66{,}0}\sqrt{\frac{717{,}0-66{,}0}{2 \cdot 66{,}0}} = 0{,}607556 \tag{51}$$

$$k_p = 2{,}2 + e^B \cdot \zeta^C = 2{,}2 + e^{0{,}43719} \cdot 0{,}607556^{0{,}83929} = 3{,}219144. \tag{52}$$

Differences between the reference calculation and the scaled simulation result can be explained by divergences between used concentration factors, material properties and heat transfer coefficient. Nonetheless the compared stresses are quite close to each other.

In the second case the simulation is performed with a constant heat transfer coefficient. The fluid inside the separator is assumed the be water during the start-up. For the heat transfer coefficient value 3000 W/m^{2}K is used. In EN 12952-3 it is advised to use value 3000 W/m^{2}K for water and value 1000 W/m^{2}K for steam [15 p. 117]. Results are illustrated in Figure 35.

a)

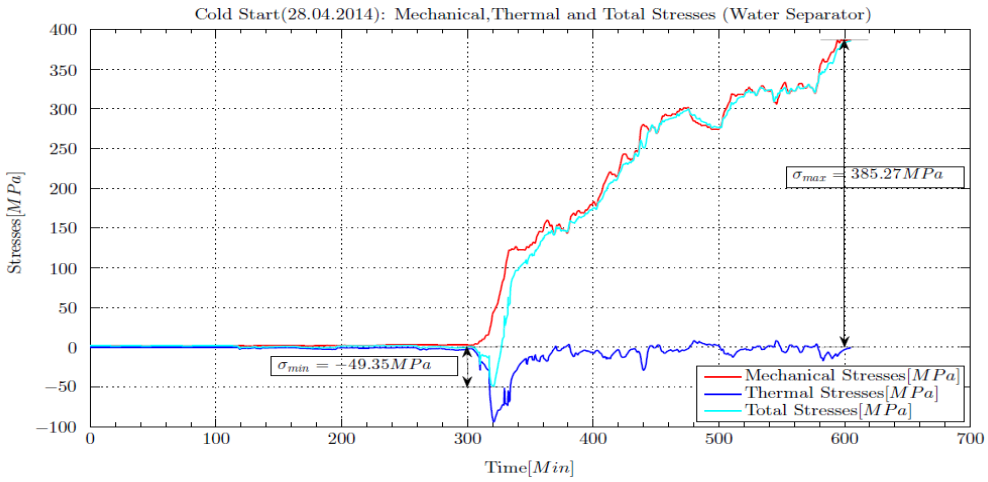

b)

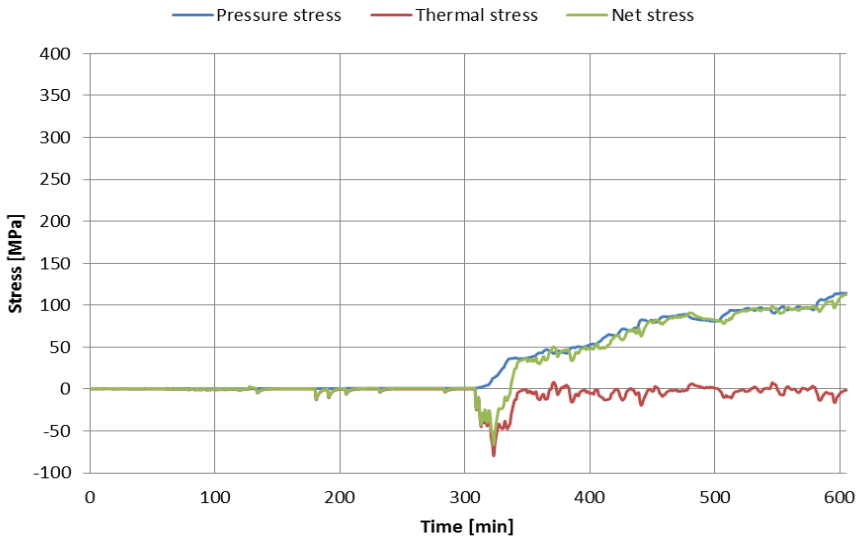

c)

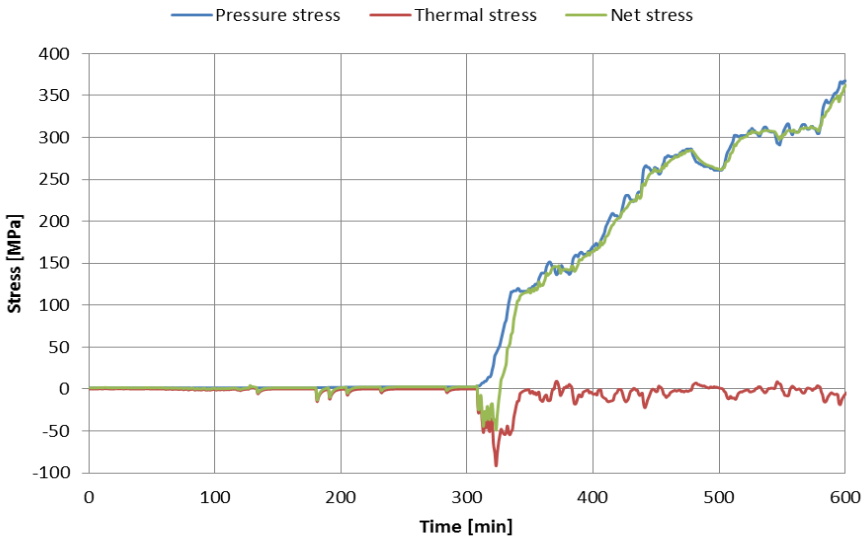

Figure 35. *a) Tangential reference stresses [49 p. 80], and simulated tangential stresses with constant heat transfer coefficient, a) without stress concentration factors and b) with stress concentration factors k_p = 3,291 and k_t = 1.151.*

The pressure stress in the second case is equal to the first case since the heat transfer coefficient does not have an impact on the pressure stress. Also the thermal stress values are nearly identical, thus the value of heat transfer coefficient did not have major impact on the results. In the first case the heat transfer coefficient varies between 3000–7000 W/m^2K, whereas in the second case heat transfer coefficient is constant 3000 W/m^2K.

Based on the validation results Apros stress calculation corresponds to calculation in reference [49], if the defined stresses are scaled with stress concentration factors. For further development purposes in Apros the user should have an opportunity to use concentration factors if the stresses are defined in pipe connections.

8.2.2 Coal mill model validation

The simulation model of reference plant A has been validated against real plant data and based on the validation results the model corresponds well to the real plant behavior. The reference simulation model has its own coal mill model, which has been tuned to correspond the behavior of the plant mills.

In contrast to the generic coal mill model introduced in this thesis, the mill in the reference plant model is an identified "black box" model. Differences between the models are visualized in Figure 36. In this section the reference model is referred as "original model" and the model including the coal mill UC is referred as "UC-model".

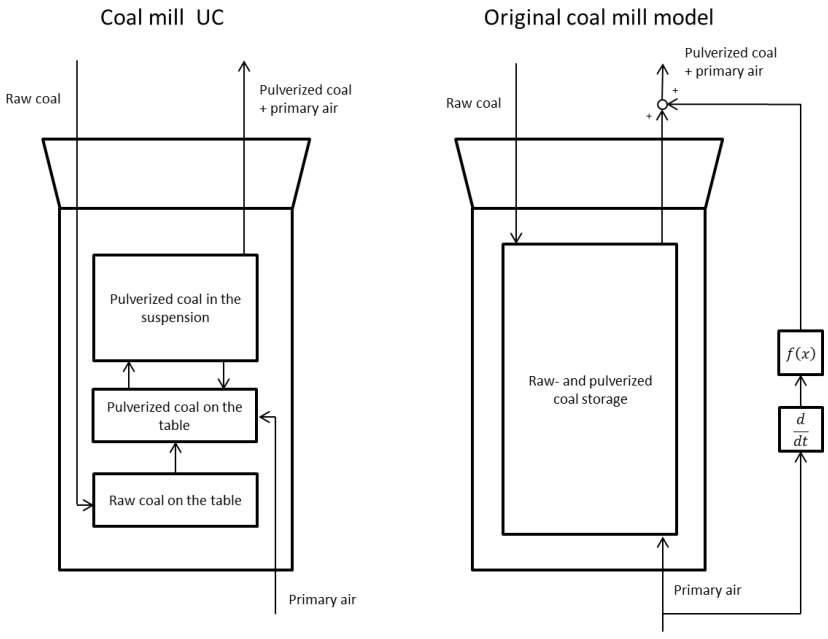

Figure 36. *Concepts of the coal mill UC and the original coal mill model.*

In this work the original coal mill model was replaced with the coal mill UC and the same transient, that has been used to test the secondary control capability of the plant, was used for the validation of the coal mill UC. During the simulation the gross electric

output of the model was changed from 652 MW to 730 MW and back to 652 MW. The duration of the simulation is 1400 s. The simulation results are compared to responses produced by the original model, which are really close to the real plant measurements.

The coal mill model was tested with multiple parameter sets, which are used in Equations (4)–(12). Parameters used in the validation are listed in Table 7.

Table 7. *Reference plant A coal mill model parameters.*

Parameter	Value	Parameter	Value
K_1	0,04	K_7	4,5212
K_2	0,064	K_8	0,0509
K_3	0,0483	K_9	0,5273
K_4	0,6	K_{10}	7,3985
K_5	0,005	K_{11}	19 800000
K_6	2,8424	ω	1,8 r/s

Due to challenging conditions inside the coal mill, mills internal variables cannot usually be measured. Pulverized coal flow from the mill to the furnace is one of these variables, which cannot be accurately measured. Even the measuring of raw coal mass flow into the mill is inaccurate due to varying content and properties of the coal. For these reasons the validation of the coal mill model is challenging.

During the coal mill model validation the following variables are monitored:

- Gross electric power output of the plant
- Raw- and pulverized coal mass flows
- Coal storage variables inside the mill
- Primary- and total air mass flows
- Ratios between coal and air flows
- O_2-volume percentage in the flue gas
- Live steam temperature and pressure

All the monitored variables, except part of the coal mill storage variables, are compared to the responses of the original plant model. Coal mill internal variables are usually not measurable from a real mill, and therefore validation of these variables is challenging.

Figures (37)–(40) show the simulation results of the coal mill validation. Gross power output of the plant is presented in Figure 40. A difference between the model responses can be noticed after the first overshoot. The original model response drops under the set point after the overshoot, whereas the UC-model response drops a bit after the over-

shoot and raises again. Reason for this can be found from the pulverized coal flow out of the mill, which is presented in Figure 37. Pulverized coal flow produced by the coal mill UC continues to grow at the point where the coal flow produced by the original model settles. This is can noticed between 300 and 700 seconds. Although the deviation between the curves is proportionally small, it has a major impact on the boiler load and furthermore to power output. The raw coal flow curves in Figure 37 are dynamically in line with each other, so the deviation in pulverized coal flow comes from internal dynamics of the mill model.

Furthermore deviation in the pulverized coal flow is a consequence of behavior of the coal storages inside the mill, which are presented in Figure 37. In the UC-model the storage is divided into three sections: raw- and pulverized coal on the grinding table and pulverized coal in the air (i.e. suspension), whereas in the original model the coal storage is not divided. Therefore the storages are not fully comparable. Also the absolute values of the coal storages should not be stared, since the amount of coal in the storages are not known from the real mills. The differences between the mill models are illustrated in Figure 36.

Based on Figure 37 the overall coal storage inside the mill starts to raise in both models when the load is ramped up and it drops back to the original level when the load is decreased. This is probably the case in real mills as well. However the pulverized coal storages on the grinding table and in the air should first decrease when load is ramped up. This would be an indication that the sudden primary air flow increase transports extra coal powder from the mill, which leads to a momentary coal flow peak. As a result the amount of coal powder inside the mill would drop momentarily. It takes a few minutes to build up a new coal powder storage inside the mill after the drop.

As can be seen from Figure 37 the pulverized coal on the table first drops a bit when the load is ramped up and an opposite action is noticed when the load is decreased. Thus the coal powder storage on the grinding table behaves like it supposed to. However the extra transportation of coal powder is not shown in pulverized coal storage in the suspension, which is the last storage before the outlet. This seems to be the deficiency of the coal mill UC. In the original model this issue is solved by adding a primary air flow-proportional derivative term to the pulverized coal flow as is illustrated in Figure 36.

Another issue related to coal storage behavior during the load changes is the coal particle categorization. In the UC-model coal particles are divided into two different categories: raw and pulverized coal particles. When the load is increased not only pulverized coal is transported from the mill to the furnace but also bigger particles go through the classifier section due to increased primary air flow. This leads to a peak in the coal flow to the furnace. Furthermore bigger particles find their way from the furnace into the flue gas duct. This has been measured as a higher ratio of unburned coal particles in the flue gas during a load increase in reference plant A. Thus the coal particle distribution in the

model has also an effect on performance of the mill model, and more coal particle sizes should considered in the model, if you want to capture the real dynamics of the mill in transient situation.

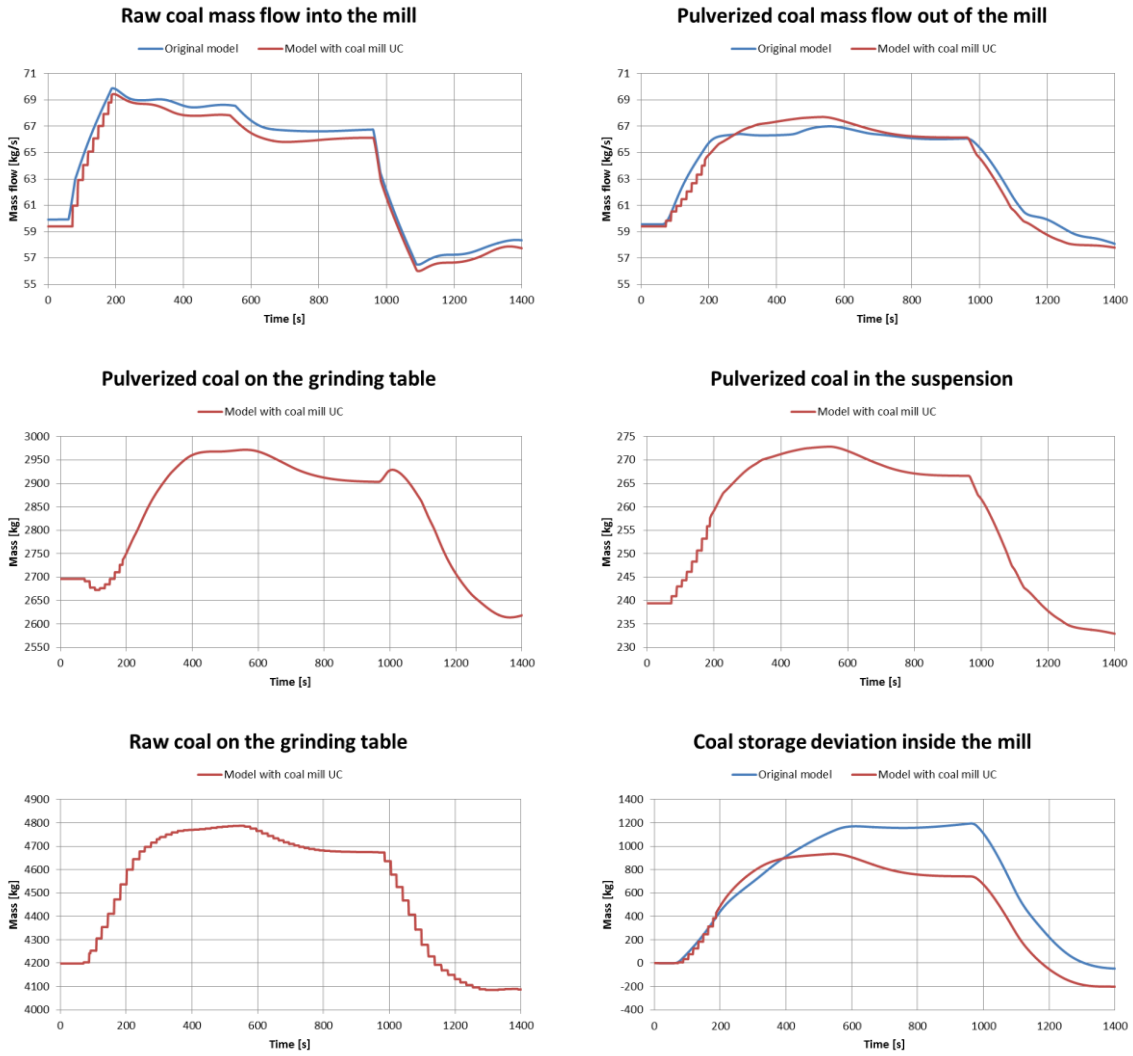

Figure 37. *Coal mill variables.*

Primary air mass flows are in line with each other, whereas there are slight deviation in the total air mass flow as can be seen in Figure 38. The deviation derives from the differences in the pulverized coal flow, which affects the O_2-content in the flue gas, and thereby has a major impact on the air feed.

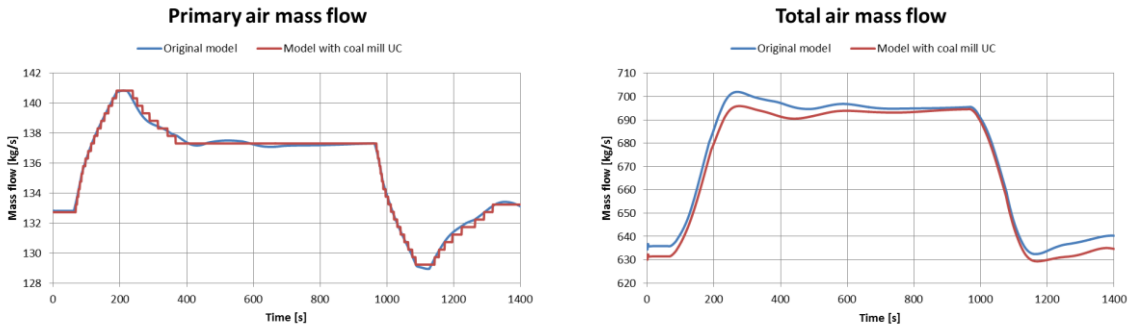

Figure 38. *Primary- and total air mass flow.*

Ratios between primary air- and raw coal mass flows as well as total air- and pulverized coal mass flows are presented in Figure 39. The primary air – raw coal ratio is slightly higher in the UC-model due to lower raw coal mass flow. Differences in the total air – pulverized coal ratio are mainly caused by deviations in the pulverized coal flow.

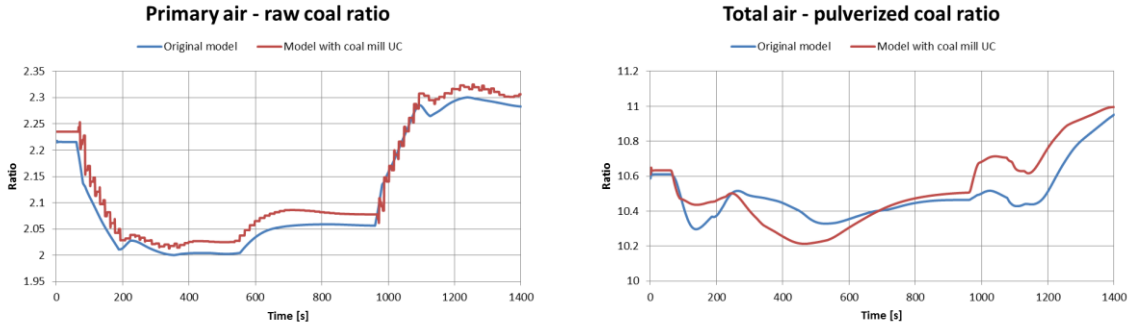

Figure 39. *Air-coal ratios.*

The are no significant differences in the live steam temperature between the models as can be seen in Figure 40. The live steam pressure follows the dynamics of the power curve since sliding pressure control is used in the plant. Therefore the steam pressure level is higher in the UC-model between the load changes. The O_2-content in the flue gas indicates the model differences in coal and air flows. For example between 300 and 700 seconds the O_2-content is lower in the UC-model due to higher level of pulverized coal into the furnace compared to the original model.

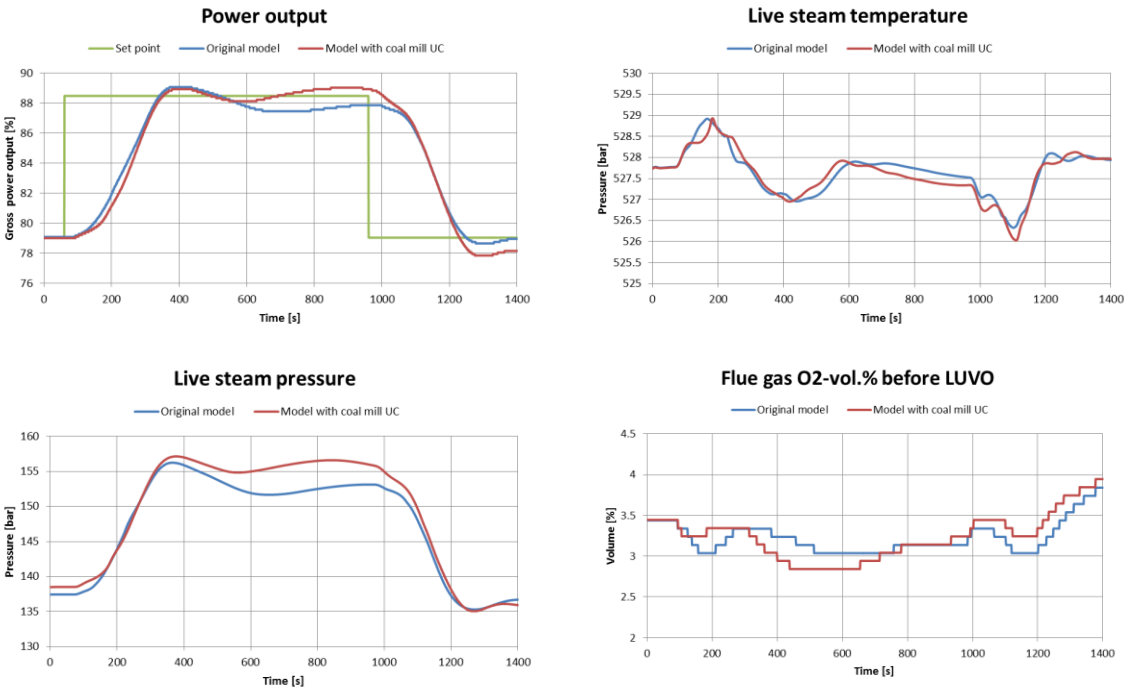

Figure 40. *Gross power output, live steam temperature, live steam pressure and flue gas O_2-volume %.*

8.2.3 Thermo-mechanical stresses during load change transient

Thermal- and pressure stresses during the load change transient in reference plant A model are discussed in this section. Same transient, that was used in the coal mill validation, is simulated to define the stresses. However the simulation time is longer, 2200 s, so that the stresses reach a steady-state condition before the simulation ends. Stresses are defined in the inner surface of a connection of a superheater header and an inlet tube attached to the header opening. This type of intersection is most prone to cyclic stresses, since the velocity of the fluid increases significantly when the cross-section of the flow area becomes smaller.

Increased velocity raises the heat transfer coefficient in the joint section, which improves heat transfer. Difference in the heat transfer between tube and header walls produces temperature differences in wall material especially in the tangential direction. Thermal, pressure and net stresses are calculated in tangential, radial and axial directions. Also combined stresses, which are typically used in permissible stress definition, are presented. Since the stresses are calculated in the connection point of a header and a tube, concentration factors k_t and k_p are used according to Equations (35)–(37). Concentration factors are determined from Equations (38)–(42), and values $k_t = 1{,}714$ and $k_p = 2{,}723$ are used in the simulations.

Superheater under discussion is the primary convective superheater in the flue gas duct. Dimensions of the superheater header and the inlet tube attached to header are listed in Table 8.

Table 8. *Reference plant A superheater header dimensions.*

Component	Outside diameter [mm]	Wall thickness [mm]
Header	355,6	54,0
Inlet tube	31,8	5,6

Material of the header and inlet tube is ferritic metal alloy 13CrMo44. Material properties of 13CrMo44 are presented in Table 9. Thermal conductivity, specific heat capacity, thermal expansion coefficient and modulus of elasticity are determined as a function of temperature, whereas in Table 4 they were determined in constant temperature.

Table 9. *13CrMo44 material properties.*

Property	Value	Unit
Thermal conductivity, λ	$46{,}462 - 0{,}0024 \cdot T - 3 \cdot 10^{-5} \cdot T^2$	W/m°C
Density, ρ	7850	kg/m^3
Specific heat capacity, c_p	$440{,}27 + 0{,}3804 \cdot T + 0{,}0003 \cdot T^2$	J/kg°C
Thermal expansion coefficient, β	$1 \cdot 10^{-5} + 2 \cdot 10^{-8} \cdot T - 1 \cdot 10^{-5} \cdot T^2$	1/°C
Modulus of elasticity, E	$212{,}42 - 0{,}0547 \cdot T - 4 \cdot 10^{-5} \cdot T^2$	kN/mm^2
Poisson's ratio, μ	0,3	-

Thermal and pressure stresses are consequences of temperature and pressure changes during the transient. Steam pressure and temperature inside the header during the transient are presented in Figure 41. Steam pressure raises when the load is increased due to increased feedwater flow and fuel feed. Steam temperature oscillates during the transient as a result of varying feedwater and fuel feed, although the steam temperature control tries to keep the temperature at a constant value.

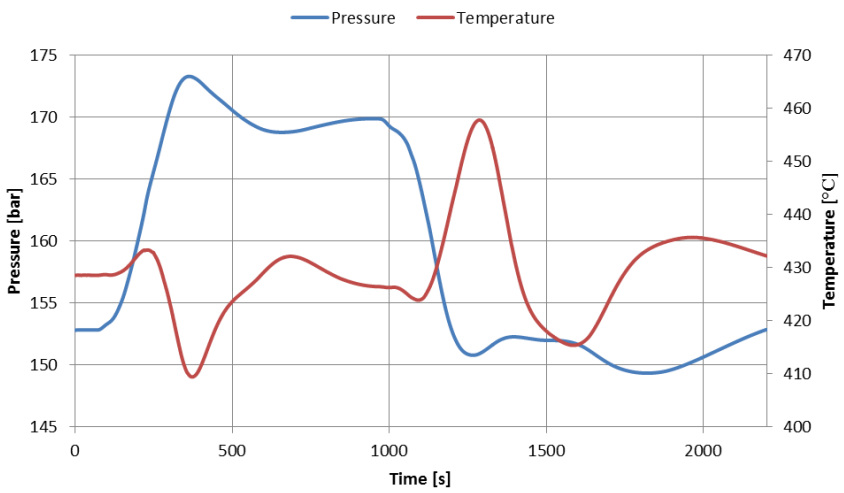

Figure 41. *Steam pressure and temperature inside the header during the transient.*

Figure 42 shows the thermal and pressure stresses in all three directions as well as the combined stress values. Circumferential stress (i.e. tangential stress) is the predominant stress component during the load transient compared to radial and axial stresses and pressure stress values change percentually much less than thermal stresses. Pressure stress forms the "steady state"-part of the stress, whereas thermal stress causes the fluctuation, which inflicts fatigue-related damages especially in materials that are not designed to withstand fatigue.

Radial thermal stress is zero throughout the transient as was described in Equation (22). The steam temperature increase causes a compression thermal stress and in proportion temperature drop causes a tensile thermal stress to the wall as was noted in Chapter 8.2.1. Compression stress is negative in sign and tensile stress positive in sign.

The combined net stress during the transient at the joint is also presented in Figure 42. For this header-tube connection the allowable stress range is around 350 MPa, and hence the three-dimensional combined net stress is within permissible region during the transient. This approximation is calculated according to EN-12952-3. The definition of allowable stresses is not included in the scope of this work due its extent. The allowable stress depends on lifetime of the component and performed load changes, which were not known for the header. Also allowable stress calculation in the standard is mainly meant for start-up and shutdown procedures.

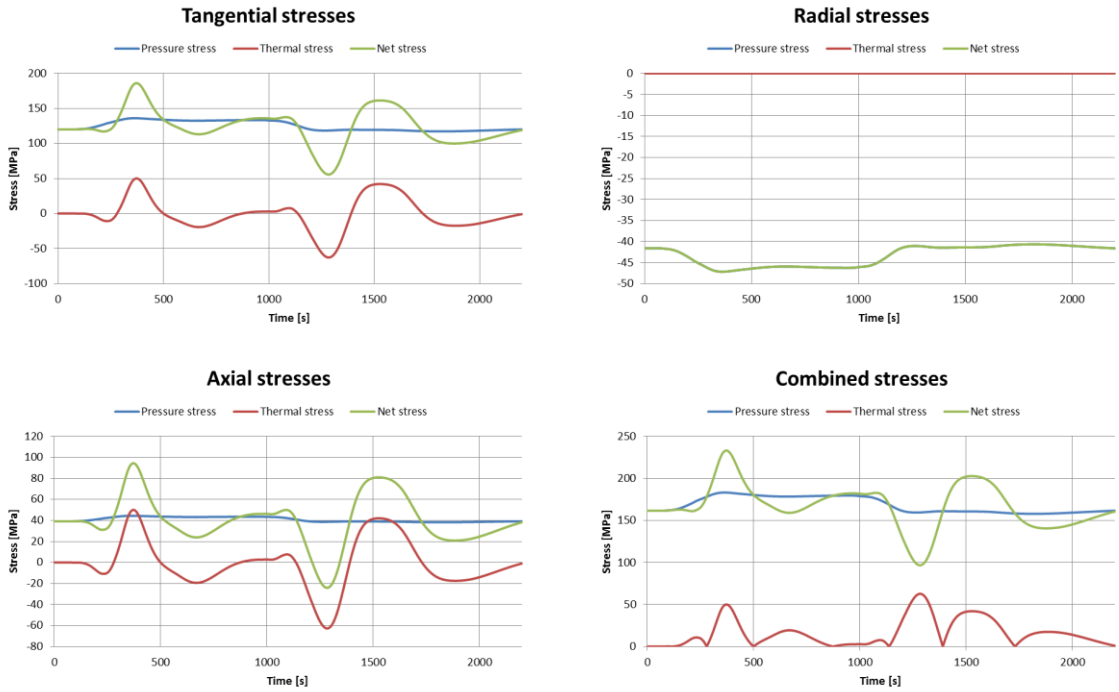

Figure 42. *Thermo-mechanical stresses during the transient.*

8.3 Reference plant B

In this section simulation experiments and results considering reference plant B model are discussed.

8.3.1 Plant- and coal mill model validation

Before the transient plant model validation, multiple steady state simulations were carried out to validate the model. First the model was tuned to full load level by modifying the model parameters. When the correspondence with the model and operational data was found, the model was validated also in various other steady state load levels at the studied power range. After the steady state investigation, dynamic validation was started by simulating a selected transient and comparing the results to measurement data.

The dynamic validation was done by simulating the model with a same transient that has been measured from the plant. The reference transient is a 6000 second period, which includes a 70 MW drop and an equal increase in gross electric power of the plant. The reference transient is used for both the validation of the whole plant model and also for the validation of the coal mill model. The coal mill parameters that was used in the validation are listed in Table 10.

Table 10. *Reference plant B coal mill model parameters.*

Parameter	Value	Parameter	Value
K_1	0,0452	K_7	4,5212
K_2	0,064	K_8	0,0509
K_3	0,0483	K_9	0,5273
K_4	0,8557	K_{10}	7,3985
K_5	0,0056	K_{11}	19 800000
K_6	2,8424	ω	2,0 r/s

During the simulation the following variables are monitored:

- Gross electric power of the plant
- Raw- and pulverized coal mass flows
- Coal mill internal variables
- Total air mass flow
- Feedwater mass flow
- O_2-volume percentage in the flue gas
- Steam temperature and enthalpy after the evaporator
- Steam temperatures in the superheater section
- Spray water flows
- Steam pressures

Figures 43–48 illustrate the results of the dynamic model validation. The coal-related variables are presented in Figure 43. Dynamically the raw coal flow curves are quite similar, although there are notable peaks in the measured coal flow when the load changes are made, and the model does not produce such peaks. This indicates that the control of raw coal flow is more aggressive at the plant and the controller might be a bit more advanced at the plant, whereas in the model an ordinary PI-controller is used. The level of raw coal flow is also a bit higher in the model. Reason for this can be found from the raw coal flow set point function which is a compromise among many other variable set point functions, since the real load-proportional set point functions were not known. In addition the composition and the heat value of the coal have a major impact on the amount of coal, e.g. if the heat value in the model is lower than is measured at the plant, more coal is supplied to the furnace in the model compared to the plant. For improving the plant model the delays and time constant of coal supply and coal mill should also be known. This would also change the pulverized coal flow curve significantly, which is now similar to raw coal flow curve.

Pulverized, raw and total coal storages inside the mill are also shown in Figure 43. The behavior of the storages is corresponding to the reference plant A simulation. When the

load is increased under 3000 seconds, the pulverized coal on the grinding table first slightly drops and then it starts to raise. However this cannot be noticed in the pulverized coal storage in the suspension. Thus the outcome seem to be equal to the validation results in Chapter 8.2.2. Naturally the amount of raw coal and the overall coal storage inside the mill drop when the load is decreased and raise when the load is increased.

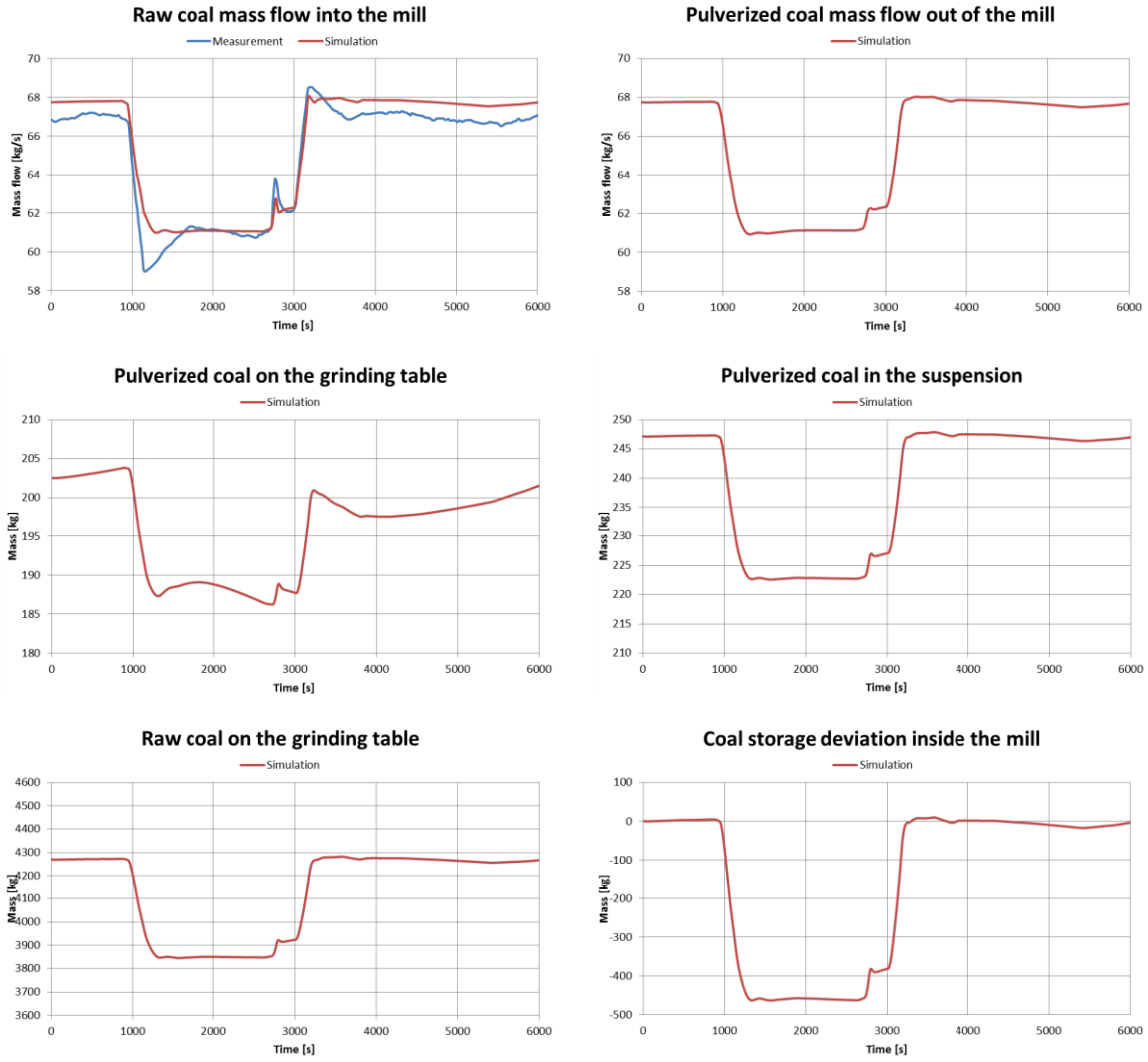

Figure 43. *Coal mill variables.*

The gross electric power output is presented in Figure 44. The model response follows fairly well the set point curve, but it does not overshoot and undershoot the set point curve as the measured power output. The deviation between the power curves is a consequence of multiple factors, since the inaccuracies of the whole plant model culminate on the power response. Also tuning of the controllers affect significantly on the shape of the power curve during the transient. The high-frequency oscillation in the power curve as well as in the feedwater flow and O_2-content curves is caused by measuring errors and backlash of valves. This type of oscillation is not needed to be included in the model.

In the model the level of feedwater mass flow is around two percent lower than measured level. Once again the main reason is the load-proportional set point function which is most probably not the same one that is used at the plant. In addition the absence of HP- and LP-preheaters, condenser, feedwater tank and the simplified extraction flow modelling have an impact on the feedwater flow. Nonetheless the curves are dynamically uniform if the high-frequency oscillation is not taken into account. The simulated total air flow and O_2-content in the flue gas are fairly well in line with the measurements.

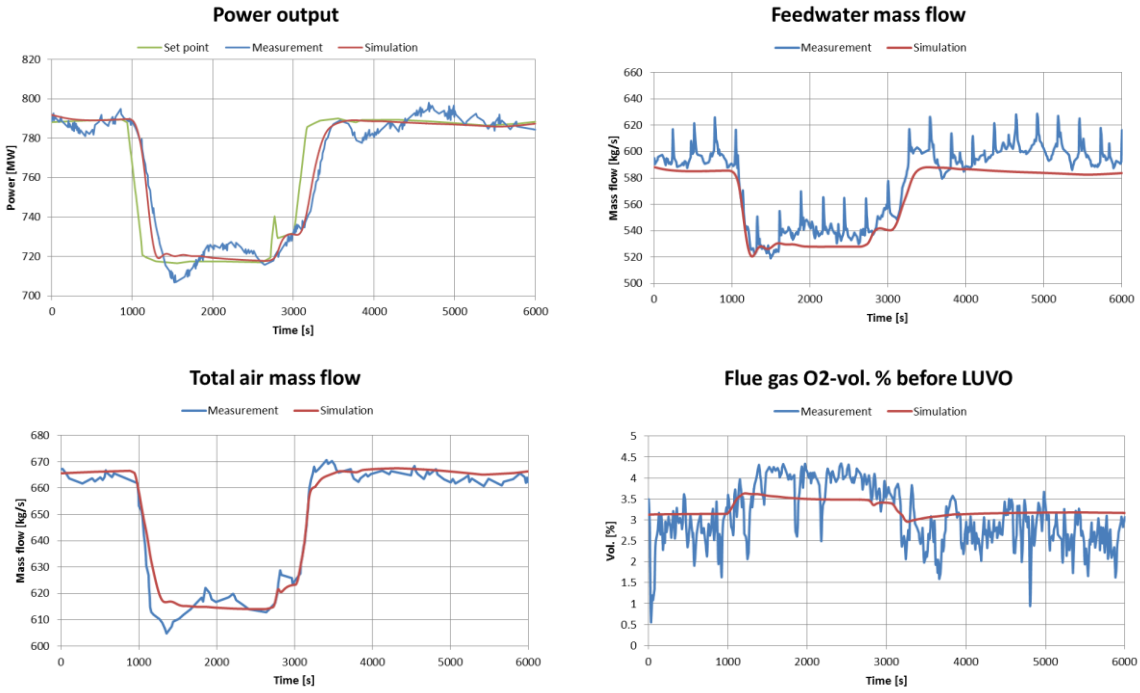

Figure 44. *Gross power output, feedwater mass flow, total air mass flow and flue gas O_2-volume %.*

Steam temperature and enthalpy after the evaporator section in the boiler are presented in Figure 45. These results indicate that the dimensions of evaporator tubes and the radiative heat transfer coefficients between the combustion flames and water-steam circuit are substantially correct, since the differences between the simulation and measurement curves are rather small.

Steam enthalpy is controlled by the enthalpy correction control, which adjust the set point of the feedwater flow according to difference between design enthalpy and measured enthalpy across the evaporator. The simulation enthalpy seems to stay well under control throughout the transient, whereas there are peaks in the measurement curve under the loads changes. The peaks are probably caused by the timing of coal- and feedwater flow controls. For example if the feedwater flow is decreased before the coal feed is decreased during a load drop, the steam enthalpy starts to raise. Also the tuning of enthalpy controller has a major impact on how the enthalpy and temperature after the evaporator behave.

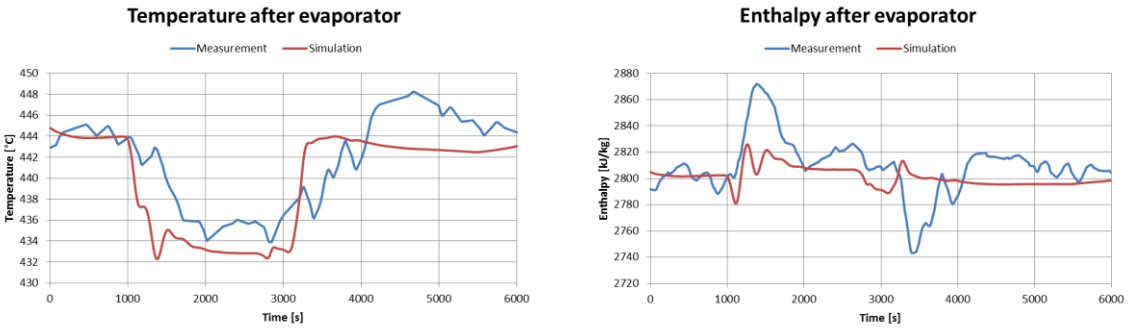

Figure 45. *Steam temperature and enthalpy after the evaporator.*

There are around two percent level difference in steam temperatures after primary, secondary and tertiary superheaters between simulation and measurements as can be noticed from Figure 46. The tuning of heat transfer coefficients and steam temperature controllers in the superheat section were one of the most difficult tasks during the modelling. The deviations between the curves depend on multiple factors, such as ratio between radiative and convection heat transfer and temperature difference set points across attemperators. Despite deviations in the first three superheaters the simulated live steam temperature after the final superheater corresponds to the measurement.

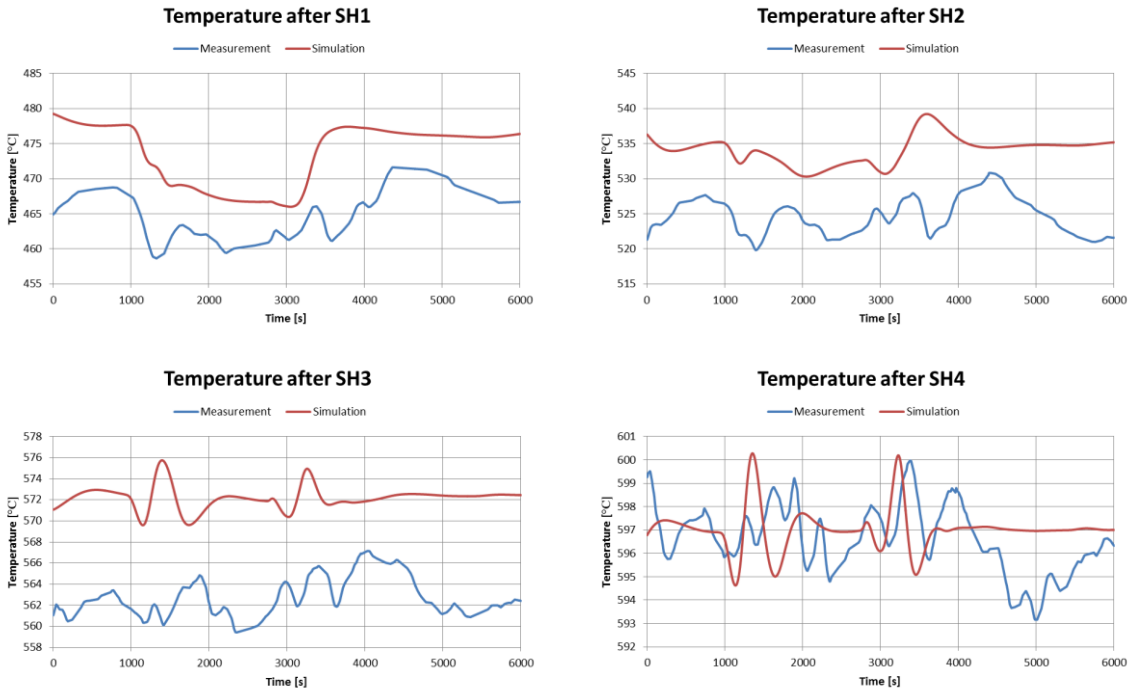

Figure 46. *Temperatures after each superheater.*

Spray water flows, which are used for steam temperature control in the superheater-section are showed in Figure 47. The level of spray water flows is slightly higher in the simulation model. Besides steam temperature control amount of spray water also affects on the whole mass balance of water and steam in the boiler. Therefore the level of spray water should approximately equate between the model and real process. However the

exact equivalence is challenging to achieve due to complexity of steam temperature control.

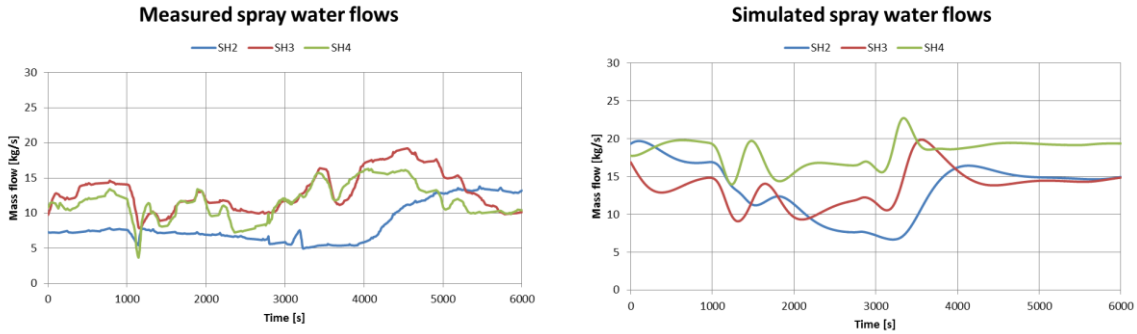

Figure 47. *Measured and simulated spray water flows.*

Simulated water and steam pressures correspond to measurements throughout the water-steam circuit as can be seen from Figure 48, where the steam pressures after the evaporator and final superheater are presented.

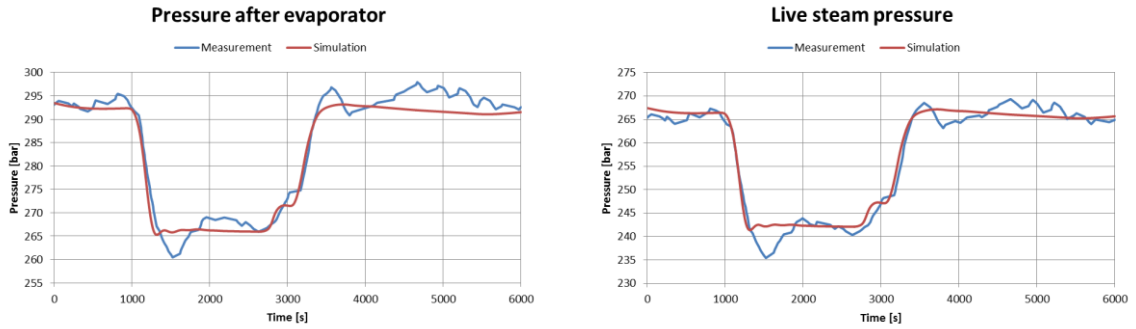

Figure 48. *Steam pressures after the evaporator and after the final superheater.*

All in all the presented reference plant B model is able to simulate the behavior of the real plant with a satisfactory accuracy in the valid gross power range between 700 and 813 MW.

As for the coal mill model the same deficiencies were detected that were discussed in the reference plant A case. These deficiencies concern the mills inner coal storage and taking into account different coal particle sizes.

8.3.2 Thermo-mechanical stresses during load change transient

As in the simulation case of reference plant A also in this case thermal- and pressure stresses in a stress-prone boiler component are determined using the Apros stress solver component during the same transient that was used in plant- and coal mill model validation.

Stresses are determined in the inner surface of an interface of tertiary superheater header and superheater tube connected to it. This location was selected because the header in

question has the thickest walls of all superheater headers of the plant. Thick-walled components, as is well known, are most prone to thermal stresses. Stress concentration factors $k_t = 1{,}66$ and $k_p = 2.74$, which were determined according to Equations (38)–(42), were used to take into consideration the geometry and the changing heat transfer coefficient in the connection. Dimensions of the header and the tube are listed in Table 11.

Table 11. *Reference plant B superheater header dimensions.*

Component	Outside diameter [mm]	Wall thickness [mm]
Header	457,0	95,0
Tube	50,8	11,5

Material of both the header and the tube is martensitic metal alloy 10CrMoVNb9-1, which properties are listed in Table 12.

Table 12. *10CrMoVNb9-1 material properties.*

Property	Value	Unit
Thermal conductivity, λ	$25{,}937 - 0{,}0097 \cdot T - 5 \cdot 10^{-6} \cdot T^2$	W/m°C
Density, ρ	7770	kg/m^3
Specific heat capacity, c_p	$440{,}27 + 0{,}3804 \cdot T + 0{,}0003 \cdot T^2$	J/kg°C
Thermal expansion coefficient, β	$1 \cdot 10^{-5} + 4 \cdot 10^{-9} \cdot T - 2 \cdot 10^{-12} \cdot T^2$	1/°C
Modulus of elasticity, E	$218{,}617 - 0{,}0456 \cdot T - 0{,}0627 \cdot T^2$	kN/mm^2
Poisson's ratio, μ	0,3	-

Steam pressure and temperature during the transient are shown in Figure 49. The steam temperature control is able to keep the temperature quite well in desired value, and therefore the biggest change is only around 6 °C. Steam pressure changes considerably, around 25 bars, when the load is modified.

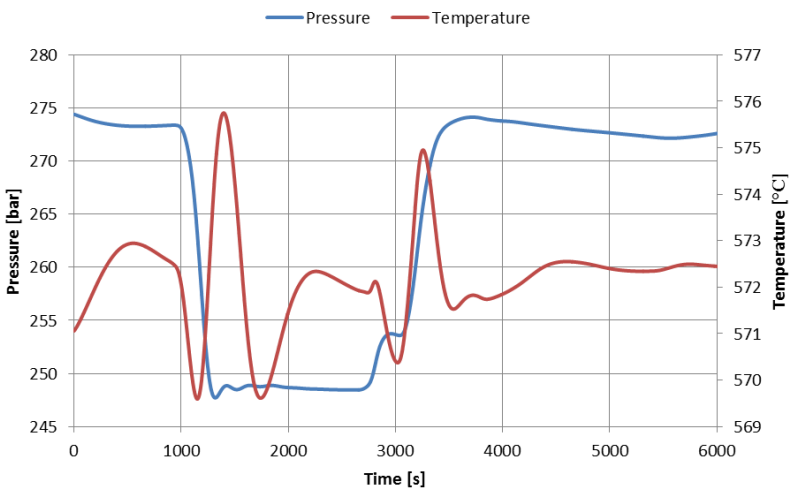

Figure 49. *Steam pressure and temperature inside the header during the transient.*

Tangential, radial, axial and combined thermal- and pressure stresses are illustrated in Figure 50. The magnitude of the stresses is substantially the same as in reference plant A stress calculation. The maximum stress is measured when the steam temperature drops, and hence thermal and pressure stresses have the same sign. Temperature increase have the inverse effect, since the stresses are opposite in sign, and therefore net stresses are at minimum value. The maximum combined stress, which would be used for allowed stress definition, is slightly bigger than in the previous reference plant A case. However if the allowed stress is assumed to be around 350 MPa based on approximative calculations according to EN-12952-3, the combined net stress remains within permissible limits throughout the transient.

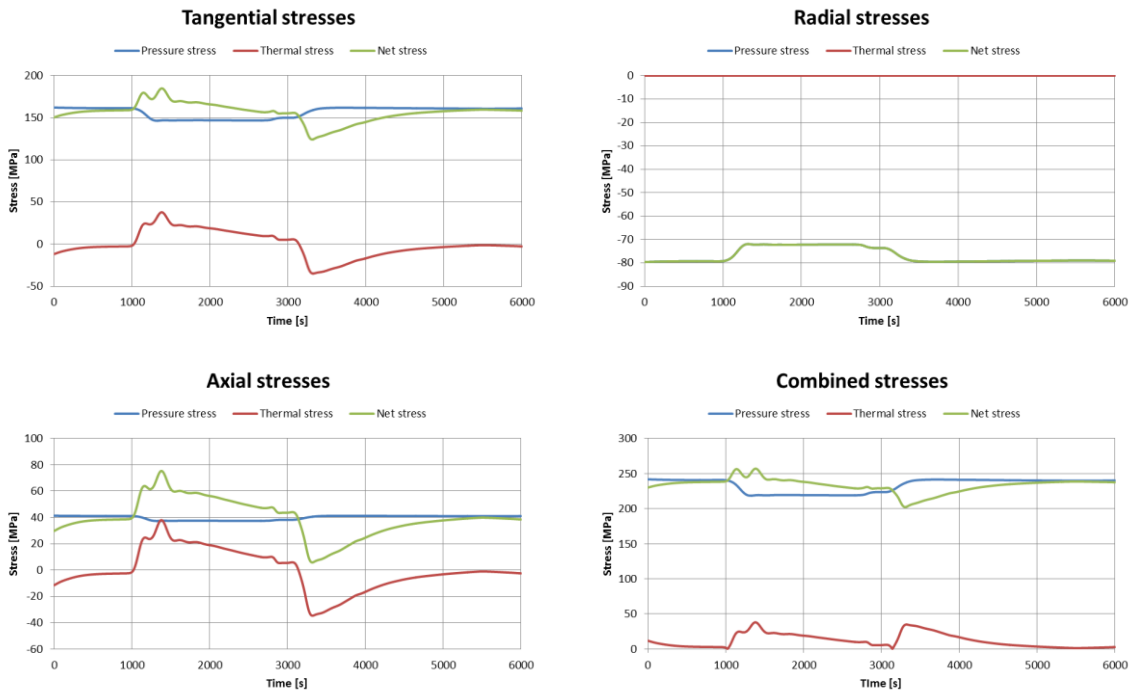

Figure 50. *Thermo-mechanical stresses during the transient.*

9. CONCLUSIONS

This thesis focused on improving the transient simulation of pulverized coal-fired power plants in dynamic simulation software Apros. By improving dynamic models and transient simulation of these plants, more accurate testing can be performed with simulation experiments. Due to intermittent renewable energy production pulverized coal-fired base load plants are increasingly operated cyclically. Cyclic operation is needed to compensate the fluctuating electricity generation of wind and solar power plants. Process changes and new control strategies need to designed and implemented to respond to challenges that load-varying operation causes at the plant. New solutions can be easily tested with transient simulation experiments in dynamic simulation software.

The first aim of this thesis was to implement a generic coal mill model in Apros using the user component feature and validate the model against operational plant data. Mill model is often considered as a bottleneck when dynamics of a pulverized coal-fired power plant is studied especially when load-varying operation is simulated. However the coal mill is essential part of the plant and the mill model should be included in the plant model especially if transient simulation is considered.

The second aim was to verify and validate the thermo-mechanical stress calculation used in Apros. Thermo-mechanical stress is the main restrictive factor during cyclic operation of load-following units, and therefore it is necessary to investigate stresses during start-ups, shutdowns and load changes by simulations. Stress calculation can be used for optimizing the plant operation.

For the validation experiments two reference plant models were utilized. Model of reference plant A was received from the plant operator whereas modelling of the reference plant B was included in this thesis. Modelling of reference plant B and the validation results of the plant model were also discussed in the thesis.

The coal mill model was validated with both reference plant models. In the first case the mill model was attached to the reference plant A model. The original model included a identified coal mill model, which was tuned to replicate the mills of the plant. The plant model, where the coal mill user component (UC) was attached, was compared to the original plant model during a load change transient. Validation showed that the main challenge related to the coal mill model seems to be the coal storage inside the mill and the coal particle size distribution, which need to be modelled with sufficient accuracy when the model is intended to be used in load transient simulation. The coal mill inter-

nal dynamic behavior is challenging to be modelled with a relatively simple model, and thus more complicated models should probably be considered.

The simulation model of reference plant B was constructed for load transient simulation use only. Therefore some significant model simplifications were done. The plant model included the coal mill UC, which was validated alongside the plant model. Validation was done by comparing the simulation results to plant measurement data. Plant model validation results were satisfactory and based on the validation model can be used in the tested gross power range between 700 and 813 MW. As in the reference plant A simulation case also in this case the coal mill model did not quite bring in the desired results. The dynamic behavior of the coal storage inside the mill during the load changes was the primary reason for the insufficient model dynamics. Both validation cases showed that the mill model that was used in this thesis should be modified to capture the complicated dynamic behavior of the mill in transient situations.

Besides coal mill and plant modelling thermo-mechanical stresses were discussed in this thesis. The Apros stress calculation was verified against literary reference and validated against calculation based on EN-12952-3 standard. The verification showed that Apros stress calculation corresponds to the literary reference in circumstances, where quasi-stationary temperature field in the component wall and a constant medium pressure were considered. Validation of Apros stress calculation brought out that stress concentration factors should be utilized when stresses are defined in pipe connections.

Also stresses were defined during the same load transients which were used in the coal mill and plant model validations. Stress calculation gave similar results in both reference plant simulation cases and the results seemed realistic. The biggest stresses in an once-through boiler are located in openings of a header or a water separator. Tangential stress is the predominant stress component during load changes, and biggest stress values are defined during load decreases since the thermal and pressure stresses are equal in sign.

This thesis brought out important information related to features that are needed to improve the transient simulation of pulverized coal-fired power plants in dynamic simulation software Apros. The development will continue based on the results presented in this thesis.

REFERENCES

[1] R. Starkloff, F. Alobaid, K. Karner, B. Epple, M. Schmitz, F. Boehm, Development and validation of a dynamic simulation model for a large coal-fired power plant, Applied Thermal Engineering 91, Elsevier, 2015, pp. 496-506

[2] A. Kettunen, M. Paljakka, Process Simulation in Power Plant Design, Foster Wheeler Energia Oy & VTT Technical Research Centre of Finland, 7 p., Available (Retrieved on 15.9.2015): https://www.automaatioseura.fi/confprog/downloadfile_public.php?conference=12&filename=12-12030.pdf

[3] J. Banks, J. S. Carson II, B. L. Nelson, D. M. Nicol, Discrete-Event System Simulation, 4th edition, Pearson/Prentice Hall, 2005, 528 p.

[4] P. Thomas, Simulation of Industrial Processes for Control Engineers, Butterworth-Heinemann, 1999, 327 p.

[5] P. Niemczyk, P. Andersen, J. D. Bendtsen, T. Sondergaard Pedersen, A. P. Ravn, Derivation and validation of a coal mill model for control, Control Engineering Practice, 2012, 6 p.

[6] P. Keatley, A. Shibli, N. J. Hewitt, Estimating power plant start costs in cyclic operation, Applied Energy 111, Elsevier, 2013, pp. 550–557

[7] National Renewable Energy Laboratory, Power Plant Cycling Costs, 2012, Available (Retrieved on 8.9.2015): http://www.nrel.gov/docs/fy12osti/55433.pdf

[8] Fraunhofer Institute for Solar Energy Systems ISE, Electricity production from solar and wind in Germany in 2014, 2014, Available (Retrieved on 8.9.2015): https://www.ise.fraunhofer.de/en/downloads-englisch/pdf-files-englisch/data-nivc-/electricity-production-from-solar-and-wind-in-germany-2014.pdf

[9] R. Raiko, H. Tolvanen, A. Pääkkönen, KEB-43500 Energiatalous - Luentomoniste, Tampere University of Technology, Tampere, 2014, 149 p.

[10] J. Sederlund, Taajuuden ylläpito sähköjärjestelmässä, Fingrid Oyj:n lehti 3/2008, Fingrid, 2008, 35 p.

[11] D. Diegel, S. Eckstein, U. Leuchs, O. Zaviska, Fulfillment of Grid Code Requirements in the area served by UCTE by Combined Cycle Power Plants, Siemens AG, Power Generation, Germany, 21 p., Available (Retrieved on 4.3.2016): http://www.energy.siemens.com/br/pool/hq/energy-topics/pdfs/en/gas-turbines-power-plants/3_Fulfillment_of_Grid_Code.pdf

[12] Transmission Code 2007, Network and System Rules of the German Transmission System Operators, Verband der Netzbetreiber – VDN – e.V. beim VDEW, 2007, 79 p., Available (Retrieved on 4.3.2016): https://www.vde.com/de/fnn/dokumente/documents/transmissioncode%202007_engl.pdf

[13] J. Kovacs, Better Technology For a Cleaner Environment, Foster Wheeler, 40 p., Available (Retrieved on 7.3.2016): https://www.automaatioseura.fi/index/tiedostot/Boiler_control.pdf

[14] Procurement of control power and energy in Germany, Amprion, Available (Retrieved on 7.3.2016): http://www.amprion.net/en/control-energy

[15] Suomen Standardisoimisliitto SFS, SFS-EN 12952-3 Water-tube Boilers and Auxiliary Installations. Part 3: Design and Calculation for Pressure Parts of the Boiler, Standard, 2012, 165 p.

[16] Holcomb Station, New Power Plant Major Components, Available (Retrieved on 7.3.2016): http://www.holcombstation.com/technology/power-plant-major-components/

[17] International Energy Agency, Energy and Climate Change, World Energy Outlook Special Report, 2015, 196 p.

[18] D. K. Moyeda, Pulverized Coal-Fired Boilers and Pollution Control, Encyclopedia of Sustainability Science and Technology, Springer New York, 2012, pp. 8347-8372

[19] ClimateTechWiki, Pulverized Coal Combustion with Higher Efficiency, 2006, Available (Retrieved on 14.9.2015): http://www.climatetechwiki.org/technology/sup_crit_coal

[20] R. Raiko, J. Saastamoinen, M. Hupa, I. Kurki-Suonio, Poltto- ja palaminen, International Flame Research Foundation – Suomen kansallinen osasto, 2002, 750 p.

[21] M. M. El-Wakil, Powerplant Technology, McGraw-Hill, 1984, 861 p.

[22] S. Teir, A. Kulla, Steam/Water Circulation Design, Steam Boiler Technology eBook, Helsinki University of Technology, Espoo 2002, 22 p., Available (Retrieved on 16.2.2016): http://www.energy.kth.se/compedu/webcompedu/ManualCopy/Steam_Boiler_Technology/Steam_water_circulation/steam_water_circulation.pdf

[23] S. C. Stultz, J. B. Kitto, Steam - Its generation and use, 42nd Edition, The Babcock & Wilcox Company, 2005, 1106 p.

[24] Y. Majanne, P. Pietilä, Prosessiautomaation sovellukset – Luentomoniste, 2012, Tampere University of Technology, Tampere, 87 p.

[25] R. Raiko, I. Saarenpää, Höyrytekniikka – Luentomoniste, 2013, Tampere University of Technology, Tampere, 254 p.

[26] I. Barnes, Upgrading the Efficiency of the World's Coal Fleet to Reduce CO_2 Emissions, Cornerstone – The Official Journal of the World Coal Industry, 2015, Available (Retrieved 16.2.2016): http://cornerstonemag.net/tag/ultra-supercritical-advanced-ultrasupercritical/

[27] P. Jayarama Reddy, Clean Coal Technologies for Power Generation, CRC Press, 2013, 309 p.

[28] S. G. Dukelow, The control of boilers, 2nd edition, ISA, 1991, 405 p.

[29] B. Lamp, K. Wendelberger, B. Meerbeck, A New Era in Power Plant Control Performance, Siemens, Reprint from COAL POWER magazine, 2009, 6 p., Available: (Retrieved on 7.3.2016) http://www.energy.siemens.com/us/pool/us/automation/instrumentation-controls-electrical-power/webfeature/Article-Control-Performance.pdf

[30] Y. Sato, Lünen – State-of-the-Art 813MW Coal-Fired USC Boiler with High Efficiency and Flexibility, Power-Gen Asia 2014, IHI Corporation, 13. p., Available (Retrieved on 16.11.2015): http://pennwell.websds.net/2014/kl/pga/papers/T3S3O2-paper.pdf

[31] C. Schuhbauer, M. Angerer, H. Spliethoff, F. Kluger, H. Tschaffon, Coupled simulation of a tangentially hard coal fired 700 °C boiler, Fuel 122, Elsevier, 2014, pp. 149–163

[32] B. Kowalczyk, K. D. Tigges, Entwicklung und Anwendung dynamischer Modelle in der Auslegung von Kraftwerken, Kraftwerkstechnik – Sichere und nachhaltige Energieversorgung – Band 4, Technische Universität Dresden, 2012, pp. 245–259

[33] U. Krüger, M. Rech, S. Tuuri. H. Zindler, Dynamischer Kraftwerkssimulator zur leittechnischen Optimierung der Sekundärantwort des E.ON-Kraftwerks Wilhelmshaven, Kraftwerkstechnik 2015 – Strategien, Anlagentechnik und Betrieb, Technische Universität Dresden, 2015, pp. 641–649

[34] P. Höök, Utvärdering av beräkningskoden APROS för användning i inneslutningsanalyser, Examensarbete, Uppsala Universitet, 2014, 55 p.

[35] V. Kakkonen, APROS model validation in case of fast transients in a boiling water reactor, Master's thesis, Lappeenranta University of Technology, 2011, 82 p.

[36] T. Polach, I. Basic, L. Strubelj, Evaluation of the Point Kinetic Model of NEK in APROS, 23rd International Conference Nuclear Energy for New Europe, 2014, 9 p.

[37] Apros Thermal Hydraulics, Thermal Hydraulic Flow Models, Fortum & VTT, Available (Retrieved on 15.9.2015): http://www.apros.fi/filebank/71-Apros_thermal_hydraulics_-_general.pdf

[38] Apros Overview, Fortum & VTT, Available (Retrieved on 17.9.): http://www.apros.fi/filebank/68-Apros_overview.pdf

[39] Apros 6 Feature Tutorial, VTT and Fortum, 2015, 458 p.

[40] C. Maffezzoni, Concepts, practice and trends in fossil-fired power plant control, Power Systems and Power Plant Control, Proceedings of the IFAC Symposium, 1986, pp. 1-9

[41] N. W. Rees, G. Q. Fan, D. Flynn (editor), Thermal Power Plant Simulation and Control, Chapter: Modelling and control of pulverized fuel coal mills, Institution of Electrical Engineers, 2003, pp. 63-99

[42] V. Agrawal, B. K. Panigrahi, P. M. V. Subbaro, A unified thermo-mechanical model for coal mill operation, Control Engineering Practice 44, Elsevier, 2015, pp. 157-171

[43] J. L. Wei, J. Wang, Q. H. Wu, Development of a Multisegment Coal Mill Model Using an Evolutionary Computation Technique, IEEE Transactions on Energy Conversion, Vol. 22, No. 3, 2007, pp. 718-727

[44] S. Härkönen, Lämpöjännitysten mittaaminen osana höyrykattilan automaatiota, Licenciate Thesis, 1981, Tampere University of Technology, Tampere, 107 p.

[45] M. Jegoroff, H. Mikkonen, M. Tähtinen, T. Leino, S. Tuuri, Dynamic Studies of Integrated Power Plants, VTT & Fortum, 2015, 14 p.

[46] R. B. Hetnarski (ed), Encyclopedia of Thermal Stresses, Springer Science+Businesss Media Dordrecht, 2014, 6643 p.

[47] G. J. Nakoneczny, C. C. Schultz, Life Assessment of High Temperature Headers, Babcock & Wilcox, 1995, 30 p., Available (Retrieved on 17.11.2015): http://www.babcock.com/library/Documents/br-1586.pdf

[48] O. Kwon, M. Myers, A. D. Karstensen, D. Knowles, The effect of the steam temperature fluctuations during steady state operation on the remnant life of the superheater header, International Journal of Pressure Vessels and Piping 83, 2006, pp. 349-358

[49] A. Toradmal, Optimization of Conventional Power Plant Start-up Through Heating of Thick Walled Components, Master of science thesis, University of Duisburg-Essen, 2015, 122 p.

APPENDIX A: APROS GRAPHICAL USER INTERFACE

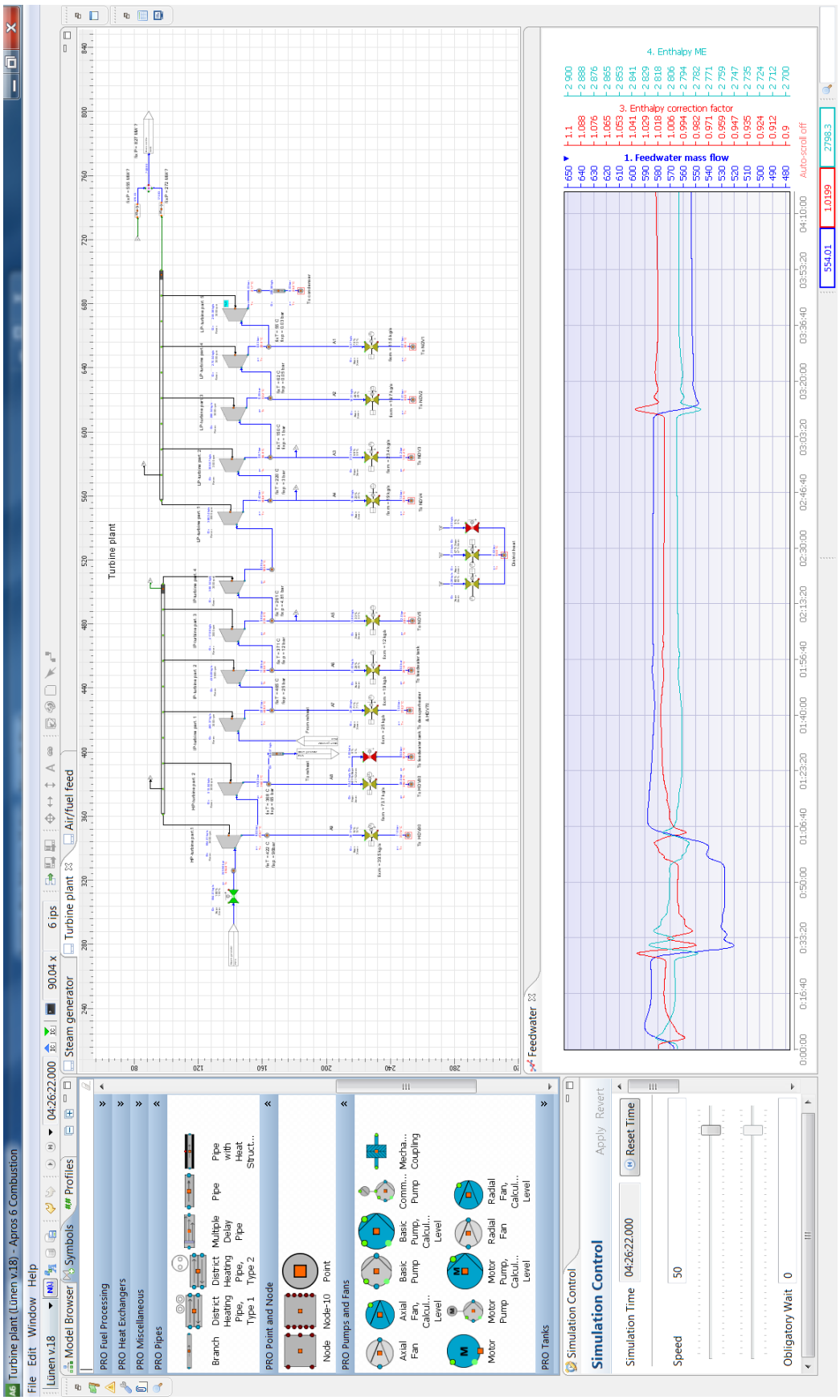

APPENDIX B: REFERENCE PLANT B APROS-MODEL DIAGRAMS

B 1 Air and fuel feed diagram

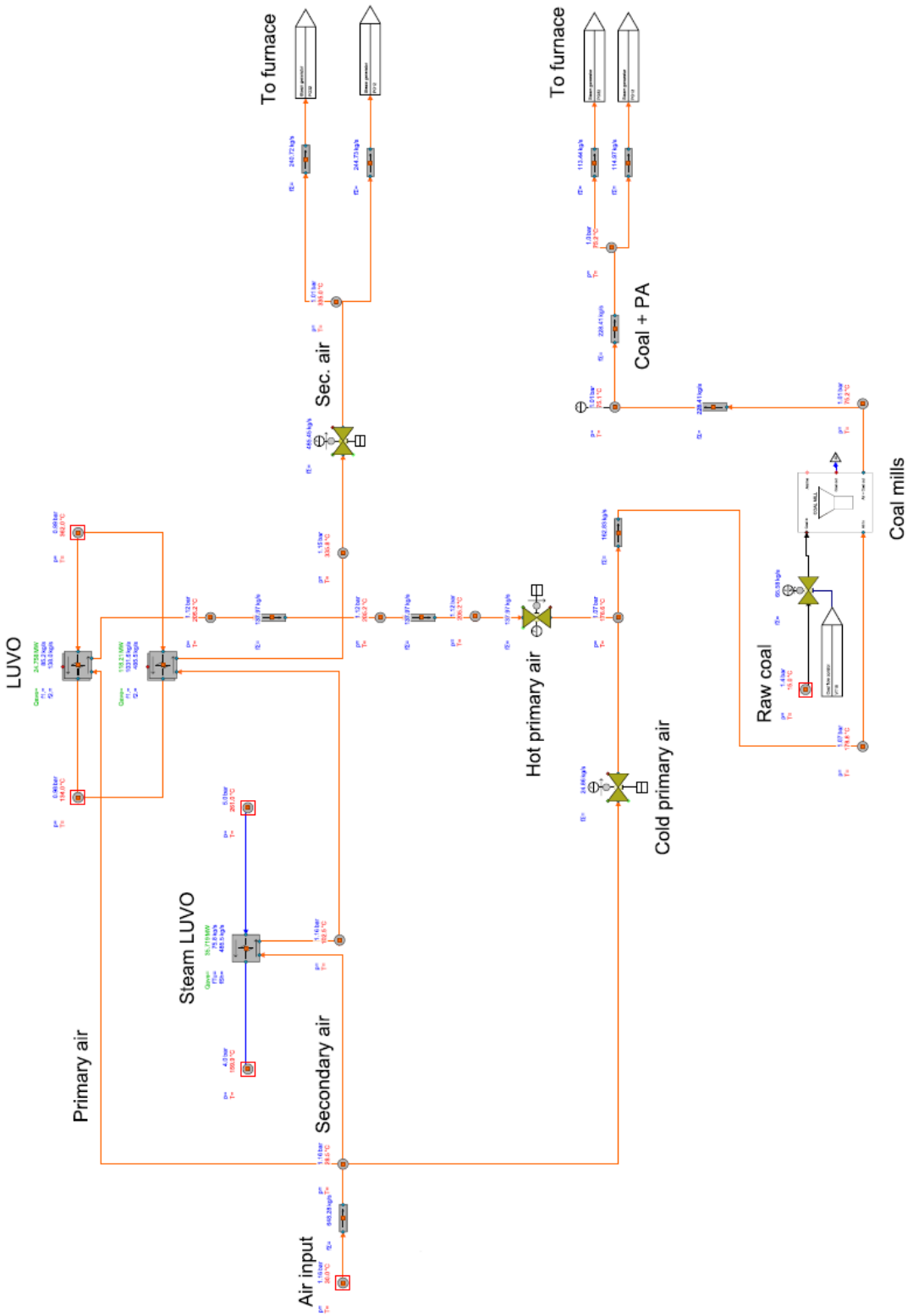

B 2 Boiler diagram

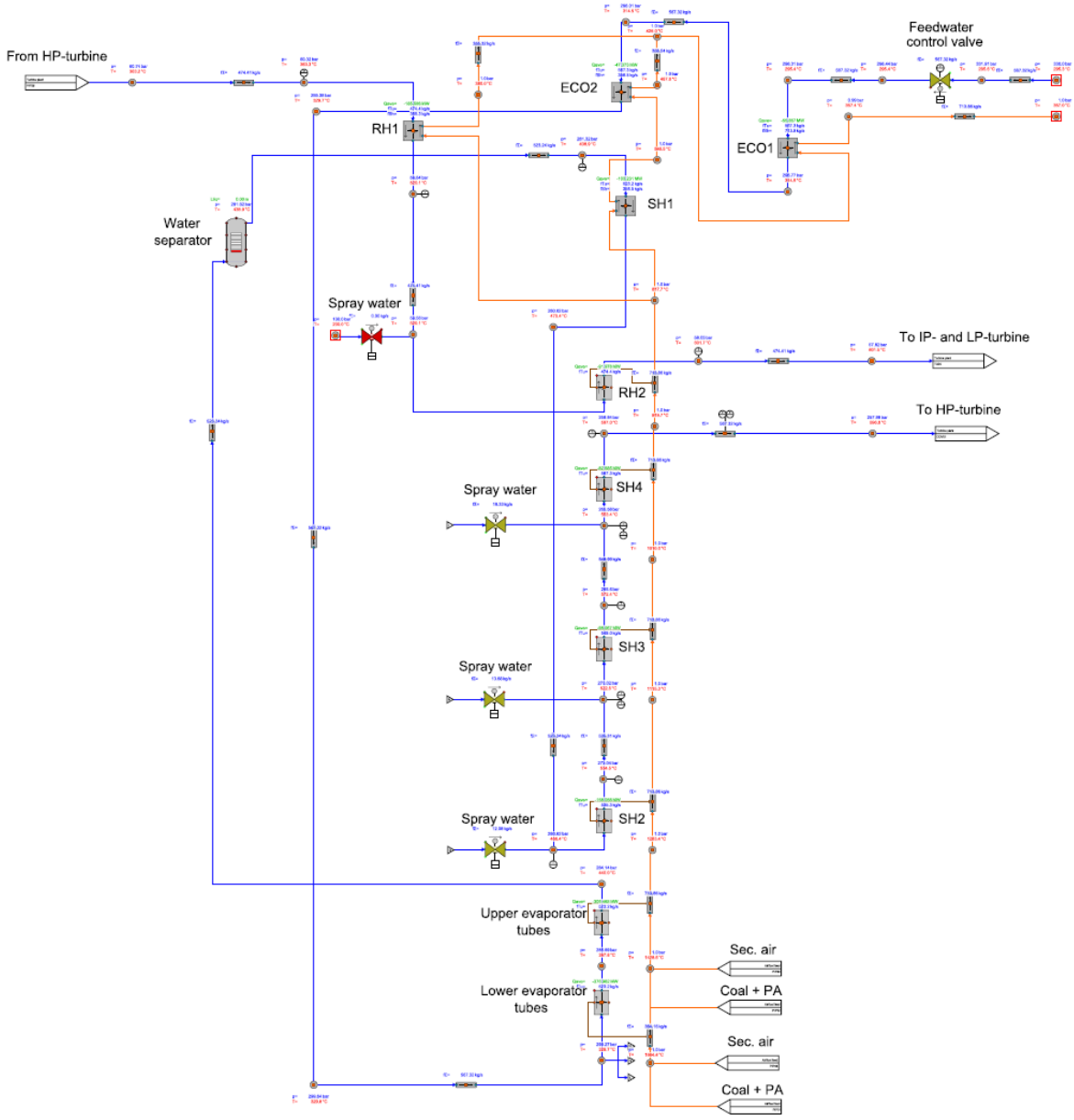

B 3 Turbine plant diagram

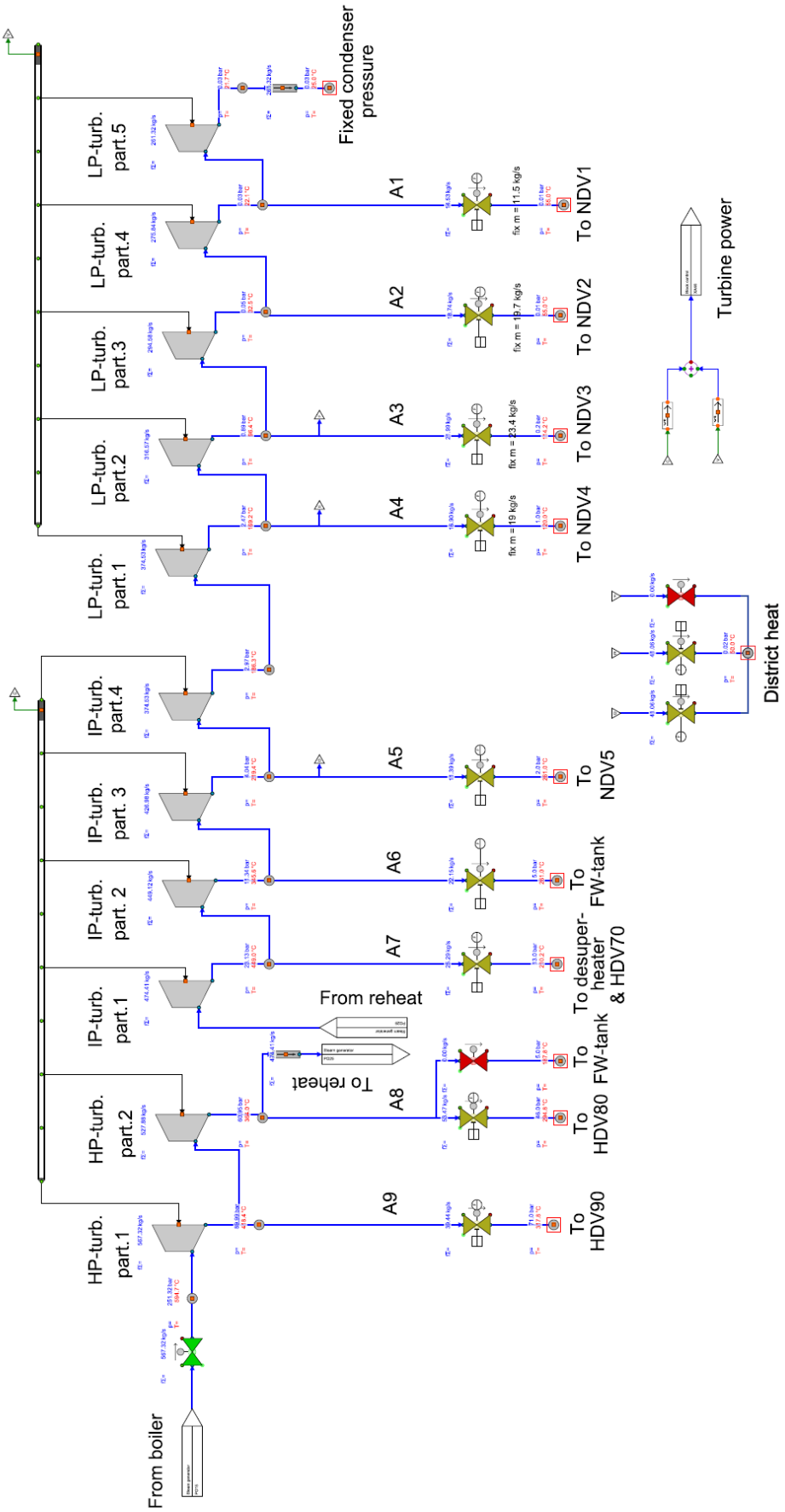

B 4 Block control diagram

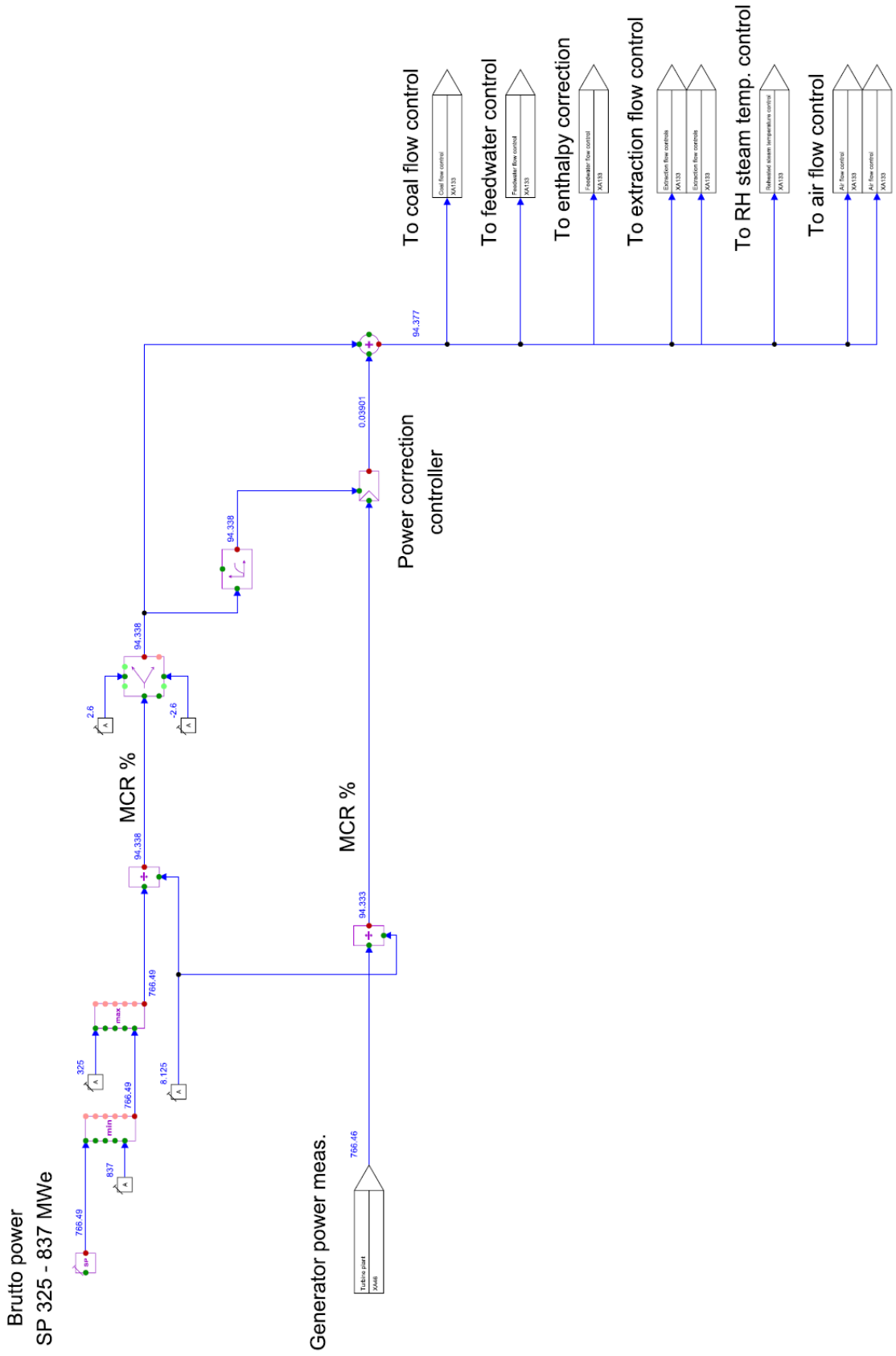

B 5 Coal flow control diagram

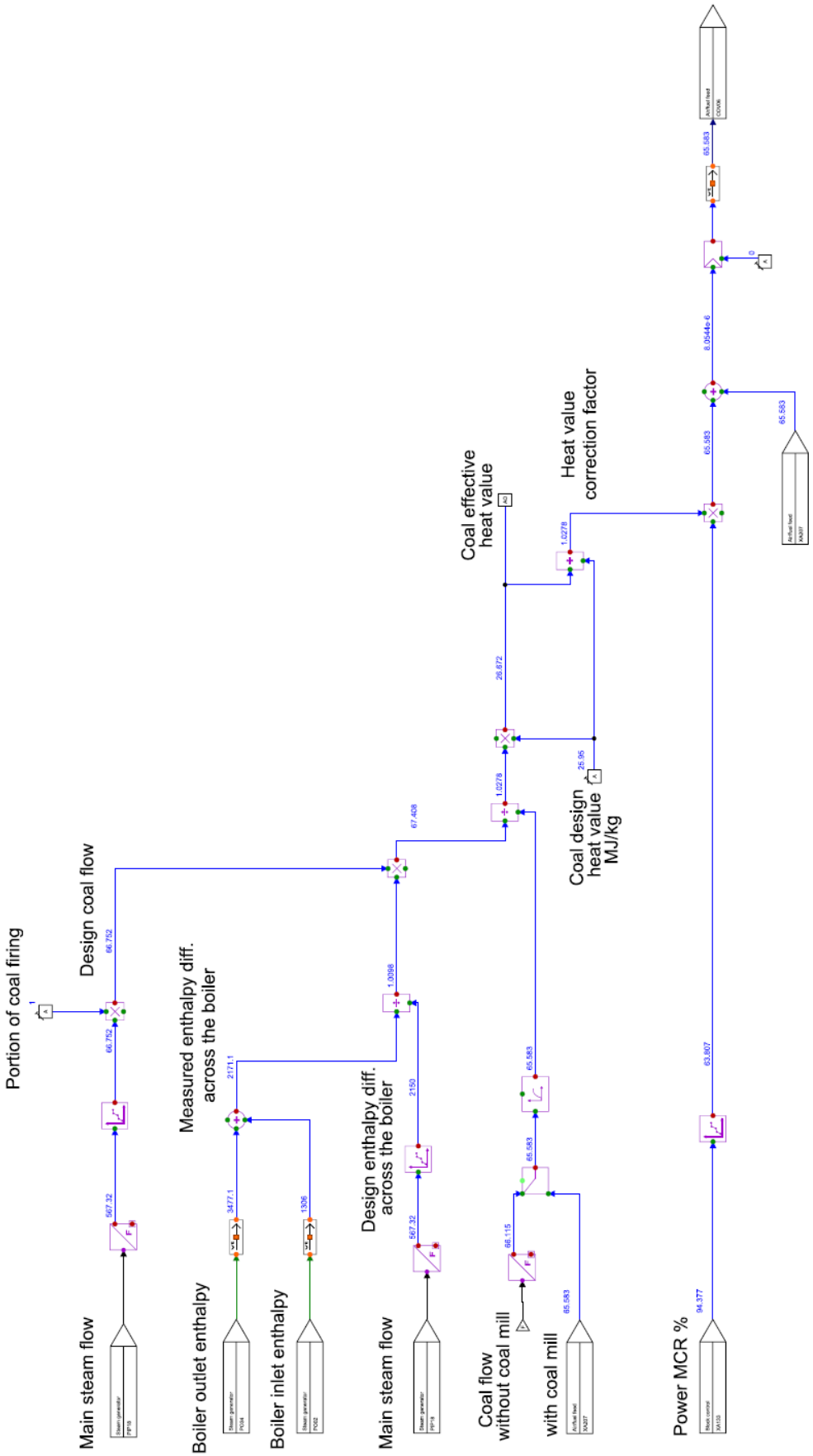

B 6 Air control diagram

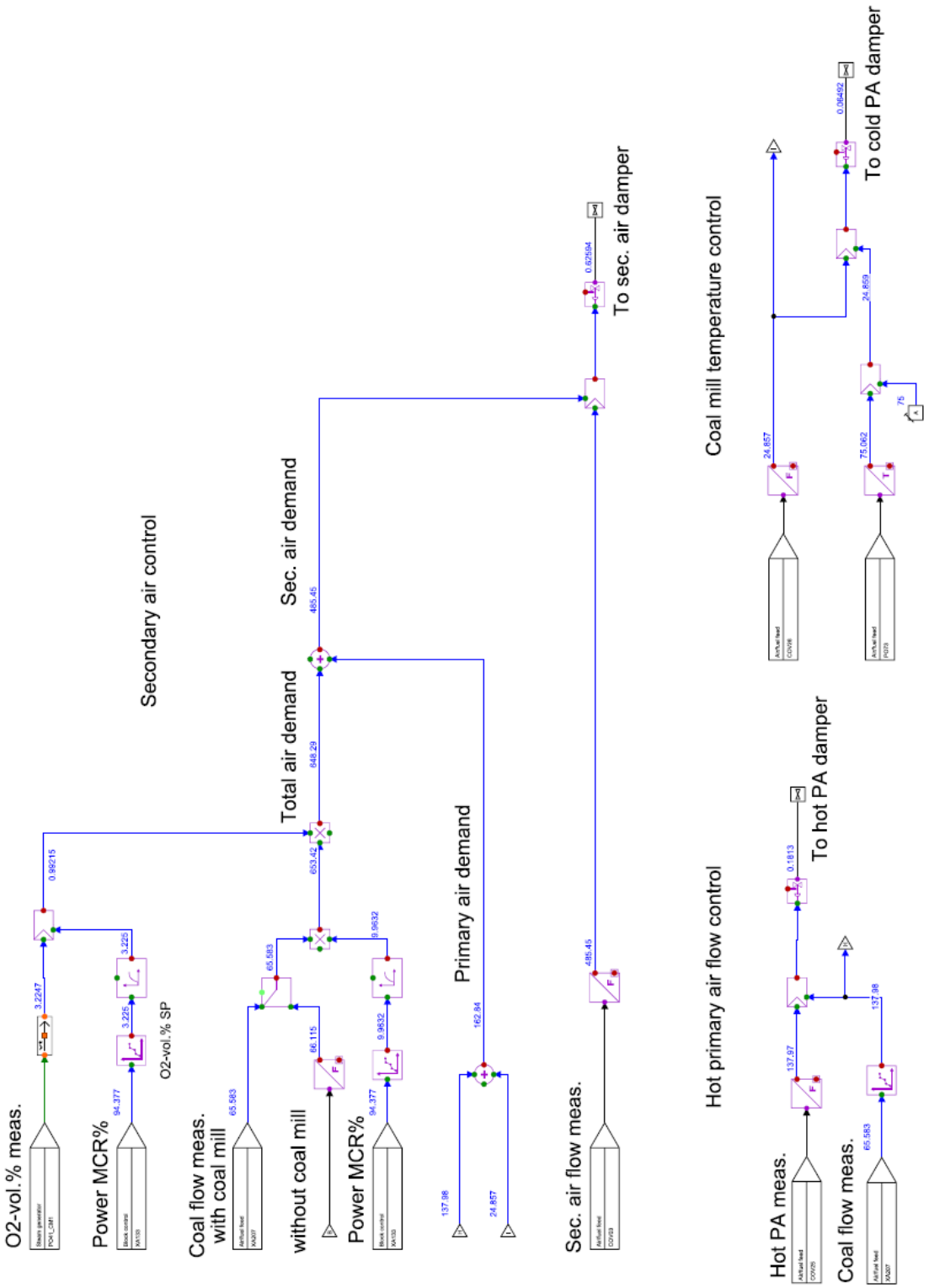

B 7 Live steam temperature control diagram

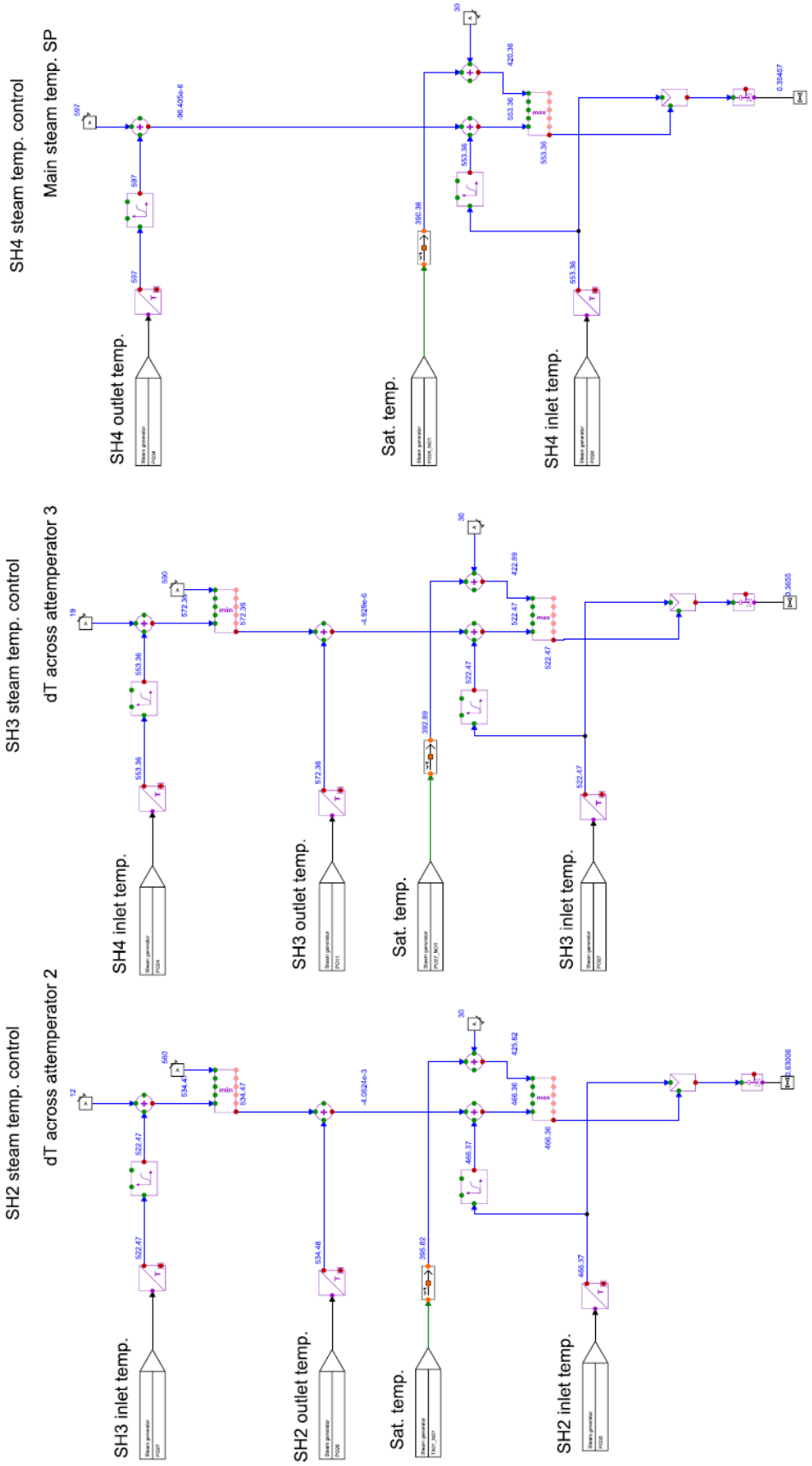

B 8 Reheated steam temperature control diagram

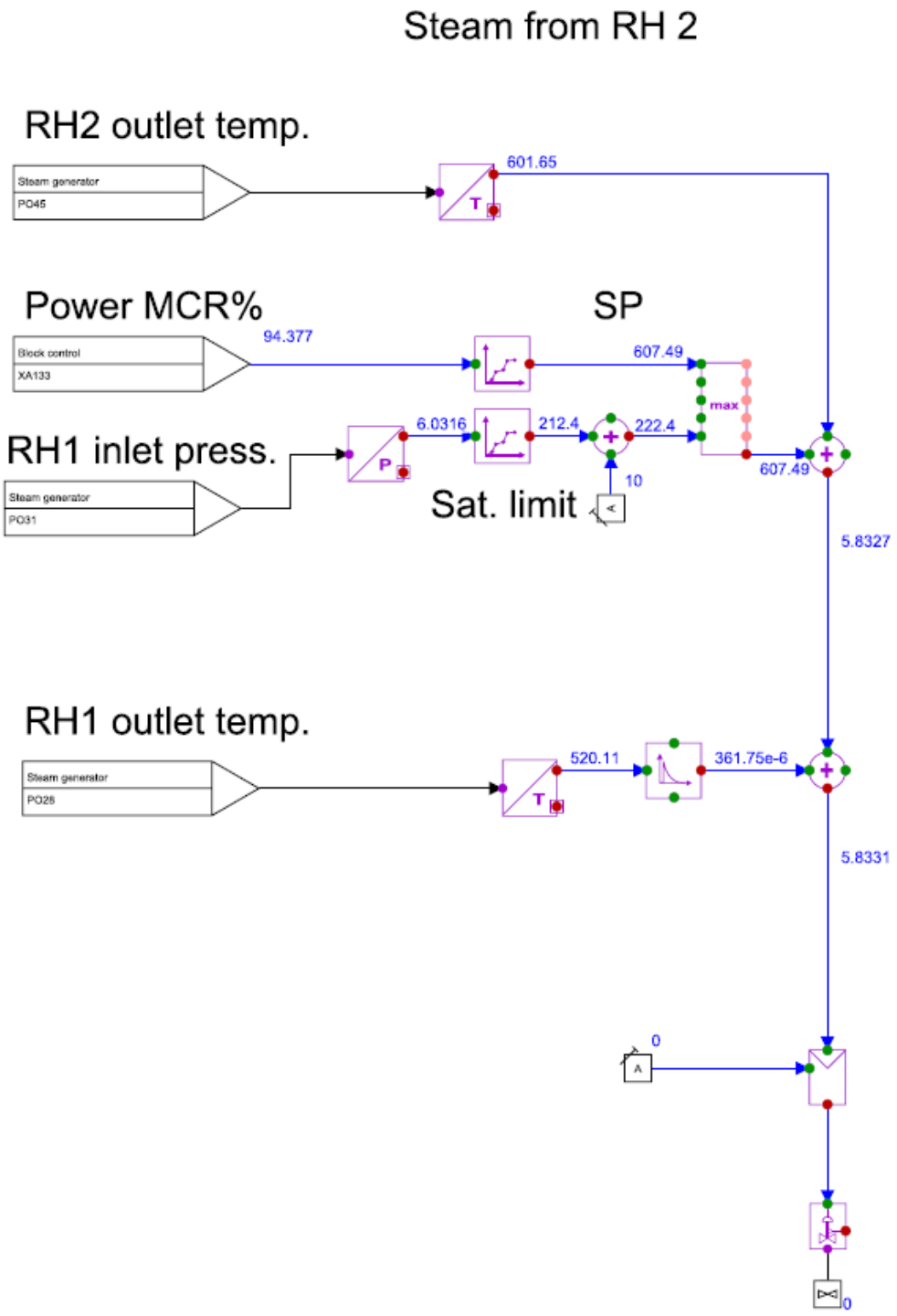

B 9 Feedwater control diagram

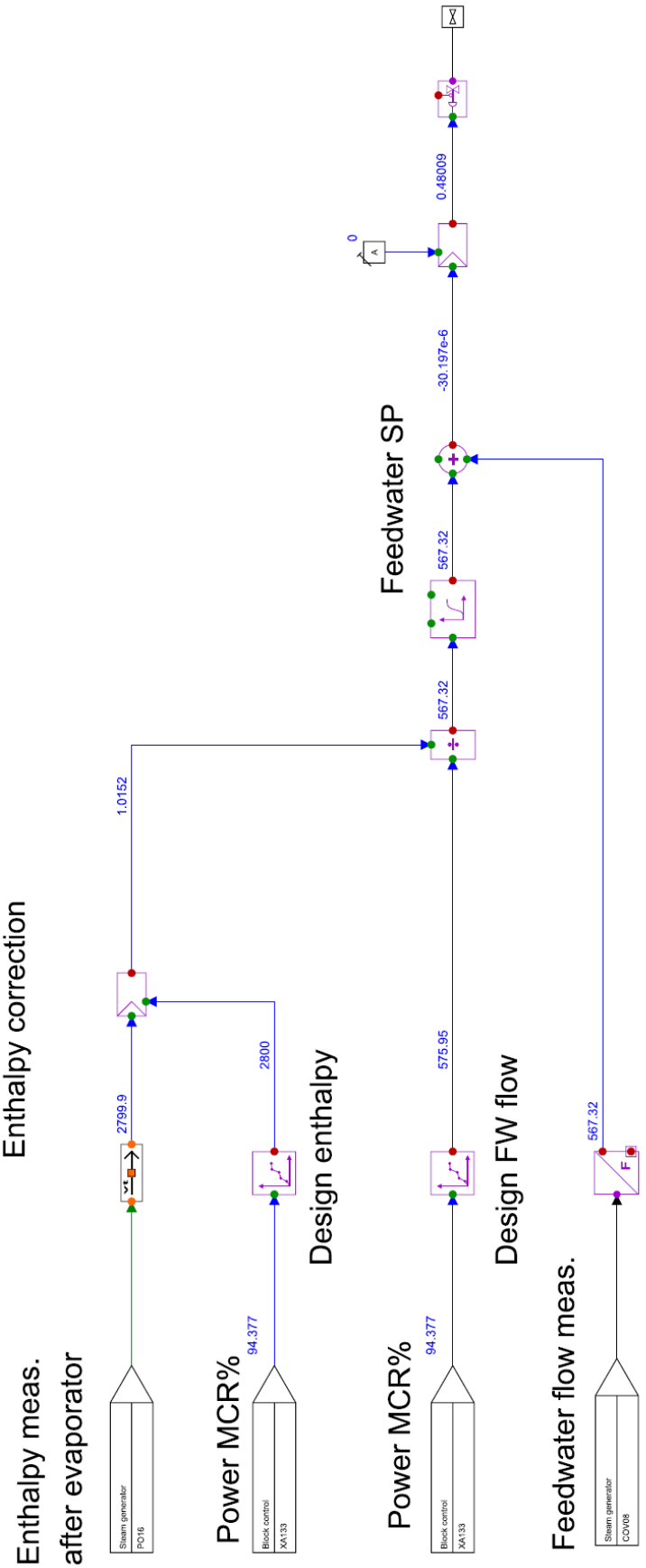

B 10 Extraction flow control diagram